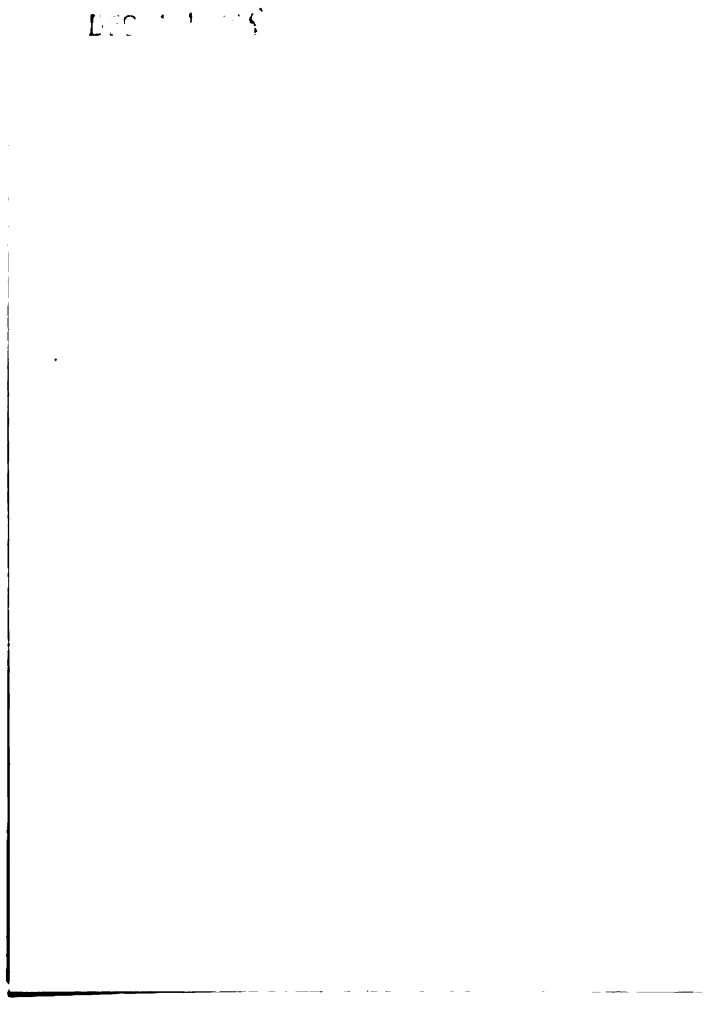

ABSTRACT

AN EXPERIMENTAL MEASUREMENT
OF COSMIC-RAY MUON SCATTERING BY ALUMINUM,
IN THE MOMENTUM REGION OF 1.60 Bev/c

by Ronald Wilbur Beery

An account is presented of an investigation into the scattering behavior of (1.60 + 0.05, - 0.04) Bev/c μ+ mesons from cosmic rays. The muons were allowed to traverse a spark chamber triggered by a counter telescope. The aluminum plates of the spark chamber provided the scattering material for the incoming muons. A description of circuits and equipment developed for this experiment is presented.

Momentum selection was made by using a lead absorber to slow muons having the above momentum, stopping them in a scintillation counter. Final selection of events required observation of a proper μ-e decay signature in oscilloscope photographs made of the signal from the stopping scintillation counter. The oscilloscope display was also arranged to distinguish between protons, pions, and the desired muons. This served as a method of eliminating the former two types of events from the muon data. As a further verification of the particle selection, the apparent muon lifetime was measured and was in excellent agreement with the accepted value. The narrow limits of momentum obtained and the positive particle-identification procedure represent an improvement over previous cosmic-ray experiments of this kind.

The track photographs obtained were measured on

semi-automatic scanning equipment, the output of which was analyzed by a computer program developed for this experiment to determine the scattering angle of the particle in the chamber. Details of this analysis program are presented. The results of the scattering measurements, in the form of an integral distribution of projected angles, are compared with the distributions predicted by the theories of Moliere, of Cooper and Rainwater, and of Drell and Schwartz. Details of the computer calculations required for the theoretical predictions are also presented.

The results of the present experiment demonstrate agreement with both the theory of Cooper and Rainwater and of Drell and Schwartz throughout the range of scattering angles observed: 0 - 4.5 degrees. This range corresponds to momentum transfers up to 190 Mev/c. Good agreement with Cooper-Rainwater and somewhat better agreement with Drell-Schwartz rather than with Moliere is clear. This experiment does not display the excessive appearance of high-angle scattering reported in early cloud chamber experiments with cosmic-ray muons. This experiment, using cosmic-ray muons, corroborates the results of the recent experiment performed by Masek et al., with 2 Bev/c muons obtained from the Bevatron.

AN EXPERIMENTAL MEASUREMENT OF COSMIC RAY MUON SCATTERING BY ALUMINUM, IN THE MOMENTUM REGION OF 1.60 Bev/c

By

Ronald Wilbur Beery

A THESIS

Submitted to
Michigan State University
in partial fulfillment of the requirements
for the degree of

DOCTOR OF PHILOSOPHY

Department of Physics and Astronomy

1966

ACKNOWLEDGMENT

I wish to acknowledge my appreciation to Professor Joseph Ballam for his suggestion of the problem and direction in the early stages of the work. I am grateful also for his interest and willingness to continue the responsibility of seeing the work completed even after his transfer to Stanford University.

The valuable suggestions and advice of Dr. John Scandrett during the construction of the spark chamber equipment are acknowledged. I am also grateful to the many professors and staff of the Department of Physics who have given encouragement during the long-term construction and operation schedule of a cosmic-ray experiment such as this. With regard to construction assistance I am indebted to the late Mr. Charles Kingston and to Mr. Richard B. Hoskins as well as the entire staff of the machine shop for their counsel and assistance in the design and mechanical construction of the experimental apparatus. I am also indebted to Mr. Ernest F. Brandt and the staff of the electronics shop for their assistance in constructing the electronic equipment necessary to the experiment.

My thanks go to Mr. William M. Patmos and to Professor David Marker for their assistance in the early stages of the computer programming for the data analysis and the theory calculations respectively. My thanks also go to Mr. Michael Yarnold who, as an undergraduate, headed up my film-scanning staff, and to the other students on the scanning staff for their interest and help in the work.

I wish to express finally my appreciation to my wife Alice for her patience and encouragement throughout the work and for her efforts in typing the manuscript and final copies of this work.

The construction and operation of the apparatus for this experiment were made possible by a grant supported by the National Science Foundation.

TABLE OF CONTENTS

TABLE OF FIGURES

I. INTRODUCTION

A. Background of muon investigations

The characteristic properties of muons have in recent years been the subject of considerable interest among those working in particle physics. The following characteristics measured in these muon investigations are of interest here:

1) Muon mass found to be 206.767 ± 0.003[21] times that of the electron.
2) Muon mean lifetime found to be 2.2001 ± 0.008 useconds[22].
3) $\nu_\mu - \nu_e$ distinction. In an experiment by Danby, et al.,[23] it was demonstrated that the muon has its own neutrino, quite apart from that associated with the electron. This was concluded from the fact that neutrinos, produced by π-μ decays and allowed to interact subsequently with protons, caused the appearance of numerous muons but no observed electrons. This provided an answer to the problem of the forbiddenness of the decay mode $\mu^+ \rightarrow e^+ + \gamma$.

Of particular interest are other characteristics in which the muon displays a high degree of similarity to the electron. The following are of interest here:

1) Muon charge found to be 1.00002 ± 0.00004[1,2,21] times that of the electron.
2) Muon-electron similarity in weak interactions.

A value for the μ^- + p capture rate has been calculated[24] using the observed rate of neutron decay (an electron-producing process) to evaluate the required constants. This calculated rate is in good agreement with the capture rates measured with both bubble chambers[25,26] and counters[27,28].

3) Muon-electron similarity in electromagnetic interactions.

   a) Measured value of $g_\mu = 2(1.001162 \pm 0.00005)$[1,2,29]. This measured value gives a comparison ratio $g_\mu/g_e = 1.000001 \pm 0.000005$. Thus the muon is a spin $\frac{1}{2}$ particle, obeying Fermi-Dirac statistics as does the electron.

   b) Comparison of e-p and μ-p scattering. Extensive work on electron scattering by protons as well as by various nuclei has been carried out by R. Hofstadter[30], D. G. Ravenshall[31], L. N. Hand et al.,[32] and J. R. Dunning, Jr. et al.,[33] among others. Work with μ-p scattering is more recent, having been carried out notably by H. F. Davis et al.,[34] and R. Cool et al.[35] The latter work presents a detailed comparison between e-p and μ-p scattering, with the conclusion that there is no observable difference throughout momentum transfers ranging from 450-1100 Mev/c.

It has seemed on the basis of these results that the muon may be described by essentially the same theoretical formulations as have been developed for the electron. Results of scattering experiments of muons upon atomic nuclei, however, have not always been in agreement with the above results, particularly when compared with the e-p, μ-p similarity cited above. Discrepancies were first noted in the behavior of muons obtained from cosmic rays, which, of course, were the original sources for these particles. For higher energies, where the momentum exceeds 600 Mev/c, excessive scattering contributions--particularly at higher angles--have been reported by a number of cosmic-ray researchers, beginning with the first systematic search for this effect by Amaldi and Fidecaro in 1950[3]. Outstanding among the experiments since 1950 is the work of Whittemore and Shutt[4] in 1952 with 0.3-3 Bev/c muons, McDiarmid[5] in 1954 with 0.2-4 Bev/c muons, Lloyd and Wolfendale[6] in 1955 with 0.6-10 Bev/c muons, and Lloyd, Rossle and Wolfendale[7] in 1957 with 5-.50 Bev/c muons. Without exception their results show high-angle scattering in excess of that predicted by theories based on a nuclear-charge distribution of finite extent. The fact that the muon-scattering results between 1950-58 seemed to agree more nearly with the Moliere[10] "point-charge nucleus" theory than with the "finite-nucleus" theories advanced during that time was not taken to imply that the nucleus was acting in fact as a point charge, but rather as suggesting either a deficiency

in the theory or that the muon has some mode of interaction not covered by the "finite-nucleus" theories. An increasing anomaly for greater momenta was not found to occur in an experiment by Lloyd and Wolfendale[7]. Also a short-range interaction with nucleons was not indicated, since the amount of large-angle scattering in light elements is much less than would be expected from the cross section per nucleon obtained from muon-scattering results for lead[2].

"Finite-nucleus" theories with which the experimental results have been compared include primarily those of Olbert[8], of Cooper and Rainwater[9], and of Drell and Schwartz[17]. Olbert's theory is a modified version of the Moliere[10] theory, where the finite extent of the nucleus is accounted for by forcing the single-scattering law to be $\equiv 0$ for scattering angles greater than a cutoff angle φ_c. The Olbert theory provides an underestimation of large-angle scattering whereas the Moliere theory provides, of course, an overestimation of scattering in this region. The Cooper-Rainwater theory using the same general approach represents a more accurate treatment of the effects on the scattering to all angles due to a nucleus of finite extent. The Drell-Schwartz theory, however, approaches the problem by developing a sum rule which yields the scattering distribution resulting from both inelastic and elastic scattering. This sum rule is particularly useful since it does not require knowledge of the complicated final-state wave functions associated with the final excited states in which the scattering nucleus may be found. A knowledge of the

ground-state wave function is sufficient.

The experiments conducted previous to 1959 were plagued by several serious limitations, typical of cosmic-ray work during that period, which included:

1) poor statistics at large angles, caused by the slow data-gathering capability of cloud chambers
2) measurement errors in determining particle momentum and/or deflection angles
3) contamination of results by events involving particles other than muons, pions being the major concern.

An experiment by Fukui, Kitamura, and Watase[11] in 1959 with 1 Bev/c muons gave results consistent with the Cooper-Rainwater theory. This experiment though showing a degree of improvement in some of the above areas was shown to be inconclusive by Lloyd and Wolfendale[12] in 1960, primarily because of uncertainties in momentum determination and in particle identification.

To fill the need for a conclusive experiment on this subject Masek, Heggie, Kim and Williams[13] performed an experiment with the Bevatron at Berkeley using 2 Bev/c muons obtained from decay of the pion beam. Scattering was done both in lead with momentum transfers up to 265 Mev/c, and in carbon with momentum transfers up to 400 Mev/c. A total muon flux of 2.5×10^7 particles was obtained in the experiment. Momentum spread was not more than $\pm$ 3.5

percent, and the fractional contamination by pions was of the order of 4.9×10^{-6}. The scattering in lead was compared with the predictions of the Cooper-Rainwater theory and excellent agreement was found. The scattering in carbon was compared with the predictions of the Drell-Schwartz theory and again excellent agreement was found. Thus the question appeared settled, for machine-made muons at least, that no anomalous scattering exists.

B. Motivation for the present experiment

There remained a need, however, for a cosmic-ray experiment to demonstrate conclusively whether the anomalous scattering observed by so many cosmic-ray workers was indeed due solely to the inaccuracies encountered in the three categories listed above. Such an experiment should provide significant improvements in each of these three difficult areas. The present experiment was designed to fill this need by applying the capabilities of a number of recently-developed research tools to a cosmic-ray scattering investigation.

C. Approach of this experiment

The approach of this experiment was first of all to utilize a spark chamber to replace the cloud chambers used almost exclusively for cosmic-ray work in the past. This allowed a greater rate of data collection and greater accuracy of angle measurement. Plastic scintillation counters were used in place of the trays of Geiger-Mueller tubes common to cosmic-ray work. These provided

a significant improvement in the momentum determination and made possible the type of particle identification technique developed for this experiment. This technique provided for, among other things, direct observation and removal from the data of pion events seen. Also computer-programmed scattering-angle calculations developed in this experiment replaced the hand deflection-angle measurement methods previously employed. Thus significant improvements have resulted in areas (2) and (3) above. Some improvements were made in (1), with further improvement available in this area upon continued pursuit of the method of this experiment.

II. EXPERIMENTAL APPARATUS

A. General description

The apparatus for this experiment consisted of an aluminum-plate spark chamber located in a cosmic-ray counter telescope, which was composed of three scintillation counters: an aperture counter, a stopping counter, and an anticoincidence counter. The three-channel coincidence system provided a mode of event selection which required double coincidence between the first two counters and anticoincidence with the third. The output of the coincidence circuit then triggered the spark chamber.

The visible track formed in the spark chamber was recorded on 35mm film by a motor-driven camera which automatically advanced to the next frame after each spark-chamber event. In addition, the pulse from the stopping counter was displayed on a fast oscilloscope and photographed by a second automatic camera, synchronized to the first. This provided a simultaneous photograph of the stopping pulse corresponding to each chamber event selected by the coincidence system.

In view of the low rate of data collection inherent in this experiment, the apparatus was designed to be fully automatic in its operation. Use of 100-foot rolls of film in each camera allowed eight-hour periods of operation before film changes were required.

The data was analyzed with the help of the following basic items of equipment:

1) A Gilliland motorized film-projection machine on which the oscilloscope film was scanned for event selection,
2) A Hydel digitized film scanner tied to an IBM 526 summary card punch by which the coordinates of each spark in the chamber photograph of a given event were digitized and punched on IBM cards for processing,
3) The Michigan State University Control Data Corporation--3600 computer by which all calculations upon the raw data were performed.

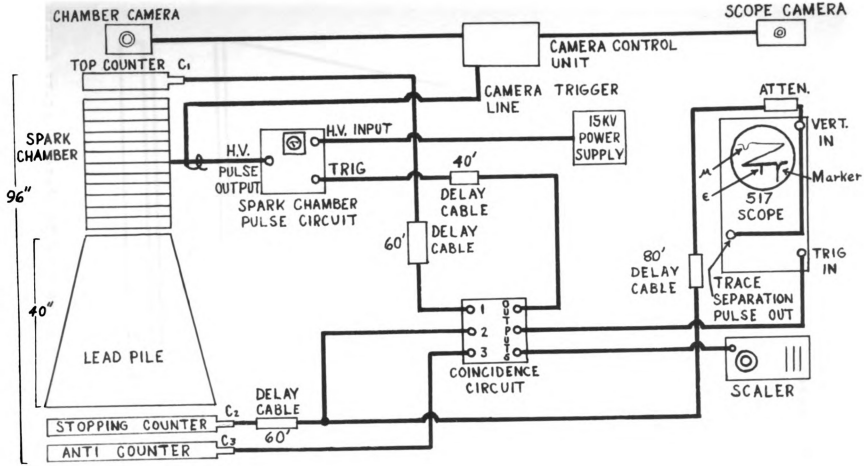

FIGURE II-1.

BLOCK DIAGRAM OF EXPERIMENTAL ARRANGEMENT

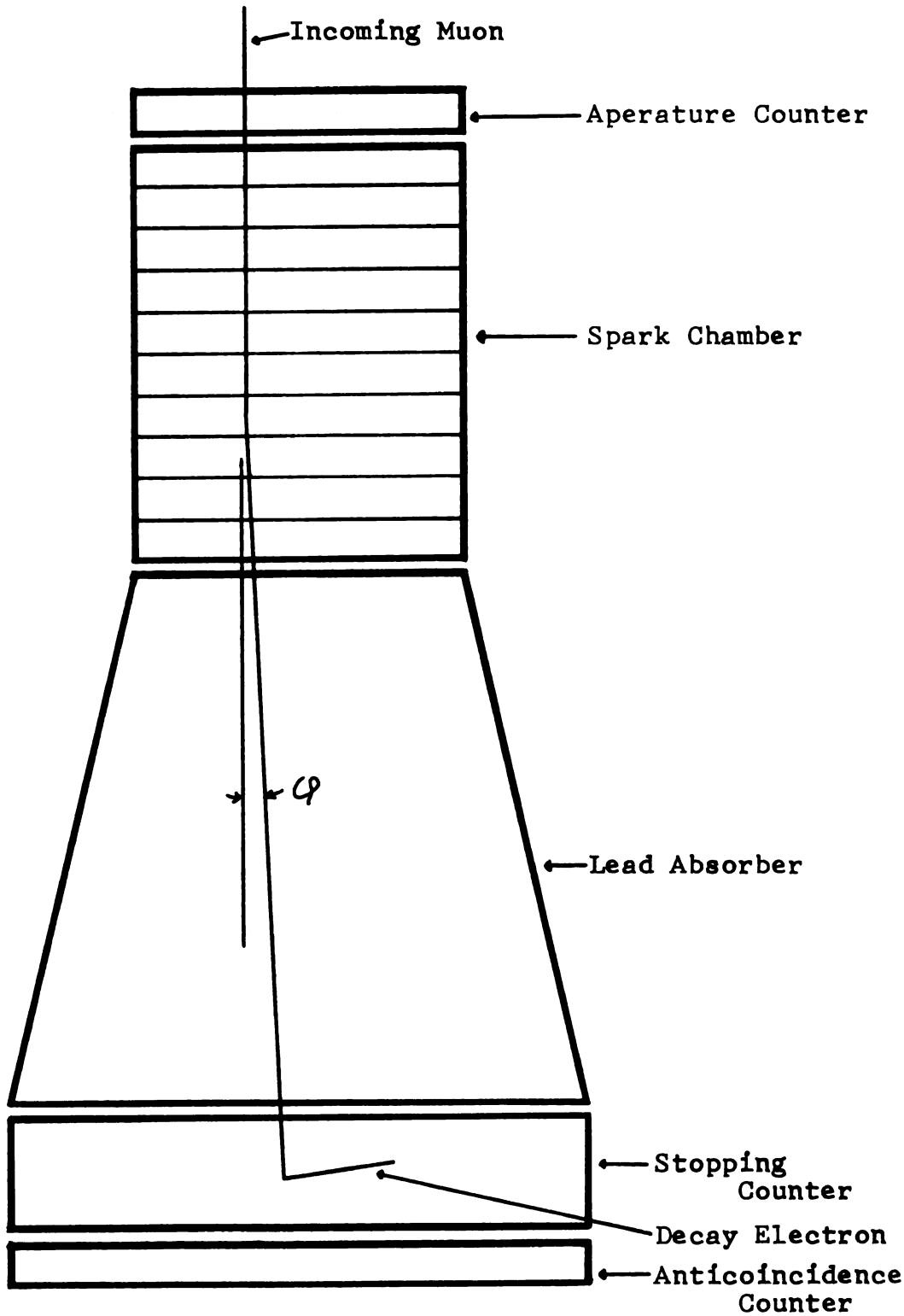

Figure II-1a. Detail of scattering apparatus.

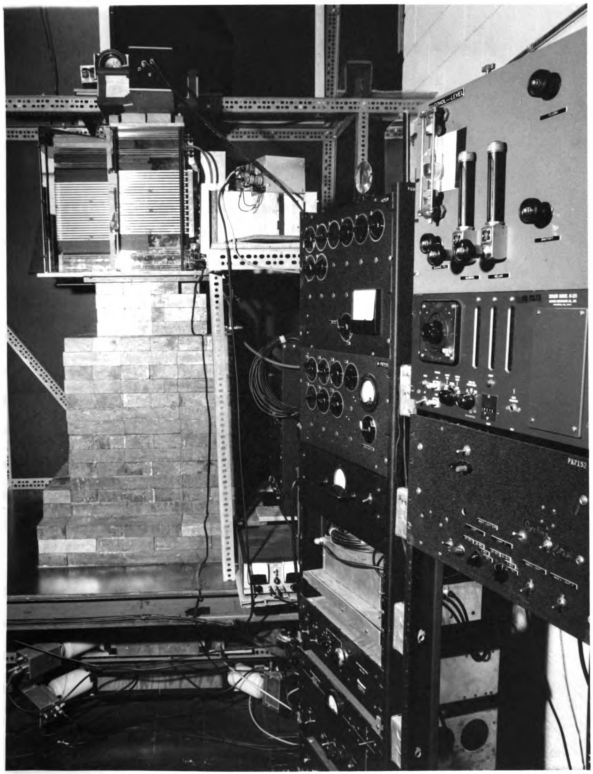

Figure II-2. Overall view of experimental apparatus.

B. Spark chamber system

The spark chamber used in the present experiment was divided into three sections: (1) the main chamber, in which the usable events took place, and (2) an upper and (3) lower thin-plate chamber used for more accurate determination of the incoming and outgoing directions of the particle. The main chamber section is a laminated assembly of $10\frac{1}{2}$-inch by $10\frac{1}{2}$-inch aluminum plates 5/32-inch thick, separated by clear plexiglas spacing strips 1/4-inch thick placed around the perimeter of each pair of plates, to form a series of closed cells. Twenty-two such aluminum plates and plexiglas spacers comprise the main chamber. The aluminum plates themselves were used as the scattering material. The upper and lower chambers are constructed of 3/64-inch aluminum plates assembled into milled slots in the sides of a closed plexiglas shell, with the gap spacing being identical to that of the main chamber.

To provide a helium atmosphere within the chamber for formation of the ion trail, a series of small holes were drilled through the right face of the chamber (one through the center of each cell spacer). Into each of these holes was cemented the free end of a short length of soft plastic surgical tubing branching from a manifold block mounted on the side of the chamber. To complete the flow system, a similar manifold was used to collect the exhaust gas into a single tube, for flow control purposes, which is vented to the atmosphere. Tanks of ordinary

welder's helium were used as a gas supply. The helium passed first through a liquid-air cold trap and on to the flow control panel. The cold trap was necessary because considerable water and traces of oil were found in the helium. Removal of these impurities improved the chamber performance in terms of the gap firing efficiency and spark uniformity and also allowed chamber operation over a longer period before disassembly and cleaning of the plates in caustic potassium hydroxide solution became necessary.

The flow control panel consisted of a branching valve arrangement with a separate flow gauge and metering valve in each branch. Helium passing through the main branch proceeded directly to the chamber distribution manifold. A flow rate of 215 liters per minute was maintained in this branch for best operation. Helium passing through the remaining branch was made to bubble through a glass tube containing 2.5 inches of ethyl alcohol. The helium flow rate through this branch was kept at the low rate of one bubble per second from an orifice 1/32-inch in diameter. This minute quantity of alcohol dissolved in the helium and served as both a quenching agent for the ionization process and, to some extent, as a wave-length shifter to bring the wave-length of the light emitted from the spark discharge nearer the blue region where the film sensitivity is higher.

To supply the high-voltage pulse necessary to fire the chamber, a thyratron pulsing unit was used which was

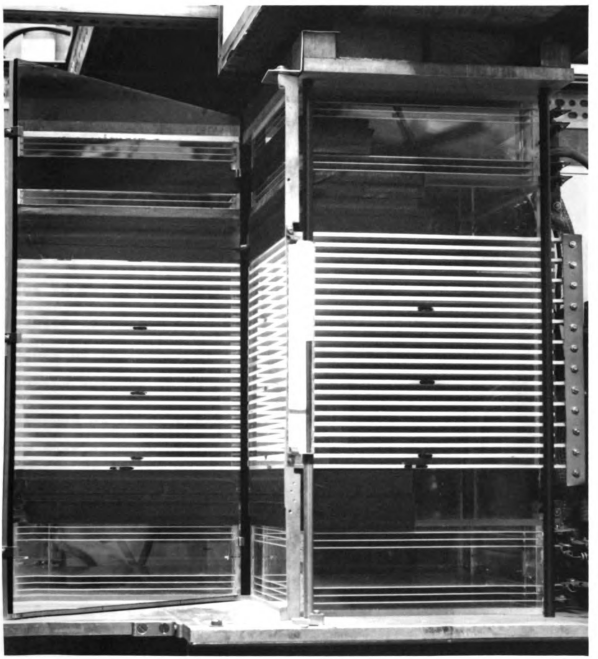

Figure II-3. Close-up of spark chamber.

C. Counter telescope system

A vertical counter telescope system subtending a solid angle of 0.15 steradian was constructed as shown in Fig. II-1,2. This solid angle allowed reception of approximately 5 percent of the available cosmic-ray intensity. Plastic scintillation counters viewed by 6810A photomultiplier tubes were constructed for each position in the telescope system. The aperture counter at the top consisted of a circular block of scintillating plastic 9 inches in diameter by 3 inches thick with a flat region cut on one side to which the photo tube was attached. The stopping counter consisted of a block of scintillating plastic 24 inches by 24 inches by 7 inches with each of the four corners cut off at 45 degrees so that phototubes may be attached at those positions. The corners are cut in such a way that as many as four phototubes could be attached at each corner.

For reasons of cost only two phototubes were actually installed, giving a total of eight in all for this counter. This provided a ratio of photo-cathode area to total counter surface area of 0.96 percent, which is considerably smaller than recommended by the experience of others.

The "anti" counter consisted of another block of scintillating plastic 24 inches by 24 inches by 2 inches with one phototube on each corner mounted as in the above case. In this counter the ratio of photo-cathode area to surface area was 0.65 percent, notably smaller than the

value for the stopping counter. Indeed it was observed that the anti counter was less efficient than was the stopping counter as it was not able to produce the expected reduction in count rate compared to the doubles rate (i.e., integral count rate). Fortunately this deficiency only caused film to be wasted, since the burden of the momentum determination as well as particle identification rests upon the film record of the stopping pulse with its required decay signature. For this reason the cathode-area fraction was allowed to remain at the above value throughout the experiment.

The power for the phototubes was derived from two Hamner N-4035 power supplies. The aperture counter and the anti counter were operated from one of these supplies and the eight tubes on the stopping counter were operated from the second supply. In addition the voltage on each tube in the entire system was adjustable within +0 percent, -20 percent of the power supply output in 16 steps for the purpose of matching the sensitivity of all the phototubes in each counter by equalizing pulse height or count rate.

The signals from the three counters were fed to the appropriate coincidence or anti coincidence input in the tunnel diode coincidence unit which was also built during the course of the present research work. This unit used gallium arsenide tunnel diodes throughout as monostable multivibrators, each triggered by the previous stage, and the first triggered by its respective scintillation counter signal. The primary features of this design were its

narrow coincidence resolution time (2 to 3 nanoseconds), short dead time, and reliability for input signals ranging in amplitude from 50 millivolts to 50 volts approximately. This latter feature is particularly important in working with relatively large scintillation counters. A detailed circuit description and schematic of this unit is given in Appendix B. A delay cable 60 feet long had to be inserted in each coincidence channel to assure the condition that the anti signal, whenever present, arrived at the coincidence circuit before the coincidence signals from the aperture counter and stopping counter. The tunnel diode coincidence unit has an output circuit consisting of a transistor amplification stage and individual emitter follower output stages to supply isolated coincidence output signals to the spark chamber, the 517A oscilloscope and a count rate monitoring scaler.

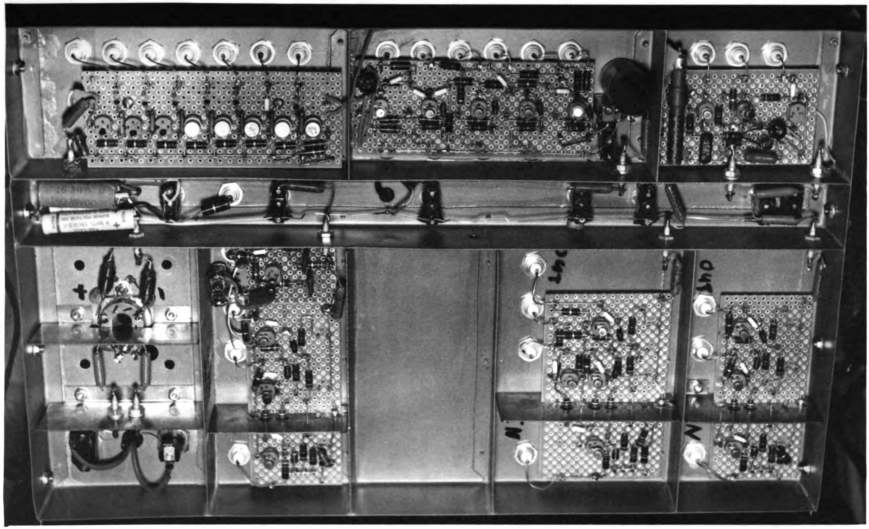

Figure II-4. Close-up of coincidence circuit.

D. Automatic photographic system

The photographic aspects of this experiment required two cameras. One photographed the particle tracks in the spark chamber; this was done three-dimensionally by means of a mirror to provide a stereo view of the chamber. The remaining camera photographed the traces appearing on the screen of the 517A oscilloscope. These traces displayed the pulse signature produced in the stopping counter by the particle making the track in the chamber.

1. The optical arrangement

The optical schematic of the chamber camera arrangement is shown in Figure D-1. A large chamber-to-camera distance was chosen in order to assure an adequate depth of field and to compensate for the fact that the spark chamber plates were parallel. These requirements were made more demanding by the use of a 45 degree mirror to project a 90 degree steroscopic view of the chamber onto the film. As can be seen from the figure, a useful depth of field twice the chamber depth is required for this type of view since the two images are not located at equal distances from the lens. This results in a minimum f number of 5.6 at a distance of 20 feet. In the room which housed the experiment, space considerations required the use of an additional plane mirror to fold the viewing beam back upon itself, allowing the chamber camera to be mounted directly above the chamber.

As is also apparent from the figure, the image of

the stereo view will be smaller than that of the direct view by the ratio of their distances. Correction for this effect as well as that of parallax was made in the analysis procedure. A separate section of the analysis program performed this task.

2. The operational system

The camera system was designed for fully automatic operation. This was accomplished by using camera units built to expose 1200 frames per 100 foot roll of 35 mm film and by the construction of a camera control unit capable of automatic sequencing and control of all film advance functions. The following basic functions are performed by the camera control unit (in order of occurrence):

a. Blank the grigger circuit of spark chamber. Blanking is accomplished by relay interruption of the signal line to the grid of each 5C22 thyratron.

b. Start film drive motor in each camera. The sprocket motor in each camera operates on 24 volts AC.

c. Advance frame number in each camera. Solenoid-activated six-digit counters are used for the purpose of registering on the film the frame number of each event.

d. Apply braking to film drive motors. The discharge of 250 mfd at 30 volts into the motor coils is used to provide the DC braking necessary to obtain positive frame position control.

e. Illuminate, for a set duration, the

chamber itself and the frame numbers thus recording these on the film prior to the next event.

f. Unblank the trigger circuit of spark chamber to accept the next event.

These operations were performed in a properly timed sequence by the use of appropriate relays controlled by the R-C timing circuits, as described in greater detail in Appendix D. The complete film advance sequency requires approximately 0.85 seconds. With an event rate of 2.5-3 per minute the dead time due to this operation was of the order of 5 percent.

E. Stopping-pulse display system

A positive particle identification was sought for this experiment in an attempt to avoid some of the problems inherent in the earlier work with cosmic-ray muons as mentioned previously. Photographic recording of the pulses from the stopping counter provided, in principle, the means necessary to make positive particle identification. The muons may be distinguished from stable protons or electrons and from pions by the number of pulses observed and from other singly-decaying particles on a statistical basis by a check of the characteristic lifetime of the events accepted. Thus a satisfactory mechanism of selection is available if the pulses registered in the stopping counter are suitably displayed for photography. A specialized means for doing this has been developed in the present experiment. Of the multiply-decaying particles the most significant constituent in the cosmic-rays is, of course, the pion. It was the large time scale difference between the two steps in the decay of a pion via a muon to an electron that made the development of a satisfactory display method such a challenge.

An attempt was made to record stopping π^+ mesons as well as μ^+'s. This was done by a complex scan pattern for the 517A oscilloscope which worked by following a single fast sweep (6 pion lifetimes long) with a displaced slow sweep (5 muon lifetimes long).

A Z-shaped trace was decided upon, of which the top trace was set at 25 nsec/cm for a total sweeptime of 140 nsec to resolve π-μ-e decays occurring in the stopping counter. Next the sweep rate was changed automatically to 2 μsec/cm and the beam retraced ready for the second trace at this slower rate to display μ-e decay pulses. The change of sweep rate was effected by connecting a new timing capacitor corresponding to the slower rate in parallel with the one corresponding to the initial fast sweep. This connection was made by a triggered thyratron just as the first trace was completed. The thyratron was extinguished again upon completion of the slow trace ready for the next event. Proper retrace between the fast and slow traces was an automatic result of the above procedure since the sweep system in the 517A consisted simply of a timing capacitor whose voltage rose linearly with time, and was applied to the deflection plates via a DC amplifier. Thus the voltage accumulated upon the first timing capacitor was immediately reduced, upon connection of the new uncharged timing capacitor, to 1 per cent (by the ratio of sweep rates) of its value at the end of the first trace. The sole reason the beam retraced between times was that the second capacitor was initially uncharged and was larger by a factor of 100 than the first. Thus the beam should return essentially to its starting point on the screen. Retrace instead to

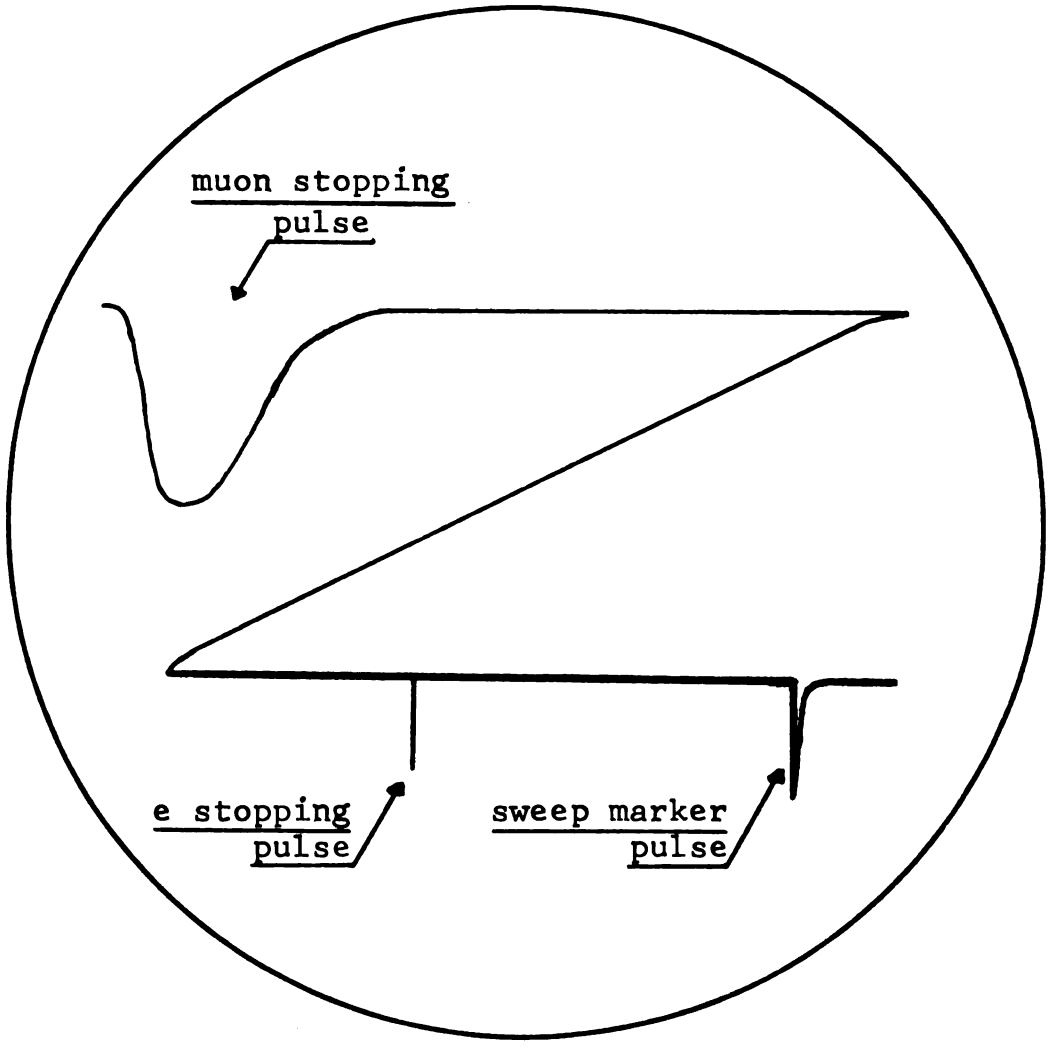

Figure II-5. Characteristic oscilloscope trace, showing μ-e decay signature.

approximately 10 per cent of the full scale value was the practical result, due to stray capacitance in the sweep amplifier and deflection plate leads. The retrace required approximately 0.80 μsec, thus placing the beginning of the second trace at about 1 μsec after the passage of the particle through the apparatus.

Two additional modifications were added for analysis convenience. A negative step pulse was generated and applied to the vertical input along with the regular signal to displace the second trace to a position below the initial fast trace. The particular portion of the trace (three in all, including the retrace) to which each observed pulse belongs could in principle be determined from the apparent pulse width, since all pulses are essentially the same width in reality. It is, however, much more satisfactory to have the traces separated into a Z-pattern as mentioned above. The other feature was the addition of a negative marker pulse introduced in the vertical input at a time of 10 μsec after the top trace. This was included for purposes of sweep calibration monitoring. The position and height of this pulse at the end of the second trace in every photograph gave immediate indication of any trouble developing in either the sweep timing or vertical amplifier sections of the oscilloscope.

The above predetermined sweep sequence was

iniated by a single external trigger pulse from the coincidence circuit. The delay encountered in initiating conduction in the 5C22 thyratrons that fire the spark chamber was $\approx$ 300 nsec so that the first fast trace of the oscilloscope was completed before large amounts of RF from the chamber discharge could appear in the scope picture. It is, of course, in the top trace where problems of pulse identification and resolution are most difficult. Slight timing adjustment to assure this desirable condition was made by adding 20 feet of cable to the chamber trigger line.

The scope display system had a stopping pulse width of $\approx$ 40 nsec width at half maximum. This is somewhat more than desired as only pions persisting for more than two lifetimes can be expected to display the μ pulse in a π-μ-e decay. Efforts to materially improve this condition have thus far been unsuccessful, but a major effort at such improvement is scheduled as a primary task preceeding further research to be done with the apparatus.

F. Analysis system

The analysis system consisted primarily of two film scanning machines, one equipped with an IBM 526 key punch, which were used to prepare the data for use on the Michigan State University computer (a C.D.C. 3600) on which the computations were carried out.

The first of the two scanners is a Gilliland vertical projection model modified for continuous film traversal by means of a foot-operated speed control. This facilitated the scanning of the oscilloscope film for suitable events. The corresponding chamber film photographs of events judged as having been muons that came to rest in the stopping counter were measured on the second scanning machine, a Hydel unit. This unit equipped with a Datex digital encoder system and an IBM 526 summary key punch was used to provide on IBM cards data describing the x, y coordinates on the film of each spark in the particle track. These coordinate positions were punched on the cards as five-digit numbers which were linearly related to position on the film. The scale is arbitrary and must be converted to position in real space; this is done in the geometry subroutine of the program.

All computation related to track behavior in each event was carried out in the SCOPE program especially written for this experiment. This program performs the following major tasks for each event:

1) Sorting and identification of each event

2) Geometry conversion to real-space coordinates

3) Storage of all converted real-space data on magnetic tape

4) Elimination of events having an insufficient number of data points present

5) Calculation of least-square line fits to spark positions for incoming and outgoing directions in both the direct and stereo views

6) Calculation of the total deflection angle for each event from the line fits in the direct and stereo views

7) Partitioning of the data with respect to how many events in a given run display a track deflection angle in each 0.25 degree increment from 0 degrees to 7 degrees.

The partitioning supplies the necessary information from which the differential scattering distribution may immediately be plotted. This same partitioning operation is performed upon the calculated values of azimuth angle for each of the track segments as well.

A more detailed description is presented in Section III-B and a program listing is given in Appendix F.

III. ANALYSIS PROCEDURE

A. Analysis of oscilloscope photographs

1. Types of events identified

The types of events identified by analysis of the oscilloscope photographs made of the signal emitted by the stopping counter may be categorized according to the number of individual stopping pulses observed for each event. An interpretation of each such category follows:

a) One-pulse event: Such an event would have been caused by a particle which either was not stopped within the counter or did not undergo a subsequent decay within the observation time of the oscilloscope (which includes stable particles, of course). In either case all events of this type were rejected as not representing muon events. Since the observation time of the oscilloscope was 11 μseconds, i.e., five muon lifetimes, less than 0.7 percent of the real muon events were lost by rejecting such one-pulse events.

b) Two-pulse event: Such an event was taken to be due to a muon which was stopped in the counter and subsequently decayed into an electron and two neutrinos. The electron, being given an initial kinetic energy as a result of the decay process, produces another stopping pulse in the scope trace, identifying the time of the decay. All such events were marked for subsequent track measurement. As described in section (2) below, a random sample from events in this category yielded a

measured mean lifetime in close agreement with the accepted value for muons.

A false two-pulse event could have been caused by a single pulse event together with a second pulse caused by the appearance in the counter of another cosmic ray particle within the oscilloscope observation time. As is shown in the next section, the fractional occurrence rate for this is of the order of 3×10^{-4} for muons. Thus out of the 2,266 events used in the final results of the experiment only of the order of 0.7 such spurious muon events would be expected. As a practical matter this must be increased by a factor of 2 due to the fact that in most of the oscilloscope photographs there is a second trace triggered by persistent transients in the apparatus. In the upper and middle portions of the trace the real and spurious traces are easily distinguishable by the presence of the initial stopping pulse and the residual radio-frequency pickup in their respective portions of the real trace. In the lower slow trace, however, these two traces are indistinguishable and thus provide a duplicate time interval in which a pulse from the cosmic ray background could appear. It is asserted that the presence of this second trace in the oscilloscope photographs does not affect the reliability of identifying two-pulse μ-e events. This is because the occurrence of any false μ-e event having its second pulse in the lower trace of the spurious sweep would be governed by the above mentioned

expectation of 0.7 such occasions out of 2,266 events. Even this total of 1.4 possible false μ-e events causes a negligible effect on the resulting scattering distribution of the experiment. The μ-e lifetime plot shown in part 2., of this section was made assuming all two-pulse events to have occurred within the original trace. No inconsistency with this assumption is apparent in the lifetime results.

The contribution of spurious two-pulse events in which one of the particles was a proton is expected only in the ratio that protons are present with muons in the cosmic rays. This ratio of protons to muons in the cosmic rays above 0.7 Bev/c is less than 1 percent according to Rossi[16]. Thus only $(10^{-2})(3 \times 10^{-4})(2,266) = 6.8 \times 10^{-3}$ events out of 2,266 events are expected to be of this type. Contamination of the data due to protons may thus also be neglected.

c) Three pulse event: Such an event was taken to be one of the following: (1) a π-μ-e event, (2) an event in which another charged particle entered the counter within the observation time of the scope trace in addition to a bona fide μ-e event, or (3) an event in which two additional charged particles entered the stopping counter following an initial single pulse event. As can be seen from the several possibilities mentioned, the rejection of all observed three-pulse events constitutes a more than sufficient means by which to eliminate from the scattering data such pion events as produced a π-μ-e decay in the stopping counter.

Events involving pions which traverse the chamber but decay into muons in flight before reaching the stopping counter cannot be eliminated from the data by the above selection method if the muon formed in flight subsequently decays in the normal manner in the counter. However, because of the relatively short time of flight at relativistic velocities for the distance of 4.5 feet from spark chamber to stopping counter, together with the relativistic lifetime dilatation existing through the greater portion of this distance, the number of pion events not identified because of in-flight decay was considered negligible.

The relative number of three-pulse events caused by mechanism (2) and (3) may be estimated in the following manner. First of all the total muon intensity must be calculated for the apparatus of the experiment. The integral muon intensity, I_v, at sea level due to the hard component of the cosmic rays is given as 0.008/cm^2-sterad-sec by Rossi[16]. The total count rate may be obtained from this by integrating over the area and solid angle of the counter.

The count rate $$\frac{dN}{dt} = A \int_0^{2\pi} \int_0^{\theta_{max}} (I_v \cos^2\theta) \sin\theta \, d\theta \, d\phi$$

Taking I_v = 0.008/cm^2-sterad-sec, A = 2600 cm^2 for the stopping counter, and $\theta_{max.}$ = 70° from vertical due to cutoff by depression of basement laboratory below surrounding terrain, gives

$$\frac{dN}{dt} = 2\pi I_v \left[-\frac{1}{3}\cos^3\theta\right]_0^{70^\circ} A = 41.8 \text{ /sec}$$

This is only a rough estimate since no account was taken of the shielding effect of the lead pile above the stopping counter.

A more careful estimation is next obtained by considering the total solid angle in three zones: $0 \leq \theta \leq 9^{\circ}$; $9^{\circ} < \theta \leq 27^{\circ}$; and $27^{\circ} < \theta \leq 70^{\circ}$. The value of 9° was chosen because it represents the half angle of the cone subtended at the stopping counter by the area of the top of the lead pile. The next interval of 18° was chosen to be equal to the full angle of the central cone for symmetry purposes. For each zone a different value of I_v was taken according to the approximate amount of effective absorbing material present in each particular zone.

$$dN/dt = (\pi/3)\{[2(.0045)(930) + (.0045)(2600-930) + (.0062)(2600-930)][1-(.987)^3] + [2(.0053)(930)+(.0053)(2600-930)+(.0062)\cdot(2600-930)][(.987)^3-(.888)^3] + [2(.0062)\cdot(930)+(.0053)(2600-930)+(.0073)(2600-930)]\cdot[(.888)^3-(.342)^3]\}$$

This yields dN/dt = 31.5 incident muons/sec. From this value of dN/dt the relative probability for appearance of an additional pulse on the oscilloscope within the 10 μsec observation time may be obtained. This relative probability is equal to the ratio of the observation time to the average time between background muons. Thus

$$\text{Prob.} = T_{obs}/T_{background} = T_{obs}(dN/dt) = (10 \times 10^{-6}\text{sec})\cdot(31.5/\text{sec})$$

$$= 3.15 \times 10^{-4}$$

Thus for three-pulse events having another muon in addition to a μ-e decay the above calculated probability gives an expectation of five events out of 8,000. These false three-pulse events will appear with one pulse in the top trace and the remaining two somewhere in the middle or lower traces. There are other higher order possibilities by which three-pulse events of this type may occur. These include μ-e, p; μ, μ, μ; μ, μ, p. The relative probabilities for these mechanisms are smaller than the above by factors of 0.01, 3.15×10^{-4}, and 3.15×10^{-6} respectively.

Since the sweep duration of the fast upper trace is nearly six pion lifetimes (mean pion lifetime taken as 25.5×10^{-8} sec[21]), more than 99 percent of all real π-μ-e events should appear with two pulses in the top trace. In contrast, however, the probability for a second muon pulse to appear in the top trace is

$$\text{Prob.} = 140 \times 10^{-9} \text{ sec } (31.5/\text{sec}) = 4.41 \times 10^{-6}.$$

This gives an expectation of 0.035 occurrences of an additional pulse in the top trace out of 8,000 events. The appearance of a μ-e decay in the first trace with a subsequent additional muon pulse appearing in the slow bottom trace is the only remaining first order mechanism for false three-pulse events having two pulses in the top trace. The probability of having a μ-e decay within 140 mμ-seconds is

$$\frac{N_o e^{-\left[\frac{(50 \times 10^{-9})}{(2.2 \times 10^{-6})}\right]} - N_o e^{-\left[\frac{(140 \times 10^{-9})}{(2.2 \times 10^{-6})}\right]}}{N_o}$$

$$= e^{-2.27 \times 10^{-3}} - e^{-6.36 \times 10^{-2}} = 0.059$$

This probability must further be multiplied by 3.15×10^{-4}, the probability obtained above for having an additional muon within the 10 μ-sec observation time, yielding 1.86×10^{-5}. This gives an expectation of 0.15 occurrences out of 8,000 for three-pulse events having a μ-e in the top trace followed by an additional pulse in the lower trace. There is a total expectation in 8,000 events of 0.035 + 0.15 = 0.185 false occurrences of three-pulse events having two pulses in the top trace, forming an apparent π-μ-e event. This is still, of course, a very small expectation, implying that if any decays are seen in the top trace with a third pulse later, they should be considered bona fide π-μ-e events. Of the 6 three-pulse events observed, none displayed two pulses in the top trace.

The fact that no three-pulse events qualifying as π-μ-e events were observed must be compared with the expected pion flux at sea level. This flux is, however, not very well known as yet. The best estimate which seems to be available at present is due to B. Peters and Y. Pal of the Niels Bohr Institute in Copenhagen[37]. They estimate the integral pion flux to be of the order of 10 percent as great

as that of protons in the momentum region of this experiment. The proton to muon ratio in turn is less than one percent according to Rossi[16]. Thus out of 8,000 muon events, something less than eight π-μ-e events should be expected.

Not all pion decay events occurring in the stopping counter can be observed in the oscilloscope trace due to the width of the stopping pulse. The minimum resolving time is 50 μsec or 2 pion lifetimes. Assuming a pion lifetime of 25.5 μsec[21] only the fraction 0.135 remain of the original number present. Thus out of the eight pions suggested above, at most one observed case should be expected. Indeed the figure of eight expected pions out of 8,000 muon events may well be excessive due to the fact that in looking for pion decays, one is concerned with the differential rather than the integral flux. The relative differential pion flux in the region of 1.6 Bev/c may well be notably smaller than the relative integral flux as there is indication from cosmic-ray results[37] that the differential pion flux actually decreases with momentum below several Bev/c.

Since out of 8,000 events no π-μ-e events were observed in the decay time range of 50-140 μsec, an upper expected limit to the observed pion incidence for this experiment of 1 in 8,000 may be set. Since only 0.135 of the total incident pions have their decay observable in the time range of 50-140 μsec, this corresponds to an observed total upper limit of 7 pions in 8,000 events. This value is consistent with the value of 8 pions in 8,000 events

calculated above. The value of 7 in 8,000 corresponds to a maximum expectation of 2 pions in the 2,266 events used in the final results of the experiment. It must further be borne in mind that both the calculated value of 8 in 8,000 and the observed value of 7 in 8,000 are upper limits. As indicated above there is reason to believe that both the calculated and observed figures for the number of pions included in the data of the experiment are high.

2. Lifetime study

As a check on the acceptance criteria for events chosen for measurement as muon events having the proper momentum, the muon lifetime was calculated from a sample of 1,280 events chosen at random from the data of this experiment. These were selected by choosing some 50 rolls of oscilloscope film distributed uniformly throughout the total film data and measuring the delay time to the second pulse of each two-pulse event in that film roll. Thus the sample was also taken without regard to whether that event was subsequently measured for scattering or rejected due to poor track quality. As it turned out 676 events of the 1,280 had acceptable tracks for measurement, 604 events did not. Fig. III-1 shows a plot of $N_{(t)}/N_o$ versus distance along the oscilloscope trace measured in centimeters on the scanning table. From this distance in centimeters the corresponding time t may be determined from the geometry of the system. Taking d as the distance of pulse separation on the scanning table, the conversion to time is as follows:

$$t = \left[\frac{5.3 \text{ cm on scope}}{39.8 \text{ cm on scanner}}\right] \quad \frac{(9.3\ \mu\text{sec})}{(4\ \text{cm})}$$

$$= [0.310 \text{ usec/cm}]\ d$$

The solid line of Fig. III-1 is the theoretical decay curve for muons. It was obtained from the decay law

$$N(t) = N_o e^{-\lambda t} = N_o e^{-t/\tau}$$

Differentiating gives

$$\frac{-t}{\tau} = \ln \frac{(N(t))}{(N_o)} = \ln 10 \log \frac{N(t)}{N_o}$$

$$\text{Or} \quad \ln 10 \log \frac{(N_o)}{(N(t))} = t/\tau = \frac{(0.301\ \mu\text{sec/cm})d}{2.20\ \mu\text{sec}}$$

$$2.302 \log (N_o/N_{(t)}) = (1.403/\text{cm})d$$

Choosing d = 20 cm for convenience, a ratio of $N_o/N_{(t)}$ = 16.60 satisfies this equation. The solid line in Fig. III-1 is drawn with this slope. Slight departure from a straight line at each extreme of the plot is due to nonlinearities in the oscilloscope sweep rate at the extremes of the trace. This came about in connection with the response time of the circuit causing the automatic change in sweep speed after the first fast trace. A best fit to the data in Fig. III-1 yields a muon mean life 0.6 percent less than the accepted value of 2.20 μsec[21] used above in forming the theoretical curve. This is well within the estimated 1 percent sweep calibration tolerance that it was found possible to maintain over the long term duration of the experiment. In view of the good agreement of the measured mean life with the accepted value for muons, the particle selection procedure used in this experiment is established as a satisfactory criterion for muon selection.

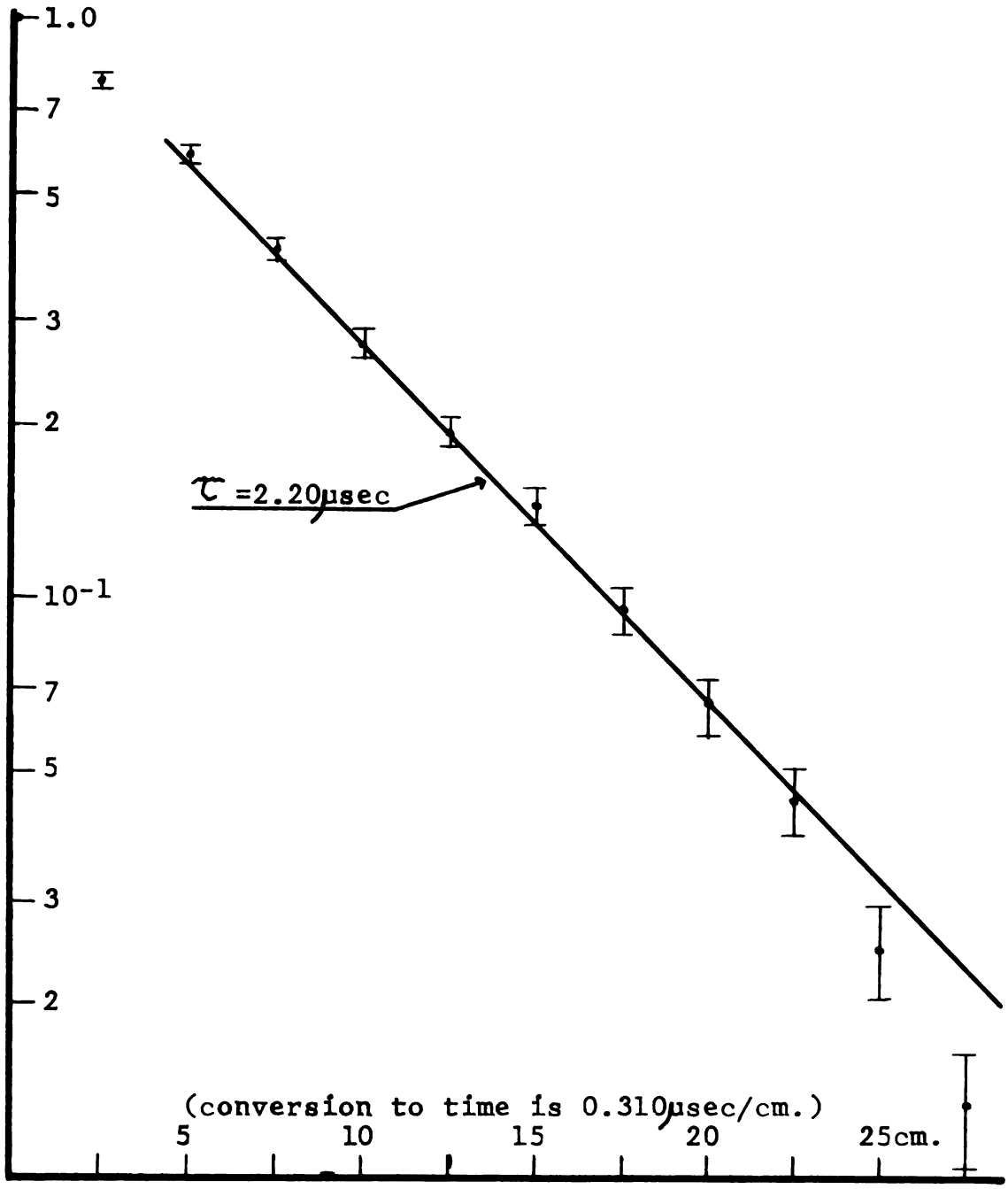

Figure III-1. Normalized lifetime plot of 1280 events selected at random from 8000 two-pulse events.

B. Analysis of track photographs

The muon track photographs taken in the spark chamber were measured on a Hydel scanning machine and the digitized output was punched out on IBM cards by the IBM 526 Summary punch attached to the Hydel. With this scanning-punching chain the x-y coordinate position of any point on the film frame may be recorded on IBM cards in 5-digit numbers having an arbitrary scale factor but bearing a relationship to position on the film which is linear to five significant figures.

Each data card contains a ten-column heading which records the film frame number being measured, the view number ("1" for direct, "2" for stereo), card number within a given view measurement (1-5 to complete the measurements in each view), and the operator number. The remaining seventy columns are available for punching data. Since both the x-y coordinates require 5 columns on the card, totalling ten columns per point on the film, each card carries the coordinate data of seven points along the track. The position of the center of the spark in each gap along the track was recorded in this manner; there are 30 such points to be recorded in each view. In addition to these 30 points the upper and lower front corners of the main chamber, which are visible in both views, were chosen as fiducial marks. These fiducial marks were used as a means of establishing both the

vertical Z axis reference direction and the scale factor pertaining to real distances in each view. This makes a total of 32 points in each view, requiring five cards per view or ten cards in all, per event. From these recorded points the complete track can be reconstructed and the desired quantities calculated using a computer program written for this experiment.

C. Data reduction

The computer program, for which a listing is given in Appendix F, performed the following tasks upon the raw track data obtained on the Hydel scanner.

1. Sorting and geometric reconstruction

a. The cards are processed ten at a time and are checked for identical frame number and sequential view and card numbers. If cards are missing or out of order, the program will cause an appropriate diagnostic to be printed, scrap that particular event and move on to the next.

b. The position data of the 32 points is first converted to centimeters measured in real space. Then the coordinate points are corrected for camera parallax, using the known optical geometry of the experimental set-up.

c. These data are then written on tape for permament storage. This phase of the calculations will thus never have to be repeated for subsequent runs with the same data. Nor will the original data cards again be needed, as future calculations can be made directly from the tape.

2. Performing the necessary calculations upon the data tape

a. First the appropriate track points are taken from memory, from which line fits are formed

to the incoming and outgoing directions in both chamber views. There are often gaps in the chamber which do not fire in a given photograph, leaving points missing from the track data. A minimum of two points in the four gaps or the thin plate chamber and two in the first four gaps of the main chamber is set as the criteria for acceptance of a given event for processing. A maximum of six points would be available for the line fit if all gaps in the thin plate chambers fired properly.

b. Having met this criteria, a least squares line fit is made to each of the projected track segments. This line fit process yields values for the slope with respect to the Z axis and the intercept in the x-y plane at Z = 0.

c. A statistical parameter called R^2 is calculated for each of the four line fits done above. This quantity defined as

$$R^2 = \frac{\sum_{i=1}^{m} \{[x_i - \bar{x}][z_i - \bar{z}]\}}{(m-1)\sqrt{\frac{\sum_{i=1}^{m} x_i^2 - m(\bar{x})^2}{m-1}}\sqrt{\frac{\sum_{i=1}^{m} z_i^2 - m(\bar{z})^2}{m-1}}}$$

where

$$\bar{x} = \frac{1}{m}\sum_{k=1}^{m} x_k \qquad \text{and} \qquad \bar{z} = \frac{1}{m}\sum_{k=1}^{m} z_k$$

has values between 0 - 1.0 and is a measure of how nearly the observed points fall exactly on the least squares line. A cutoff value of $R^2 = 0.960$ was established by correlating the values obtained for R^2 with

the appearance of the track as viewed on the scanning screen. The event was rejected if any one of the four line fits yielded a value of R^2 less than 0.960.

Causes of this could be either operator error or individual spark displacements. The former was effectively eliminated by remeasuring all events rejected for too low a value of R^2. A portion of the rejected events were recovered in this way. The latter are assumed to be caused by delta rays formed in a given gap. These events which pass the R^2 test have their line fit parameters made available to the space angle and projected angle calculation procedure that follows.

d. Another subroutine uses the values obtained in step b. above for the slope and intercept of each track segment, to determine the azimuth angle ϕ of both the incoming and outgoing tracks projected on the x-y plane. From the signs of the slopes, the quadrant in which each track segment lies around the Z axis in the upper hemisphere is determined. These quadrant values are in turn used in assigning the correct value of ϕ to the arctanϕ , yielding values ranging from 0 degrees to 360 degrees measured counterclockwise from the positive X axis.

e. The value of the apparent total deflection angle θ present in the track is calculated in a function subroutine, by a process derived upon direction cosines.

1. Next the projected angle with respect to the + Z axis of each track segment is calculated from the corresponding slope parameter. A modified value of the two projected angles in the direct view is formed by correcting for the inclination angle in the y-z plane made by the top track. This is done in order than when the projected deflection angle in the direct view is calculated from the value of the projected incoming and outgoing directions, it will be indeed the deflection angle projected in every case on a plane containing the incoming direction of the particle. This formality is dictated by the nature of the statistical scattering theories with which the experimental results are to be compared. In principle this is quite different from the deflection angle projected upon an arbitrary plane, i.e., that of the front face of the chamber, which does not necessarily contain the direction of the incoming particles coming in from random directions within the vertical acceptance cone of the counter telescope system. Yet since this cone has a maximum opening angle of 15 degrees or less, the correction to the calculated deflection angle required for track inclination amounts to only a few percent. The values of incoming and outgoing projected angles for both views are printed out on the Projected Angle Data page. Along with this are printed the calculated values of projected deflection angle in the direct

and stereo views and the projected deflection angle in the direct view, corrected as described above.

g. A calculation of the zenith angle (with respect to the +Z axis) of the incoming track was performed at this point from the values found for the slope of the incoming track in each view. Vector addition of the tangents in each view was used to find the tangent of the zenith angle.

3. Summary functions performed by the computer program

a. A partitioning operation was performed upon the resulting values of ϕin, ϕout, the total deflection angle θ, the zenith angle θin, the incoming direction in the direct view (projected) θin, and the corrected projected deflection angle in direct view θ dir. This operation consists of having the computer take successive small increments of the quantity in question, counting and storing for each interval the total number of cases, out of each group of fifty events, that yielded a value of that quantity within each such interval. This is a valuable aid to subsequent plotting of the results in the form of distribution functions for each of the above quantities. Each interval is defined to be single-ended so as to avoid ambiguity for any resulting value of the angle. In the case of ϕ in,

for example, the first interval is formed by the relation $0 \leq \phi < 10^{\circ}$; the second is $10 \leq \phi < 20^{\circ}$, et cetera, up to 360 degrees. The interval size chosen for the above quantities is 10 degrees, 10 degrees, 0.25 degrees, 0.20 degrees, 0.20 degrees, and 0.25 degrees respectively. The number of events occurring in each interval is cumulative for each successive group of fifty events throughout the entire run.

b. There is assembled at the end of each group of fifty events a list of frame numbers for all events rejected for having an insufficient number of spark points from which to form a line fit.

c. There is also assembled at this point a list of those events rejected for R^2 less than 0.960. Recovery of these events was attempted by remeasuring each such rejected event. Some 15-20 percent of such remeasured events then passed the R^2 test.

4. Print-out of results

The following information was printed out by the program in this order.

a. Information printed out at beginning of run

(1). List of events stored on tape. After storage of the data on tape, a complete list of frame numbers of all such events is printed out in groups of fifty.

(2). List of frame numbers for events not placed on tape due to cards out of order

within event, wrong event number on a card, et cetera. Along with each frame number will be an appropriate diagnostic statement describing the reason for deletion.

b. Information printed after processing of each group of fifty events throughout the run

(1). Line data page. The slopes, intercepts, correlation factors, and number of points used are listed for each of the four line fits associated with each event number. Two pages are required to list this information for fifty events.

(2). Space angle data page. On this page the computed values of azimuth angle ϕ and corresponding quadrant are printed out for both the incoming and outgoing track. Along with this the calculated value of the projected incoming direction α in and of the total deflection angle θ is listed. A final column relists all values of θ which were 1.000 degrees or more, with zeros listed for all events having θ less than 1.000 degrees. The events whose value of θ is listed in this column have their spark position data duplicated on another tape for separate storage of all events giving high deflection angles.

(3). Projected angle data page. On this page are printed the calculated values of the incoming and outgoing projected angles for both views, the values of the projected deflection angle in each view, and the projected deflection angle in the direct view,

corrected for track slant as described previously.

(4). First list of rejected events. A list of event numbers for events having less than the minimum number of spark points present is printed on the page following the projected angle data.

(5). Second list of rejected events. A list of event numbers for events not passing the $\geq$ 0.960 test on R^2 is printed on the next page. Events appearing in this list were remeasured and rerun as a group.

c. Information printed at the end of an entire run

(1). The last page number used in the run.

(2). The total number of events processed to date.

(3). The total number of events "saved" (i.e., having $\theta \geq 1.000$ degree) to date. This information is printed out so that a total count of these quantities may be accumulated over any number of runs. This is accomplished by reading these numbers back in on a data card for the next run.

(4). Also the number of events saved during this run is listed.

(5). List of the frame numbers of every event having a calculated track deflection angle θ of 1.000 degree or greater.

(6). Results of the partitioning subroutine upon ϕ in, ϕ out, θ, θ dir. (corrected), α_{in} and θ in as defined above are printed out last, using a separate page for each.

A complete listing of Program Spark is presented in Appendix F.

IV. THEORETICAL PREDICTIONS

The data of this experiment are to be compared with the scattering theories set forth by L. Cooper and J. Rainwater[9] and by S. D. Drell and C. L. Schwartz[17] for multiple scattering of fast particles by extended nuclei. These methods deal directly with the case where the scattering centers are nuclei of a known charge distribution of finite extent. This is in contrast to previous treatments of the problem, notably the Moliere[10] theory which assumes the nucleus to be a point charge and the Olbert[8] theory which, as a first approximation to treating the extended nucleus case, assumes that the single scattering law becomes identically zero for angles greater than a certain maximum angle φ_0 calculated from the properties of the scattering material in question. As can be inferred from the above listed assumptions, the former theory overestimates the multiple scattering at higher angles, while the latter underestimates predicted scattering in this region.

A. The Cooper-Rainwater calculation

The Cooper-Rainwater theory begins as does that of Moliere and of Olbert with a single scattering law which is the Rutherford scattering law, modified to account for shielding by atomic electrons. This law has the following form:

$$f_1(\varphi, \varphi_m) = Q/2(\varphi^2 + \varphi_m^2)^{-3/2}$$

where φ is the projected angle

φ_m is the equivalent screening angle

and $Q = 4\pi (Nt/A)[(Z/\beta)(e^2/m_ec^2)(0.511/pc)]^2$

$e^2/m_ec^2 = r_e = 2.82 \times 10^{-13}$ cm

N = Avagadro's number

Z = proton number of the scattering material

A = atomic number of the scattering material

t = thickness of the scattering material

$\beta = v/c \approx 1$ for the relativistic particles dealt with in this experiment

pc = momentum in Mev.

This basic single scattering law is taken as is, in the Moliere theory. In the Olbert treatment $f_1(\varphi, \varphi_m)$ is taken as above for angles φ such than $0 \leq |\varphi| \leq |\varphi_0|$ but is set $\equiv 0$ for $|\varphi| > \varphi_0$. The cutoff angle φ_0 is determined from φ_m by the relationship

$$\varphi_0/\varphi_m = a/r_n = \frac{(1.67 \times 10^4) r_e Z^{-1/3}}{r_0 A^{1/3}}$$

$$= \frac{(1.67 \times 10^4)(2.818 \times 10^{-13})}{1.1 \times 10^{-13} AZ^{1/3}}$$

where $\varphi_m = \frac{1.14\ (m_ec^2)\ Z^{1/3}}{137pc} \quad 1.13 + 3.76(Z/137\beta)^2 \quad ^{1/2}$

$$\approx \lambda\!\!\!^{-}/a = \hbar c/pca$$

and $\varphi_0 = \hbar c/pcr_n = \hbar c/pc(1.1 \times 10^{-13})A^{1/3}$

The Cooper-Rainwater theory, however, employs the above single scattering law for all angles, modified by the appearance of a form factor which also is a function of angle, thus:

$$f_1^{C-R}(\varphi) = Q/2(\varphi^2 + \varphi_m^2)^{-3/2} \quad \mathcal{F}_N(\varphi/\varphi_0)$$

where $\mathcal{F}_N(\varphi/\varphi_0) = \mathcal{F}_N(y)$ is defined by

$$\mathcal{F}_N(y) = F_N^C(y) + F_N^I(y)$$

where $F_N^C(y)$ is the term contributed by elastic scattering.

In fact $(F_N^C(y))^{\frac{1}{2}}$ is the Fourier transform of the nuclear charge distribution. $F_N^I(y)$ is the term contributed by inelastic scattering. F_N^I can be written approximately as $1/Z\ (1-F_N^C)(F_p)$ where F_p is the form factor for scattering by a single proton. This, however, can be taken as ≈ 1 for momentum transfers ≤ 200 Mev/c. Thus its effect can be neglected for all present purposes.

The exact form taken by Cooper-Rainwater for F_N^C, chosen in such a way as not to underestimate the effects due to multiple scattering, is defined by a curve drawn through a set of points for which values of F_N^C were given and then attached to an asymptotic formula

for $y = 0, 1, 2, 3$, F_N^C is taken as follows:

$F_N^C = 1.00, 0.82, 0.50$ and 0.15.

For $y \geq 4$, $F_N^C = 12/y^4$.

This form for F_N^C amounts to taking up a position between the results of assuming a uniform charge distribution in the nucleus, which gives a value of $9/y^4$ for large values of y, and the results set forth by Williams which give a value of $16/y^4$ for large values of y.

This choice of $F_N^C(y)$ results in an $\mathcal{F}_{N(y)}$ such that

$\mathcal{F}_{N(y)} = 1$ for small values of $y = |\varphi/\varphi_0|$

and becomes Z^{-1} for large values of $y = |\varphi/\varphi_0|$

with the rapid change occurring around $y \approx 2$. This is an improvement over Olbert's tacit assumption of:

$F_{N(y)} = 1$ for $y \leq 1$

and $\equiv 0$ for $y > 1$

In the present theory $\mathcal{F}_{N(y)}$ becomes Z^{-1} instead of zero for large values of y and the functional form is known by which it reaches this value from its value of 1 for y = 0.

The Fourier representation of the single scattering law can be written thus

$$f_1^{C-R}(\varphi) = \frac{1}{2\pi}\int_{-\infty}^{\infty} g(\vartheta) e^{i\vartheta\varphi}\, d\vartheta$$

$$\text{and } g(\vartheta) = \int_{-\infty}^{\infty} f_i^{C-R}(\varphi) e^{-i\vartheta\varphi}\, d\varphi$$

From this a value for the probability of a final projected angle after any number of scatterings is given by

$$M(\varphi)d\varphi = d\varphi/2\pi \int_{-\infty}^{\infty} e^{i\vartheta\varphi}\, e^{g(\vartheta)-g(o)} d\vartheta$$

The quantity $g(\vartheta) - g(0) = Q/2\int_{-\infty}^{\infty} \frac{(e^{i\vartheta\varphi'}-1)\, \mathcal{F}_N(\varphi'/\varphi_0)d\varphi'}{(\varphi'^2+\varphi_m^2)^{3/2}}$

For the sake of convenience, the variables are transformed, following Moliere, as follows:

$$x = (2GQ)^{-\frac{1}{2}}\varphi, \quad \eta = (2GQ)^{\frac{1}{2}}\vartheta$$

$$\text{and } G = -\tfrac{1}{2}\ln\left[(\gamma^2/e)\varphi_m^2/2GQ\right]$$

$$\cong 5.66 + 1.24 \log 10\left[\frac{Z^{4/3} A^{-1} t}{1.13\,\phi + 3.76(Z/137)^2}\right]$$

Thus $g(\vartheta) - g(0) = g(\eta/(2GQ)^{\frac{1}{2}}) - g(0) \equiv S(\eta)$

Whence $S(\eta) = 1/2G\int_0^{\infty} \frac{\mathcal{F}_N(x'/x_0)\left[\cos(\eta x')-1\right] dx'}{(x'^2 + x_m^2)^{3/2}}$

M(x) then becomes

$$\frac{1}{2\pi}\int_{-\infty}^{\infty} e^{i\eta x}\, e^{S(\eta)} d\eta$$

After suitable integration and expansion by powers of 1/2G as described in the Cooper-Rainwater paper, the following form of M(x) is obtained.

$$M^{C-R}(x) = e^{-x^2}/\sqrt{\pi}\left[1 + q(L,x)/4G\right] + 1/4G\sqrt{\pi}\, N(L,x)$$

$$q(L,x) = 2(2x^2-1)\left[\ln(L/1.26) + \int_0^{2Lx}(\cosh(t)-1/t)\,dt\right] + 6x^2 - (1/L^2)(\cosh(2Lx)-1)$$

$$-(2x/L)\sinh(2Lx)$$

where $L = 1/4$ and

$$\int_0^{2Lx}\left[(\cosh(t)-1)/t\right]dt \approx (2Lx)^2/2.2 + (2Lx)^4/4.4! + \cdots + (2Lx)^n/n(n!)$$

for values of $n = 2, 4, 6, 8, \cdots$

$$N(L,x) = \int_L^\infty \lambda^{-3}\, T(x,\lambda)\,d\lambda$$

$$T(x,\lambda) = \exp\left[-(x+\lambda)^2\right] + \exp\left[-(x-\lambda)^2\right] - 2\exp(-x^2)$$

B. The Moliere calculation

The Moliere multiple scattering distribution which assumes a point nucleus, is latent in the expression:

$$M^{C-R}(x) = 1/2\pi \int_{-\infty}^{\infty} e^{i\eta x}\, e^{S(\eta)}\,d\eta$$

where $S(\eta) = 1/2G\int_0^\infty \frac{\mathcal{F}_N(x'/x_0)(\cos(\eta x')-1)dx'}{(x'^2 + x_m^2)^{3/2}}$

The single scattering law used by Moliere was

$$f(\varphi) = Q/2\ (\varphi^2 + \varphi_m^2)^{-3/2}$$

This differs from the one used by Cooper-Rainwater only by the omission of the factor $\mathcal{F}_N(\varphi/\varphi_0)$. Thus the Moliere scattering distribution may be obtained from the Cooper-Rainwater calculation by merely setting $\mathcal{F}_N(y) = 1$

in the above expression for M(x). The machinery set up to calculate M(x) from the final form shown in part A above can thus be used to also calculate $M^{Mol.}(x)$. The results of this Moliere calculation are used for comparison purposes in discussing the results of the present experiment.

C. The Drell-Schwartz calculation

The data of this experiment are further to be compared with the scattering distribution predicted by the method set forth by Drell and Schwartz[17]. In this method the total differential scattering cross section (elastic plus inelastic) is constructed from a knowledge of the nuclear ground state wave functions. This method considers the specific case of high energy electrons scattering from light nuclei so that the interaction may be treated in the first Born approximation. Only values of the momentum transfer $|\vec{q}| \leq 200$ Mev/C are considered so that the nucleon recoil velocities v_{rec} are kept well in the nonrelativistic range ($\beta_{rec} \lesssim 1/5$). In this region of momentum transfer values the dominant factors in the scattering are the Coulomb forces and the magnetic forces, viz., single-particle magnetic moment interactions.

The form for the low resolution (all final energies accepted at each specified angle) differential cross section $d\sigma/d\Omega$, given as equation 19 in the Drell-Schwartz paper, is

$$\frac{d\sigma}{d\Omega} = \left(\frac{d\sigma_0}{d\Omega}\right) f_{(q)} \left\{ \mathcal{F}_{(q)} + \frac{Z q^2}{2\hbar M^2} + (2\sec^2(\theta/2) - 1) \cdot \left[(2/3)(Z/\hbar M) \langle T \rangle + q^2/4M^2 \left(Z\mu_p^2 + N\mu_n^2 + \right. \right. \right.$$

$$\left. \left. \left. + \frac{1}{3} \sum_{i \neq j}^{Z} \langle \vec{\sigma}_i \cdot \vec{\sigma}_j \mu_i \mu_j \exp(i\vec{q} \cdot \vec{R}_{ij}) \rangle \right) \right] \right\}^2$$

The term $d\sigma_0/d\Omega = \left[\frac{r_e m_e \cos(\theta/2)}{2 k_0 \sin^2(\theta/2)} \right] \frac{k}{k_0}$

r_e = 2.818 x 10^{-13}cm (classical electron radius)

m_e = 0.511 Mev (mass of electron in Mev units)

K = PC (in Mev) where P is the final momentum of the particle after scattering

K_o = P_oC (in Mev) where p_o is the initial momentum of the particle before scattering

θ = total spatial scattering angle (in radians)

Note here that only through the factor r_em_e do the properties of the electron, which was taken to be the incident particle in the Drell-Schwartz development, appear. Since, however, the classical electron radius r_e is defined as

$$r_e = e^2/m_eC^2 = 2.818 \times 10^{-13}\text{cm}$$

the product $r_em_e = e^2/C^2$ is actually independent of electron characteristics. Thus for scattering of muons no change is required in $d\sigma_o/d\Omega$ since

$$r_\mu m_\mu = (e^2/m_\mu C^2)m_\mu = e^2/C^2 = r_em_e.$$

From the kinematics of the problem the relationship between K and K_o is

$$K/K_o = \frac{1}{1 + 2K_o/AM \sin^2 \theta/2}$$

This ratio is essentially unity for the present experiment since the quantity $(2K_o \sin^2 \theta/2)/AM$ is 2.69 x 10^{-3} even for θ = 17 degrees, the largest value encountered any

place in the calculation.

The term $f^2_{(q)}$, the proton form factor given by Hofstadter[18] as

$$f^2_{(q)} = e^{-q^2/6.1}$$

The momentum transfer q, from the kinematics has the form

$$q = 2K_o \sin(\theta/2)\left[1 + 2K_o/AM \sin^2(\theta/2)\right]^{-\frac{1}{2}}$$

$$= 2K_o \sin(\theta/2)\sqrt{K/K_o}$$

Since K/K_o was shown to be essentially unity above, q is replaced by q_o, the momentum transfer as a function of θ for purely elastic scattering

$$q_o = 2K_o \sin \theta/2$$

This value of q_o was used in the present calculation wherever q appears in the expression for $d\sigma/d\Omega$ above. For use in calculating the proton form factor above, q_o must be in units of f^{-1}. This requirement is satisfied by using K_o in units of $PC/\hbar C$ where PC is in Mev and $\hbar C$ is in Mev-f.

The term $\mathcal{F}_{(q)}$ is related to the form factor for two body correlations and is given by Drell-Schwartz as

$$\mathcal{F}_{(q)} = Z + Z(Z-1)\int \varphi_o^* \, e^{i\vec{q}\cdot(\vec{r}_1 - \vec{r}_2)} \varphi_o \, d\tau$$

$$= Z + Z(Z-1) F_{(q)}$$

where $F_{(q)}$ is the form factor for two body correlations. In an electron scattering experiment by Chollet, Bounin

and Bishop[19] performed at the Linear Accelerator Laboratory of the University of Paris at Orsay, the form of $F_{(q)}$ for aluminum in the momentum transfer region of this experiment was found (in terms of x) to be

$$F_A(x) = \left[1 - (16/39)x + (5/156)x^2\right] e^{-(x/2)}$$

where $x = (aq)^2/2$ with the quantity a, the nuclear size parameter, = 1.86×10^{-13}cm according to their results. For the present experiment q may be replaced by q_o in the above expressions. The terms following $\mathcal{F}_{(q)}$ in the above expression for the cross section represent scattering contributions due to magnetic forces and are denoted herein by $\mathcal{F}_{mag(q_o)}$. The terms in $\mathcal{F}_{mag(q_o)}$ were evaluated for the present experiment using Z = 13, A = 27,

$M = \frac{13(938.256) + 14(939.552)}{27}$ = 938.8 Mev, $q \cong q_o$

$\langle T \rangle$ (the average ground state kinetic energy per nucleon) = 30 Mev, μp = 2.793 nm, and μn = -1.91 nm. The final term in the $\mathcal{F}_{mag(q_o)}$, however, was taken as negligible since it is not expected to make any larger relative contribution than was the case in the work of Masek, et al.,[13] for carbon.

The differential cross section obtained as above was converted to a differential scattering distribution by the following defining relationship.[20]

$$\left(\frac{d\sigma}{d\Omega}\right)_\theta = \left(\frac{dN}{d\Omega}\right)_\theta \Big/ N_o \rho_m t$$

where N_o = total number of incident particles

ρ_n = density of nuclei (nuclei per unit volume)

t = thickness of target in cm.

Also $d\Omega$ is defined $2\pi \sin\theta d\theta$, whence

$d\theta / d\Omega = 1/2\pi \sin\theta$

Using this in the above relationship yields

$$d\sigma/d\Omega(N_o \rho n t) = (dN/d\theta)(d\theta/d\Omega) = (dN/d\theta)(1/2\pi \sin\theta)$$

$$\text{Thus } (dN/d\theta)_\theta = 2\pi \sin\theta \rho n t (d\sigma/d\Omega)_\theta$$

Now ρn can be written as

$$\rho_n = \frac{(\text{no./mole})(\text{mass/volume})}{(\text{mass/mole})} = \frac{\text{number}}{\text{volume}} = \frac{N_A \rho_n}{A}$$

where N_A is Avagadro's number, ρm is the mass density, and A is the atomic weight.

The quantity No, the total number of incident particles, was set equal to 1.0, with the result that the quantity $(dN/d\theta)_\theta \, d\theta$ gives the probability for a given particle to be scattered to the element of angle $d\theta$ at θ. This facilitates the normalization of all distributions to unity, which has been the practice in this work.

The above expression for $(dN/d\theta)_\theta$ is written in terms of total spatial scattering angle rather than projected angles. Since, however, both the Cooper-Rainwater and Moliere multiple scattering theories,

described in parts A. and B. of this section, are written in terms of projected angles, a method was developed for converting the Drell-Schwartz single scattering distribution to projected angles. This method is based on taking a conical view of the path of an incoming particle. The point of scattering defines the apex of the cone formed by a figure of revolution done upon the deflected track about an axis along the incoming direction. Azimuthal symmetry about the incoming direction is assumed throughout. Taking such a conical view of the scattering geometry, a plane may be imagined at an arbitrary distance R_o from the scattering site along the incoming direction and perpendicular to it. On this plane may be imagined concentric circles about the point where the incoming direction vector pierces the plane. These concentric circles are constructed such that each i-th one has an equal incremental radius increase dr_i over the previous one of $R_o d\varphi$.

The relative number of projected angle events occurring within $d\varphi$ at φ were found by establishing a plane of projection containing the incoming direction vector. The contributions to the projected angle scattering distribution from the various spatial deflection angles were found by calculating the fractional area of each successive concentric ring which lies between the parallel lines in the plane of the circles, perpendicular to the plane of projection, that bound the element of projected angle $d\varphi$. For each element $d\varphi$ at projected angle φ the fractional area contributions for all $\theta > \varphi$ weighted by the

scattering distribution $dN/d\theta$ evaluated at θ, are summed to form the total value of $dN/d\varphi$ evaluated at φ.

The resulting conversion relationship is as follows

$$(dN/d\varphi)_{\varphi} = \sum_{i=io}^{} C_i (dN/d\theta)_{\theta_i}$$ where the summation is incremented by an amount $\Delta\theta$. At a given value of θ the beginning point of the summation is at $\theta_{io} = \varphi + \Delta\theta$. Thereafter the successive terms in the sum are evaluated at $\theta_i = \varphi + (i - io + 1)\Delta\theta$, where using $\Delta\theta$ is taken to be numerically equivalent to using the quantity $\Delta\varphi$. The C_i coefficients represent the fraction of each concentric ring which falls within the parallel lines bounding the zone of width $R_o d\varphi$ at angle φ. The first coefficient C_{io} arises from an area which is a segment of a circle and is bounded at $\theta = \varphi$ by a chord of the circle as it bounds the element $\Delta\varphi$ and at $\theta = \varphi + \Delta\varphi$ by the arc segment which is tangential to the remaining boundary of $d\varphi$. The area of such a segment is found from geometry to be given by

$$a_{io} = \tfrac{1}{2} r^2_{io} (2\gamma_{io} - \sin 2\gamma_{io})$$

where γ_{io} is the angle in the plane of the rings measured in either direction from the projection plane around to the intersection of the lower boundary of $\Delta\varphi$ with the outside of the io-th ring. From the above definition γ_{io} is given by

$$\gamma_{io} = \arccos\left(\frac{r_{\varphi}}{r_{io}}\right) = \arccos\left(\frac{R_o \tan\varphi}{R_o \tan\theta_{io}}\right) = \arccos\left(\frac{\tan\varphi}{\tan\theta_{io}}\right)$$

$$= \arccos \frac{\tan\varphi}{\tan(\varphi + \Delta\varphi)}$$

There are two identical area contributions such as that above, symmetrically placed about the incoming direction vector. Thus the fractional area coefficient C_{io} =

$$= \frac{2\,a_{i_o}}{A_{i_o} - A_{i_o-1}} = \frac{2\left[\frac{1}{2}\, r_{i_o}^2 (2\gamma_{i_o} - \sin 2\gamma_{i_o})\right]}{\pi\left[r_{i_o}^2 - r_{i_o-1}^2\right]}$$

$$= \left(\frac{R_o^2}{R_o^2}\right) \frac{\tan^2\theta_{i_o}\,(2\gamma_{i_o} - \sin 2\gamma_{i_o})}{\pi\,(\tan^2\theta_{i_o} - \tan^2\theta_{i_o-1})}$$

To form the remaining terms in the summation γ_{io} is generalized to

$$\gamma_i = \arccos\left(\frac{r_\varphi}{r_i}\right) \quad = \arccos\left(\frac{\tan\varphi}{\tan\theta_i}\right) \quad = \arccos\left[\tan\varphi \Big/ \tan(\varphi + (1 - i_o + 1)\Delta\varphi)\right]$$

In all cases of $i > io$ the area contributions a_i were approximated by a parallelogram whose area is given by

$$a_i = \left[\cos\varphi\,(R_\varphi)\Delta\varphi\right]\left[\frac{\cos\theta_i}{\sin\gamma_i}\left(R_{\theta_i}\,\Delta\theta\right)\right]$$

where $R_\varphi = R_o/\cos\varphi$, $R_\theta i = R_o/\cos\theta i$, and $|\Delta\theta|$ is taken equal to $|\Delta\varphi|$. Thus a_i becomes

$$a_i = \frac{R_o\,|\Delta\varphi|^2}{\sin\gamma_i}$$

It is apparent that rather than two there are four such area segments in the i-th ring symmetrically placed around the incoming direction vector. The fractional area coefficient C_i then is

$$C_i = \frac{4\,a_i}{A_i - A_{i-1}} = \frac{4\,|\Delta\varphi|^2}{(\sin\gamma_i)\,\pi\,(\tan\theta_i - \tan\theta_{i-1})}\left(\frac{R_o^2}{R_o^2}\right)$$

The values of C_i thus calculated, together with the values of $dN/d\theta$, were then used to form the sum defined above for each value of φ at which a value of $(dN/d\varphi)_\varphi$ was desired. The upper limit of the summation is set at ∞; in practice, however, this series converges very rapidly since $(dN/d\theta)_\theta$ decreases by five orders of magnitude by about 14 degrees. C_i also decreases monotonically for larger angles.

The set of values for $(dN/d\varphi)_\varphi$ obtained as described above constitutes a series of points on the differential scattering distribution for projected angle single scattering. In order to be directly comparable with the results of the Cooper-Rainwater calculation and those of the experiment, it is necessary finally to make a multiple scattering correction to this single scattering theory. This was done by calculating the function g(y), the differential distribution for single scattering from an extended nucleus developed in the Cooper-Rainwater paper[9].

$$g(y) = \tfrac{1}{2}B(y^2 + y_m^2)^{-3/2} \quad \mathcal{F}_{N(y)}$$

where $B = Q/\varphi_0^2$, $y = \varphi/\varphi_0$ or x/x_0, and $y_m = \varphi_m/\varphi_0$. Q, φ_0, φ_m, x, and $\mathcal{F}_{N(y)}$ were defined in part A., of this section. A ratio of multiple to single scattering probability from Cooper-Rainwater was then formed by dividing $M^{C-R}(y)$ by g(y). This ratio was formed for each of the 260 values of y for which values of $M^{C-R}(y)$ and g(y) are obtained during the course of the computer

calculation. This set of ratios was then employed as a correction factor to the Drell-Schwartz projected angle distribution obtained as described above. The Drell-Schwartz distribution, corrected for multiple scattering is plotted in integral form in Fig. V-2 along with the theoretical distributions of Moliere and Cooper-Rainwater and the results measured in the present experiment.

Appendix G gives a review of the computer program, written in CDC-3600 Fortran, by which each of the theoretical predictions described above was calculated.

V. RESULTS AND CONCLUSIONS

A. Discussion of experimental uncertainties

Experimental uncertainties are present in the measured values of the scattering angles determined for each muon event represented in the data here reported. These arise in two general areas:

1) failure of the track, made visible by the series of spark discharges in the chamber, to lie exactly along the original path of the particle
2) inability to transfer with complete exactness the coordinate positions of the series of sparks comprising the visible track to IBM data cards to be used by the analysis program.

The major cause of (1) is taken to be a random displacement of individual sparks in the track due to the secondary ionization effects in the helium atmosphere of knock-on electrons. This effect results in a "scattering" of the points along the track which in turn causes an apparent scattering angle in the observed track not caused by any real physical scattering phenomenon. This apparent scattering is often referred to as "noise level scattering". The uncertainty of (2) is caused by the inability of the scanning operator to position the reference indicator on the Hydel Scanner over the exact center of each spark in the track for each event. The random distribution of measured positions about the actual positions on the film introduces an additional

"scattering" of the points along the track beyond that of (1) above.

The overall error distribution resulting from both of the above causes of false scattering can be treated by the method developed by McDiarmid[14] for analysis of cloud chamber tracks. From his method the standard deviation can be obtained for the overall noise level scattering from all such causes as the above. The following scattering distribution is developed in his paper for the case of $pc\beta \to \infty$, i.e., negligible real scattering:

$$P_{(<\phi>_m)} = \frac{2}{\Gamma\left(\frac{m}{2}\right)} \left(\frac{m}{2}\right)^{m/2} \frac{(<\phi>_m)^{m-1}}{\sigma^m} \exp\left[\frac{-m(<\phi>_m)^2}{2\sigma^2}\right]$$

For the case n = 2 which pertains to the present experiment as described below, this reduces to

$$P_{(<\phi>_2)} = \frac{2(<\phi>_2)}{\sigma^2} \exp\left[\frac{-(<\phi>_2)^2}{\sigma^2}\right]$$

Setting the derivative of this expression equal to zero defines the location of the peak of the $<\phi>_n$ distribution in terms of σ

$$(<\phi>_n)^2 \text{ most prob.} = \tfrac{1}{2}\sigma^2$$

This relationship may then be inverted to yield a value for σ once the value of $(<\phi>_n)(\text{most prob.})$ is identified from a plot of the experimental results. In this manner

$$\sigma = \sqrt{2}\ (<\phi>_n)_{\text{most prob.}}$$

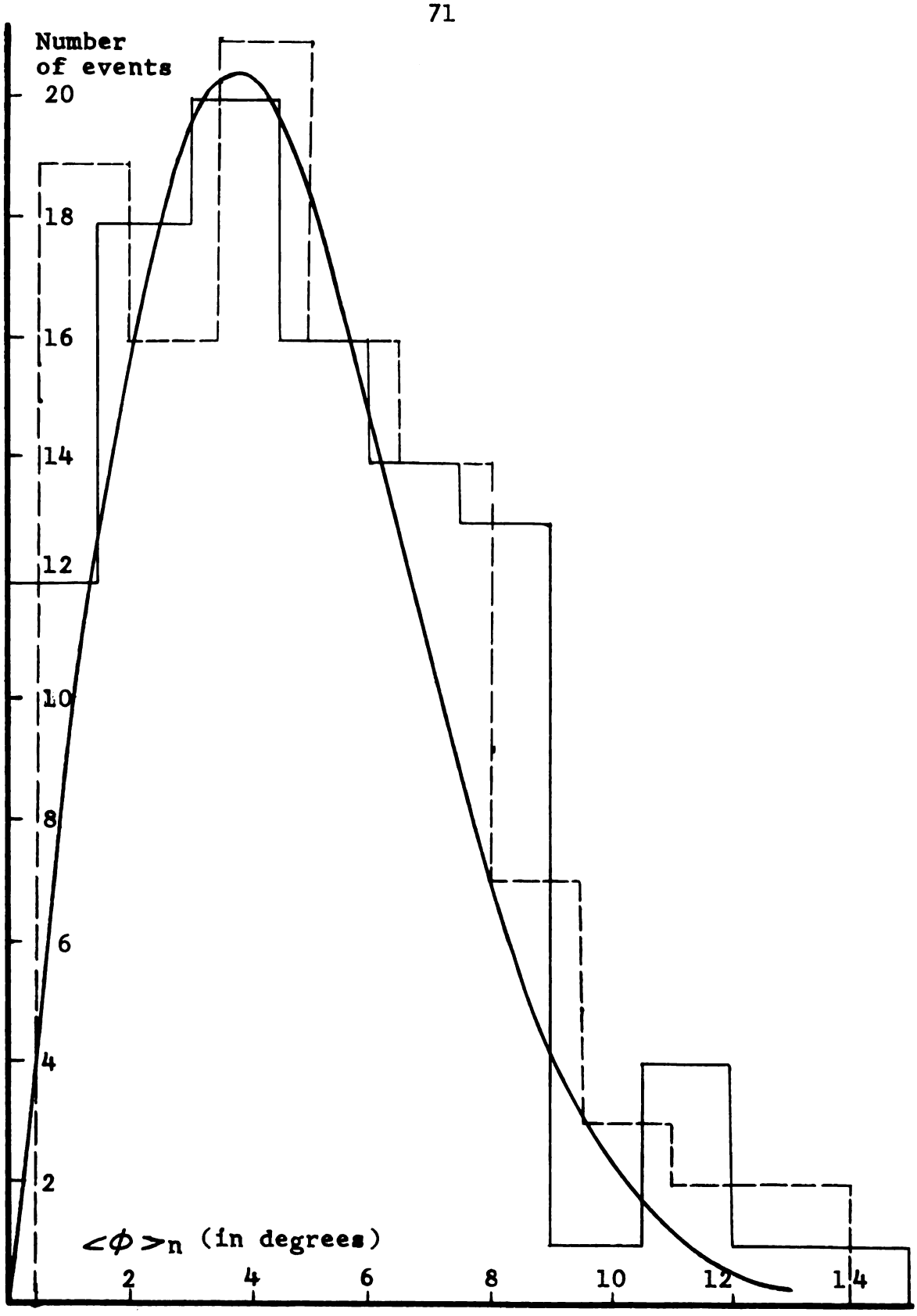

Figure V-1. Plot of 100 "doubles" events. Two groupings of the data are shown. Solid curve represents theoretical predictions for noise-level scattering.

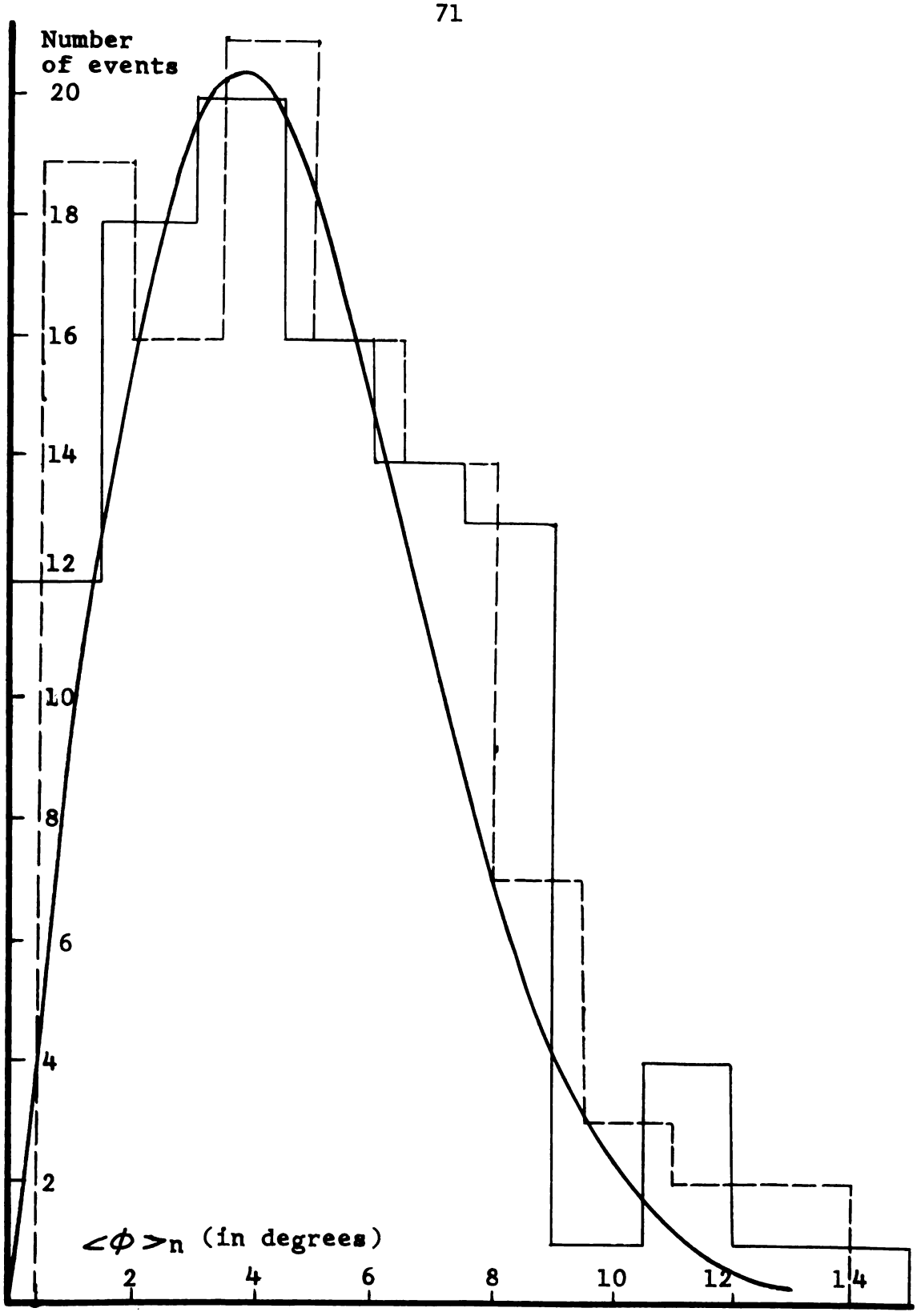

Figure V-1. Plot of 100 "doubles" events. Two groupings of the data are shown. Solid curve represents theoretical predictions for noise-level scattering.

The identification of $(<\phi>_n)_{(\text{most prob.})}$ is carried out here as in McDiarmid's paper by measuring events obtained under a "doubles" counter criteria in the apparatus. That is, these were obtained with the anticoincidence counter disabled, thus accepting particles having any momentum greater than 1.56 Bev/c in order to reduce the contribution from real scattering to a low value. A plot is given in Fig. V-1 for 100 such events upon which two measurements of the scattering angle were made, corresponding to n = 2 in the above expressions. A separate histogram for each of two groupings of the data is given. From these histograms the most probable apparent scattering, $(<\phi>_n)_{(\text{most prob.})}$ is 0.37 degrees at the location of the peak of the histogram. The solid curve in Fig. V-1 is a plot of the distribution $P(<\phi>_n)$ above for $pc\beta \to \infty$ and n = 2. The fact that this curve is a good approximation to the data establishes the assumption that the data used here had in fact negligible real scattering and thus provides a valid means of measuring σ. The value of 0.525 obtained for σ was then used in the determination of the theoretical distributions presented in Fig. V-2.

B. Comparison of observed scattering with predicted values

In the present experiment a total of 2,266 usable events identified as muon events were obtained upon which track measurements and deflection angle calculations were performed. Many events beyond this number were identified

as muon events but were not usable due to subminimal track quality of one type or another. Most of the events rejected in this way either failed to pass through the entire chamber (i.e., entering or leaving through one side), had too few sparks present to obtain an accurate line fit, or had too many displaced sparks due to knock-on electrons set in motion along the track.

Figure V-2 shows the resulting integral scattering distribution for the 2,266 accepted events. The curve is normalized to unity. This is a plot of the relative number of events displaying a measured projected scattering angle equal to φ or greater. These measured projected scattering angles were calculated from the data for each event in the manner described previously in Section III-C and Appendix F. Also shown in Fig. V-2 by solid lines are the predicted integral scattering distributions for this experiment which follow from the theories of Cooper and Rainwater[9], of Drell and Schwartz[17], and of Moliere[10]. These curves were obtained from calculations done as described previously in Section IV and in Appendix G. The error bars shown on the experimental points are statistical only. The effect of other measurement uncertainties, discussed in Section V-A, are accounted for in the calculation of the predicted distributions.

The contribution to the scattering distributions due to multiple scattering are as follows (evaluated for the Drell-Schwartz theory):

Scattering angle	1.0°	2.0°	3.0°	4.0°	5.0°
Multiple scattering	69%	27.4%	12.6%	9.5%	8.2%

In comparing the experimental results with the theories as shown in Fig. V-2, it is apparent that the data are in best agreement with the predictions of the Drell-Schwartz calculation within the statistical uncertainties shown. This calculation gives predicted values about 10 percent higher than those of Cooper-Rainwater for angles greater than 2 degrees. The Drell-Schwartz calculation represents a slightly better fit to the experimental data than does that of Cooper-Rainwater.

The Moliere distribution, while differing from that of Cooper-Rainwater only by a factor of 3.2 at the highest angle use, nevertheless does not represent a suitable fit to the data. A χ^2 test was made on the data with respect to each of the theories from the relationship

$$\chi^2 = \sum_{i=1}^{M} \left[\frac{N_i^{exp.} - N_i^{Th.}}{\sqrt{N_i^{exp.}}} \right]^2$$

This gives values of 4.76, 4.92 and 11.40 respectively for the Drell-Schwartz, Cooper-Rainwater, and Moliere theories. The χ^2 tables[38] give the following predictions for these values. The probability is approximately 92.5 percent that the data are consistent with the first two theories, as compared to a 40 percent probability that the data are consistent with the Moliere theory.

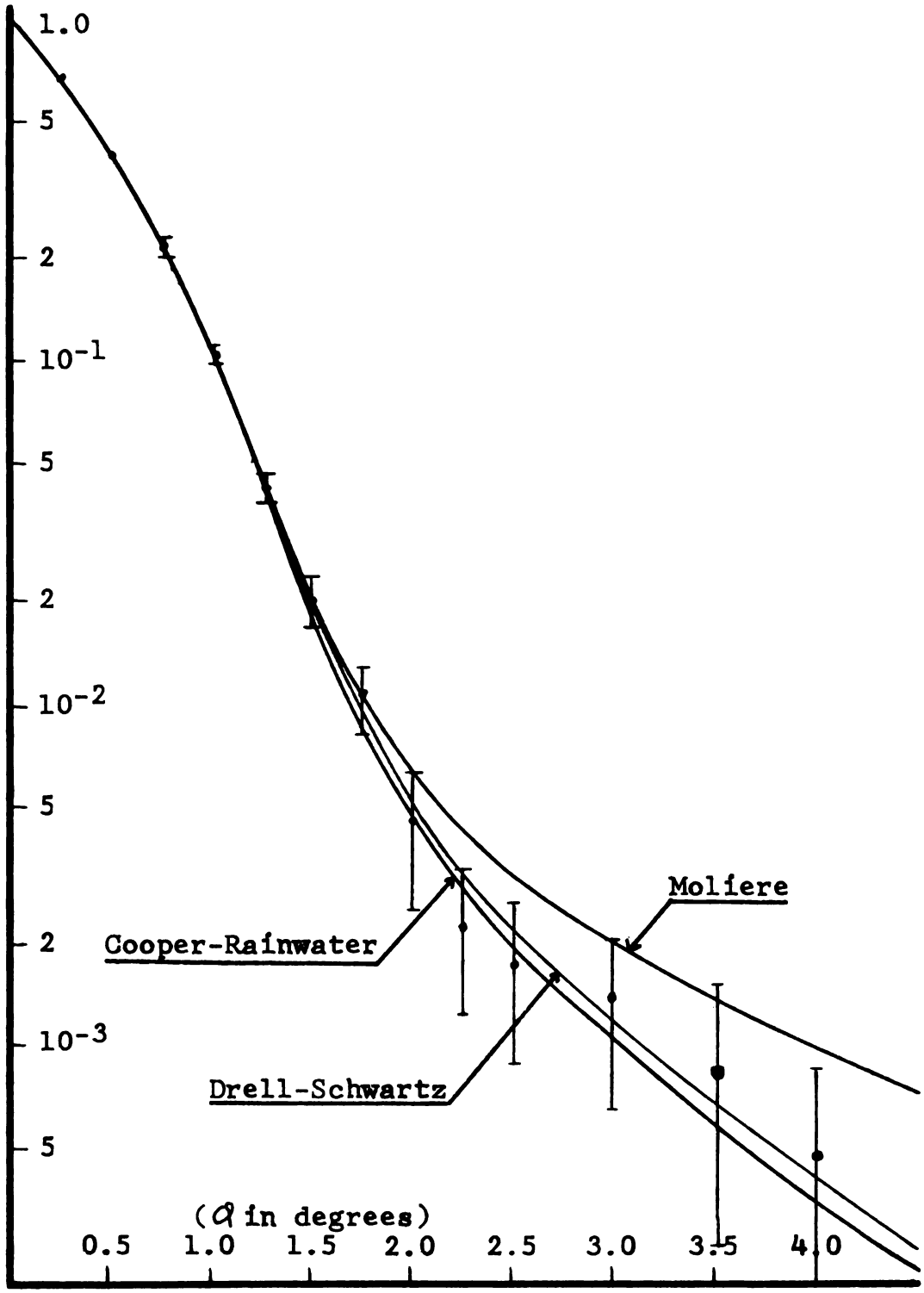

Figure V-2. Normalized plot of experimental and theoretical integral scattering distributions.

C. Summary and conclusions

The work presented herein was an experimental investigation of the scattering behavior of 1.60 Bev/c muons experiencing momentum transfers up to 190 Mev/c in the aluminum plates of a spark chamber. Cosmic rays were utilized as the source of these muons. Details of the experimental equipment constructed for operation of the spark chamber, particle detection and identification, and automatic track photography have been presented along with details of the computer programs developed for data analysis and theoretical predictions.

The muon track data obtained was analyzed to yield measured values of projected angle scattering. It was found that within the uncertainty limits shown in Fig. V-2 the observed scattering was in good agreement with the extended-nucleus theories of Cooper and Rainwater[9] and of Drell and Schwartz[17], rather than with the point-nucleus theory of Moliere[10]. Thus the results of the present experiment are in good agreement with the results of Masek, et al.,[13] and of Fukui, et al.[11] At the same time the data and results of the present experiment are given with somewhat firmer bases, with respect to improved momentum determination and particle identification as described earlier, than those upon which the results of the latter were felt by some[12] to have rested.

Having observed no identifiable "anomalous" scattering in an experiment where both the momentum determination and particle identification were good, it is concluded that upon careful investigation the similarity of muons and electrons with respect to electromagnetic scattering indeed holds for cosmic ray muons as has been shown for machine made muons[13]. The present experiment represents the best cosmic ray muon scattering experiment to date with respect to the above critical features.

APPENDIX A: Spark chamber system

The spark chamber system consists of three principal divisions: (1) the spark chamber structure itself, (2) the helium gas flow system, and (3) the thyratron pulsing unit.

1) Spark chamber

As mentioned in the text and as shown in Fig. II-3, the spark chamber used in this experiment is constructed in three sections: the upper, main, and lower chambers. The main chamber is composed of 5/32-inch aluminum plates 10 1/2-inches square with a tab on one corner of each for electrical connection. These plates were assembled with tabs alternated with respect to location at front and rear of the right-hand chamber face to facilitate the connection of alternate plates to the thyratron pulser and the remaining ones to ground. To handle the high current pulses without excessive voltage drop, one-inch copper straps were used to connect the chamber plates together, and one-inch braid carried the current from the thyratron circuit.

The gap spacing between plates was formed by plexiglas spacing strips sliced from 3/4-inch sheet stock and machined to 0.25-inch within a ten thousandth. A close gap tolerance was necessary in an attempt to obtain uniformly high spark efficiency in each gap. The spacing strips were assembled to form a square around the outside of each successive plate. The next plate was

placed upon the spacing strips forming a closed cell, and then another set of spacing strips was placed upon it in the same manner. Twenty-two such gaps form the main chamber. The entire assembly including the upper and lower chambers is held together by tensioning bolts at each corner bearing upon a 1/2-inch thick aluminum plate on top and bottom.

The upper and lower chambers were each constructed by milling 1/16-inch grooves in plexiglas pieces at 0.25-inch spacing in such a manner that the pieces are assembled into a closed box having continuous grooves around the inside wall at every 0.25-inch increment. The 3/64-inch thick aluminum plates used for these chambers were inserted in the box grooves just before the final side was mounted in place. Both the upper and lower chambers were built with four gaps in pairs of two, separated by a distance of 1 1/16-inch. Electrical connections to the plates were brought out in a similar manner to that described above for the main chamber.

2) The helium gas flow system

The gaseous medium for spark production decided upon for this experiment was helium with a trace of ethyl alcohol vapor as an additive. Of the gasses commonly used for spark chamber work, helium was chosen since it is the only one economically feasible in a free flow system which exhausts into the atmosphere.

This flow method was chosen because it is mechanically impractical to attempt to seal for evacuation a chamber constructed as described above.

Helium, of the grade most readily available from welding suppliers, was first run through a cold trap containing liquid air. This procedure was adopted when after only a few months' operation a noticeable deterioration of gap efficiency was observed. It was determined that a trace of both oil and water as well as some hydrogen was present in the welder's helium. The latter could not conveniently be eliminated, but the liquid air trap effectively removed the oil and water before it entered the system. The result was a considerably longer time period before disassembly and cleaning of the chamber again became necessary to restore gap efficiency.

The helium flow control panel consists of two Hoke metering valve and flow gauge units, one on each branch of a two-way flow path. Most of the helium passed through the main branch and on to the distribution manifold on the spark chamber. A flow rate of 2.5 liters per minute was maintained in this branch. A small amount of helium, however, was diverted into the second branch through a second metering valve and flow gauge to a 1/32-inch orifice at the base of a glass tube containing ethyl alcohol. The tube was filled to a depth of 2.5 inches and helium was bubbled

through the alcohol at a rate of one bubble per second. The purpose of the alcohol is described in the main text.

The gas flowing in the two branches was again combined and sent to the chamber. Each of the three sections of the chamber was fed from a separate flow control valve to its own manifold block. At this point individual flow control to each of these divisions was necessary in order to keep the helium flow rate per cell equalized among the three sections, since each contained a different number of cells.

3) The high voltage pulsing unit

As described in the main text the spark chamber was fired by discharging into the chamber a bank of capacitors charged to 15 KV. The discharge of each capacitor bank was controlled by a separate 5C22 hydrogen thyratron being triggered ultimately by the coincidence circuit. The Amperex 6279/5C22 version was chosen because of its superior rise time characteristics and higher voltage handling capabilities. Biasing the grid of each thyratron at +15 V (adjustable to best operating point) further decreased the rise time into conduction. An Amperex EFP60 secondary emission tube, used in a single-shot blocking oscillator circuit, delivered a fast-rise 150 V pulse to the grid of the 6279/5C22. The EFP60 was triggered by the positive pulse delivered to it from its respective 6688 cathode follower stage. The three cathode followers, each

driving its own EFP60 and 6279, received their signals from the coincidence circuit via a 6688 input amplifier-inverter stage. A negative pulse having an amplitude of 0.1 V or greater triggered the spark chamber discharge, but a larger input pulse was desirable for reducing the rise time to a minimum. A negative input pulse of one volt or more produces an overall spark discharge delay time of $\approx$ 200 nsec. The circuit of the thyratron unit is shown in Fig. A-1. This unit was constructed in 1961 following the general plan of a similar unit just completed at that time by Prof. D. Meyer and Prof. K. Terwilliger of the University of Michigan, Ann Arbor.

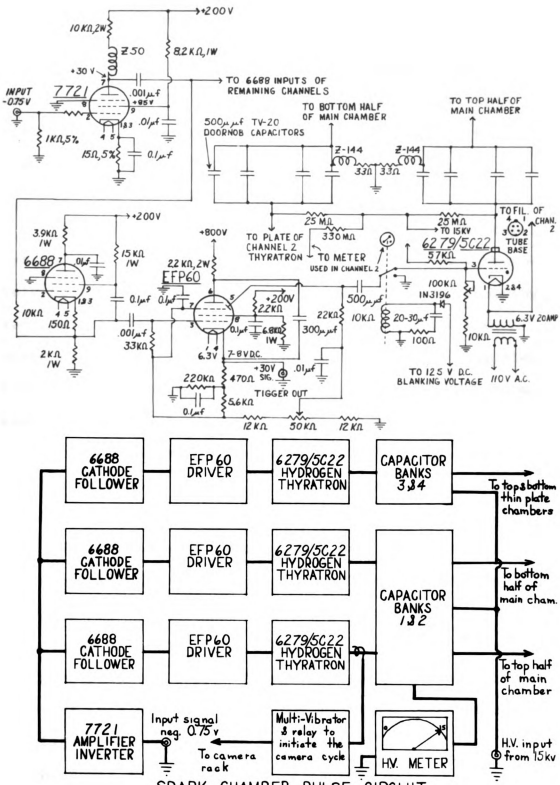

SPARK CHAMBER PULSE CIRCUIT

FIGURE A-1.

APPENDIX B: Circuit description of the counter telescope system

The counter telescope system consists of two divisions: (1) the scintillation counters with their circuit boxes and power supplies, and (2) the tunnel diode coincidence circuit.

1) Counters and phototubes

The three scintillation counters in the telescope system are fitted with one, eight, and four 6810A photomultiplier tubes corresponding to the aperture, stopping, and anti counters respectively. Each phototube was wired for negative pulse output according to a suggested circuit found in the data sheet supplied with each tube, except that the bleeder resistances were multiplied by a factor of 6.5 to conserve power supply current. This was feasible only because of the low average count rate involved.

The DC operating voltage for each phototube circuit was supplied via a distribution panel from two Hamner N-4035 power supplies. One of these power supplies was associated with the eight tubes on the stopping counter; the remaining one supplied both the aperture and anti counters, via a second distribution panel. Each phototube voltage could be adjusted to a desired level below that of the power supply voltage. A voltage drop ranging to minus 20 per cent in 16 steps was provided by this method.

The purpose of this arrangement was to allow independent voltage adjustment of each tube to equalize pulse heights among the several tubes on the same counter.

The aluminum mounting sleeves of each phototube were connected to the power supply at negative cathode potential to reduce dielectric stress on the glass walls of the phototube. It has been the experience of many that failure to do this causes noise in the phototube output.

2) Coincidence unit

The tunnel diode coincidence circuit constructed for this experiment (see Fig. B-1,1a) was designed from the basic circuit given by Whetstone and Kounosu[36]. Basically it consisted of an input module for each scintillation counter with a number of tunnel diode univibrators cascaded to provide a high degree of isolation from the input signal as well as standardization of signal shape. Once the input signal is standardized in this manner, the coincidence function may then be performed by merely feeding the signal from each coincidence channel into a current adder, which in turn triggers another univibrator whenever there is a signal present in all inputs at the same time.

Anticoincidence operation is also available by arranging that the signal from the "anti" input module be used to gate the coincidence channel at a subsequent stage in the circuit. It is necessary in this mode of

operation that the "anti" signal arrive in the circuit before the coincidence signal. For this reason the signals from the aperture and stopping counters were each delayed 60 nsec by means of additional cable length.

As shown in Fig. II-4 the entire unit was constructed in a copper chassis to minimize troublesome effects arising from pickup of RF radiation from the spark chamber. Use of silverplated finger stock on the tight-fitting bottom plate provided a highly effective closed conducting shell for shielding of the circuit. Within the chassis are copper dividers to decrease signal pickup from one point in the circuit to another. The necessity of this measure was evident from experience with a pilot model in which the degree of singles rejection was limited by dependence on the amplitude of the input signal. Partitioning the chassis effectively eliminated this problem.

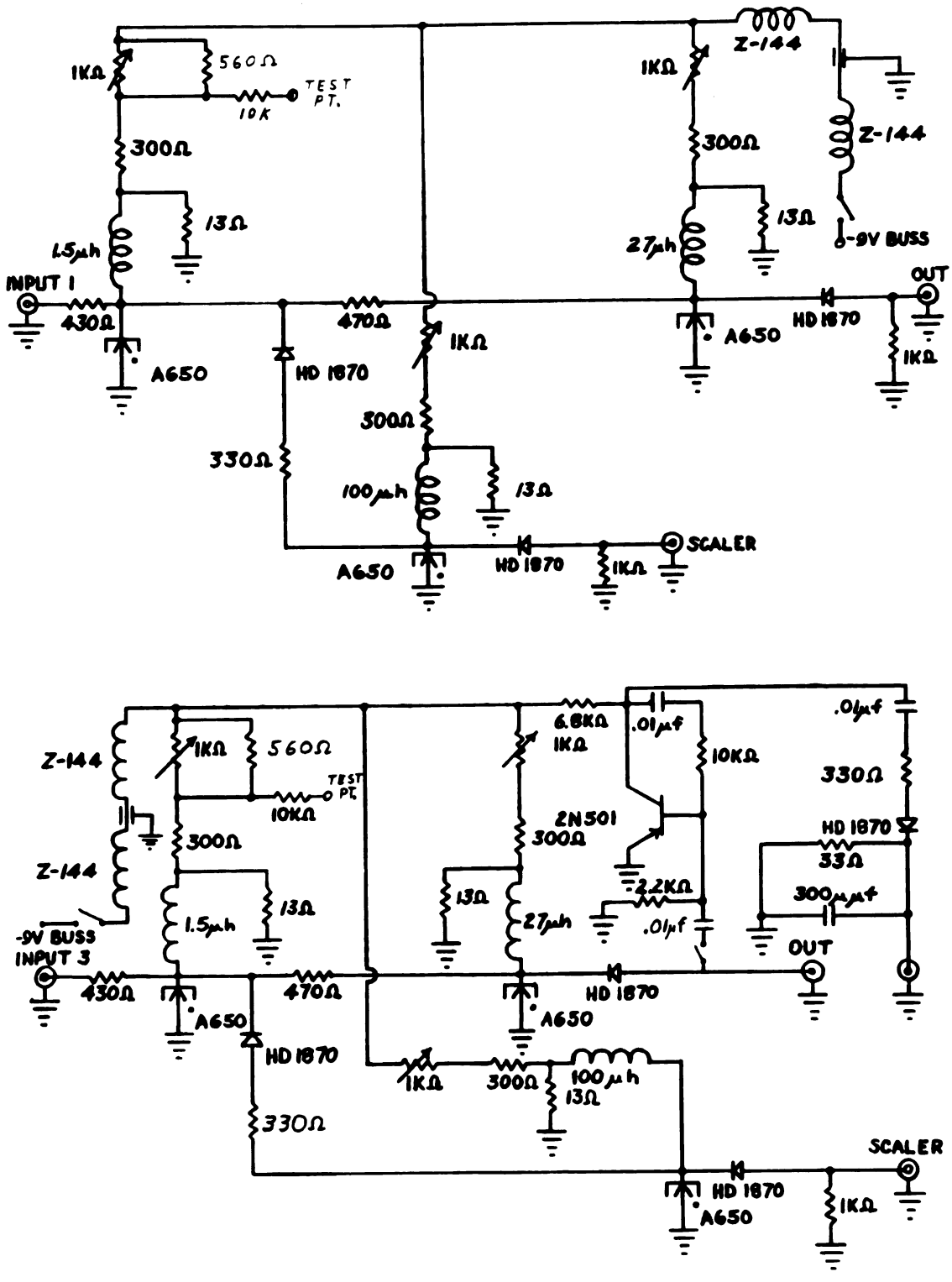

Figure B-1. Coincidence circuit diagrams.

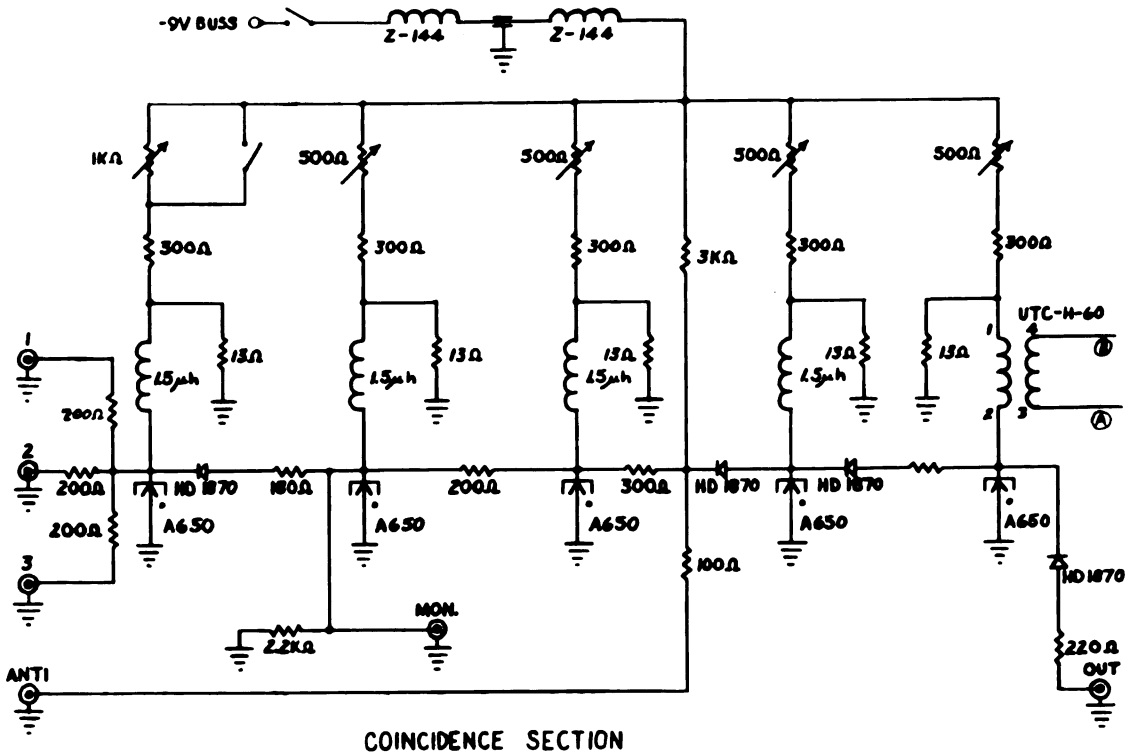

COINCIDENCE SECTION

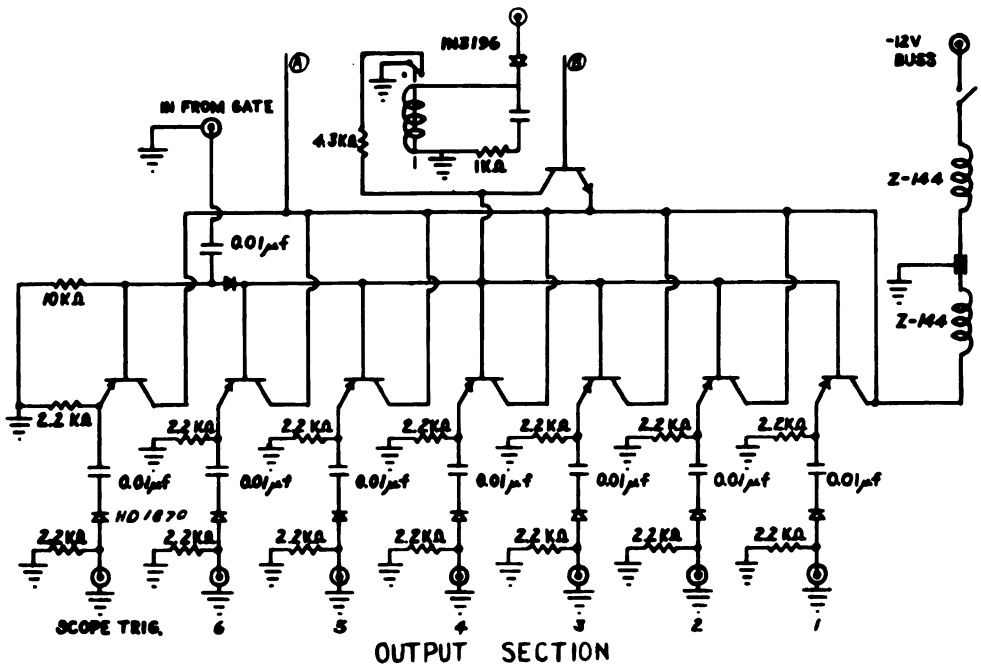

OUTPUT SECTION

Figure B-1a. Coincidence circuit diagrams, cont'd.

APPENDIX C: Modification of Tektronix 517 oscilloscope for π-μ-e display

As described in the main text, more than one method of identifying π-μ-e decay pulses on the 517 was attempted. The one which proved most reliable in the presence of large quantities of RF radiation from the spark discharge consisted essentially of programming the sweep of the 517 to produce a characteristic Z-trace as described in the main text.

To accomplish this several rather extensive modifications were made to the sweep gate and sweep amplifier circuits of the 517. A diagram of the most crucial modifications is given in Fig. C-1. These are the circuits responsible for (1) automatic sweep speed change after the first trace and (2) trace separation and marker pulse presentation.

As may be seen in Fig. C-1 the automatic sweep speed change was accomplished by using a 5727 thyratron to switch in a new timing capacitor (1200 $\mu\mu$f) for the slow sweep, after completion of the fast trace. The original timing capacitor C129J is adjustable to calibrate the fast trace, while the 25K rheostat shown serves to calibrate the slower trace. The 150 $\mu\mu$f capacitor serves for the duration of the first trace to effectively short the two resistances across which it is connected, but becomes of negligible effect in comparison with 1200 $\mu\mu$f by the time the second trace

is fully underway. The use of this 150 μμf capacitor proved to be an effective means of providing the proper charging resistance for each timing capacitor, in order to maintain a linear sweep.

The delay required before switching in the 1200 uuf capacitor for slow sweep was provided simply by the inherent delay involved in establishment of conduction in the thyratron, following application of plate potential. The plate potential is simply the potential appearing across C129J as it charges during the first sweep. The firing delay is a function of the bias potential present on the control grid of the 5727. Thus a variable bias potential was provided by the 10K rheostat by which it is possible to calibrate the firing of the thyratron to occur precisely at the end of the first trace.

When set for double sweep operation, the action started from the initial trigger pulse proceeds on its own, including horizontal retrace between sweeps. Automatic horizontal retrace is a direct consequence of the fact that in the 517 the sweep voltage appearing on the deflection plates is simply an amplified version of the instantaneous potential across the timing capacitor C129J as it charges with time. Thus when the uncharged 1200 μμf capacitor is switched across the fully charged C129J at the end of the first trace, the potential across it is reduced to approximately 1 per cent of its "full-

sweep" value. This action is passed along by the DC sweep amplifiers to the deflection plates as a very effective retrace (limited slightly by stray capacitance in the amplifier and deflection plates). The second trace begins immediately after retrace since the 1200 μμf begins to charge immediately upon being connected by the thyratron.

A ramp and marker generator was designed to produce a step voltage by which to separate the slower trace to a position on the screen below that of the fast trace. A schematic for this circuit is given in Fig. C-1. The rise time of this negative step function produces the vertical movement in the cross bar of the Z-trace as the beam is lowered after the first trace at the same time that the change of the timing capacitors is causing horizontal retrace. By the time the sweep speed change and retrace are complete the negative step function will also have reached its full amplitude where it remains throughout the slow trace.

The negative step function for sweep separation was obtained from the square negative pulse present at the first triode section of the 6DJ8. The leading edge of this wave form was delayed by a two-section RC delay network and then fed to the base of 2N501 transistor. This transistor was connected as an emitter-follower to provide a low impedance output to drive the vertical input of the scope.

The purpose of the 1N67 is to clip the signal into

the 2N501 at -10V. This method of signal limiting retains the short rise time associated with the high amplitude signal from the 6DJ8 circuit without overdriving the 2N501. The purpose of the 1N39 is to block passage of the negative step function back into the differentiation circuit attached to pin 6 of the 6DJ8.

A negative marker spike was obtained by differentiating the negative-going trailing edge of the wave form generated by the 6DJ8 monostable multivibrator circuit. The 2.5K trimpot which controls the period of the circuit was used to set the time of the marker pulse to be precisely 10 μsec after the arrival of each phototube pulse accepted by the coincidence circuit. The appearance of this marker pulse in each scope picture served as a continual calibration monitor on overall sweep time.

In addition to the modifications described above, several other incidental changes and additions were made in the 517. The two 6AG7 clamping tubes V112 and V113 used to discharge the timing capacitor following each trace were replaced by eight 6CL6 tubes for greater discharge current capacity and hence faster retrace. Two additional 6CL6 clamping tubes were inserted between pin 8 of V117 and ground to more quickly discharge the effective shunt capacitance of the positive deflection plate during retrace. This treatment should in principle have also been applied to the negative deflection plate. This was not done since sufficient benefit was obtained

from clamping the positive deflection plate as to make it no longer mandatory that it be done on the negative plate as well. Also because of the reversed polarity on the negative plate, clamping is difficult without arranging a more sophisticated circuit to control conduction in the clamping tubes than was required for the ones that were installed.

The R126 and the L105 in the trigger amplifier were increased by a factor of 5, to 1600Ω and 60 μh respectively, to increase the trigger signal for more stable triggering of the sweep gate circuit of V111 and V119.

The circuits added required power supply capabilities exceeding that of which the 517 power unit was capable. For this reason a supplemental power supply was constructed and installed in the scope to supply 6.3 V AC at 12 amperes, 6.3 V AC at 1 ampere, and -90 V DC regulated with 90C1 VR tube.

All of the above equipment was constructed on chassis plates and installed within the case of the 517 indicator unit. Subsequently, however, it became apparent that the 180 V DC regulated supply within the scope was being overloaded by portions of the modification circuits. Therefore an additional 180 V DC supply was used to supply the new circuits. No further overload symptoms in the main power supply were encountered.

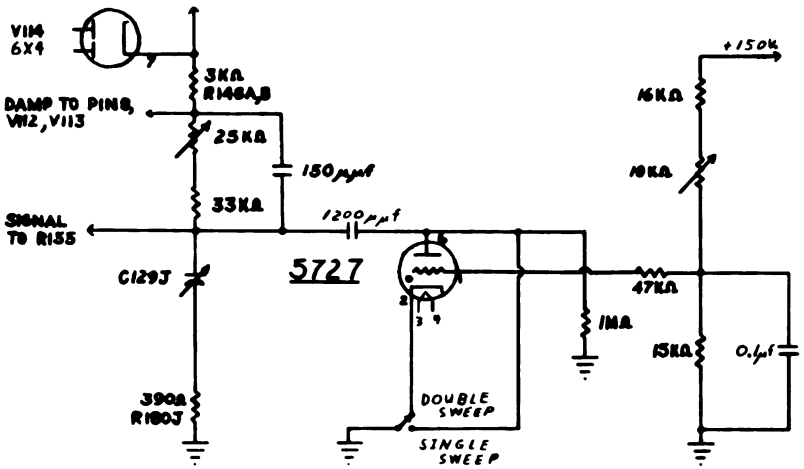

AUTOMATIC SWEEP CHANGE CIRCUIT

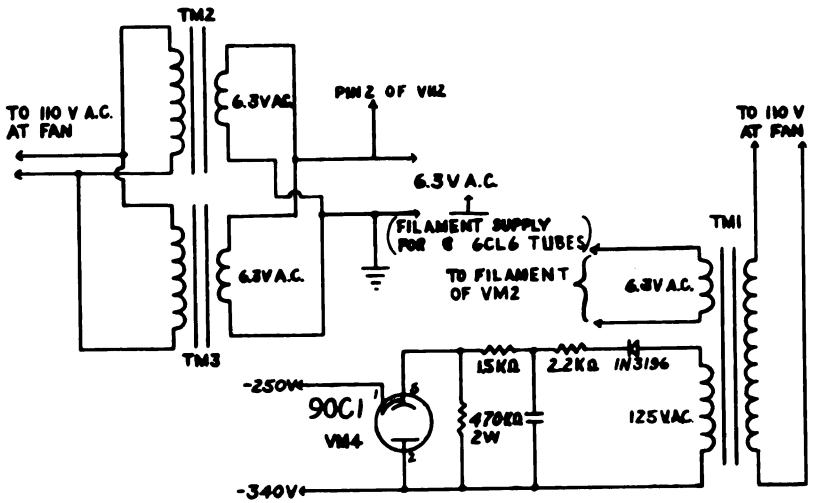

SUPPLEMENTARY POWER SUPPLY

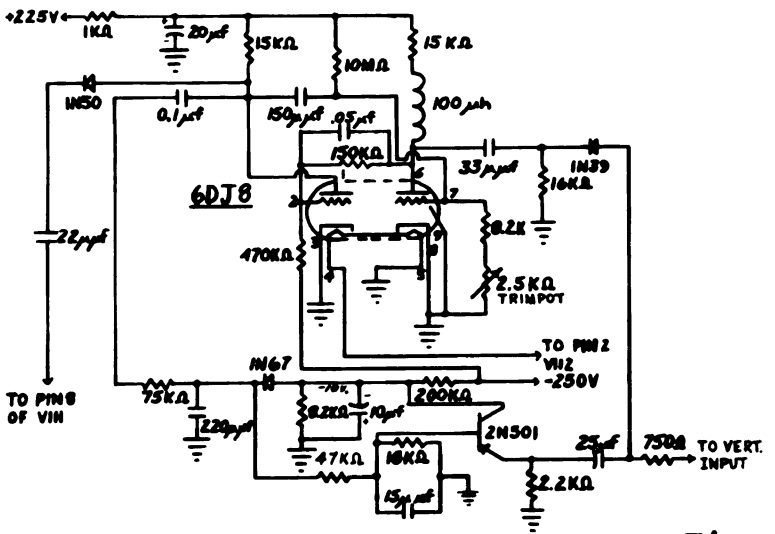

RAMP & MARKER GENERATOR

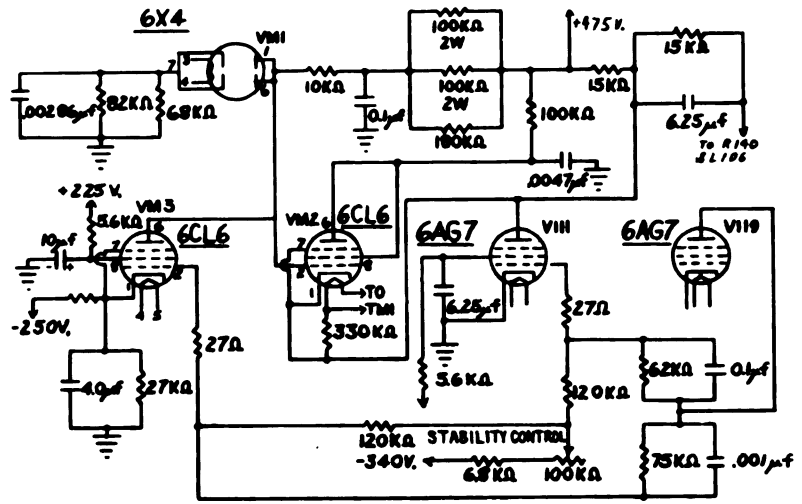

SWEEP GATE CIRCUIT (AS ALTERED)

Figure C-1

APPENDIX D: The automatic camera system

To make continuous automatic operation of the spark chamber possible an automatic film advance camera system was designed and constructed for this experiment. The cameras used were Graflex units accepting 100 foot rolls of 35 mm film. These were motorized by the addition of a 120 rpm gear motor on each to drive the sprocket directly, with a cam attached to the sprocket shaft to operate a microswitch upon each one-third turn of the shaft. Short framing was employed in order to obtain as many photographs on a 100 foot roll of film as possible. For each frame the film was advanced approximately one inch by a 120 degree rotation of the sprocket shaft. This allows 1200 frames per roll instead of 800 for the standard one and one-half inch frame spacing used for 35 mm film.

The camera motors were controlled by a circuit for which a schematic diagram is given in Fig. D-1. Each motor was a two pole induction type operating on 24 V AC, which can be very effectively brought to an abrupt stop by substitution of 30 V DC for the AC driving voltage. This DC braking procedure made possible accurate frame spacing as indexed by the cam and microswitch assembly on each motor. The central motor control circuit also controlled the synchronized advance of frame indexes placed in view of the cameras. To simplify spark gap identification during analysis, illuminating lights were

also controlled by this circuit to expose the frame count on the film in each camera, and to expose the front edges of the spark chamber plates upon the film of the chamber camera.

A resume of the sequence of camera advance operations is as follows: In the spark chamber high voltage pulse chassis was located a sensing circuit to trigger the camera circuit upon each spark chamber discharge. This was accomplished by looping a current pick up around the plate lead of one of the 6279 thyratrons. The signal induced in this lead upon discharge triggers a 6DJ8 monostable multivibrator which in turn energizes a 6C4 triode having the coil of a DPST relay in its cathode. The closing of this relay completes the 24 V AC circuit to start the camera motors and switches the 125 V DC to the sequencing relays that control the remainder of the camera and lighting functions.

The first step in the sequence that follows is that simultaneous with the starting of the camera motors is the activation of the blanking relays: three in the chamber circuit (one for each 6279 to prevent discharge during the camera advance operation, see Fig. A-1), and one in the coincidence circuit (see Fig. B-1). Each of these relays has its own timing capacitor to determine the hold time after the 125 V DC sequence-starting voltage has been removed. Also the starting of the camera motors activates relay RL2 through which their AC current flows. This

3PDT relay connects the two 10 μf capacitors in the light timing circuits to 125 V DC for charging while the motors are advancing the film. The third pole on RL2 serves to activate another relay which controls the frame indexes, advancing them one count. The duration of the voltage pulse delivered to these indexes was lengthened by the timing capacitor on this index advancing relay, for more reliable index response. When the film has been advanced one frame, the motors are stopped by the DC braking current. Following automatic termination of the braking current relay RL_2 releases. Release of RL_2 connects each of the light timing capacitors to its respective light relay which in turn illuminates the chamber and scope frame indexes for the respective durations for which S_{1A} and S_{1B} are set. The timing range available for these lights is 1/2, 1/4, 1/8, 1/16 second, with the setting chosen for suitable exposure of the frame numbers in each case.

The control of the motors for proper frame spacing occurs as follows: Upon initiation of the camera advance cycle, relay RL_4 receives 125 V DC as do the blanking relays, etc., as described above. The adjustable series resistance and shunt capacitor preceding this relay provide a delay in the operation of RL_1 sufficient to assure that both camera motors have turned far enough from their rest positions to release the microswitch from its "index" position to the "run" position. In this

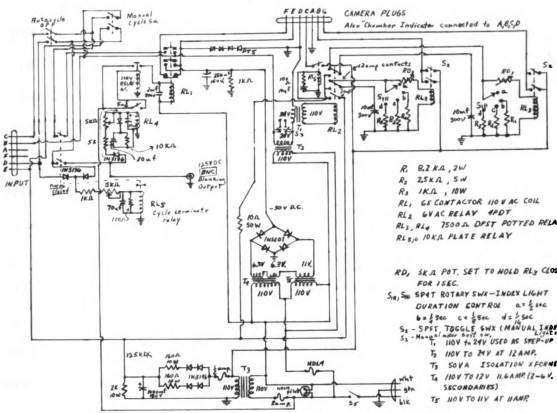

CAMERA ADVANCE CIRCUIT

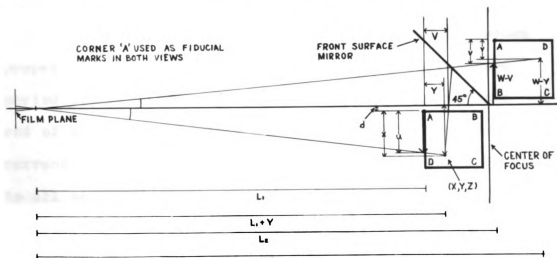

OPTICAL GEOMETRY OF EXPERIMENT

FIGURE D-1.

run condition the motor receives 24 V AC directly. The time delay on RL_4 is such that the large contactor RL_1 is activated soon after the time when the microswitch in both cameras has been placed in the run position. At this time the index lead to the motors is converted by RL_1 from 24 V AC to 30 V DC. Thus whenever each motor again reaches its index position at the next frame location, its microswitch transfers the motor coil to the index line where the 30 V DC present there provides sufficient DC current to effect complete braking in less than 1/30 of a revolution of the sprocket (based on a maximum of 1/2 revolution of the motor shaft and 14:1 gear reduction to the sprocket shaft). This is equivalent to frame indexing to better than 10 per cent in less than 0.2 second motor travel time per frame. This short camera cycling time was desirable to minimize the dead time of the apparatus.

The cycle terminating relay RL_5 served to assure proper termination of the cycle after a predetermined period for protection of the motor coils which at the end of their travel carry a high value of DC braking current. Relay RL_5 served to interrupt the 125 V DC to all sequencing relays, each of which in turn released at a time governed by its own timing capacitor as described above. A further purpose served by RL_5 was the uniform termination time it provided for the entire sequence, especially on manual camera cycling, regardless

of how long the manual switch may be depressed. Following termination by RL_5 the main motor relay RL_1 is deactivated at a time controlled by RL_4 such that both cameras have certainly completed their framing and have come to rest. The blanking relays in the chamber and coincidence circuits (mentioned above) were set to drop out last of all, making the apparatus sensitive once again to the transit of the next acceptable particle. The coincidence circuit blanking relay is in fact the last to return to normal operating position to prevent the arcing of any other motor relay from inducing a spurious signal in the coincidence unit, as this would have resulted in continuous cycling of the camera system.

The camera cycling system described above proved to be a very reliable one. There was a fairly regular mortality rate on the microswitch operated by each motor cam and this was due to a calculated risk taken on the current rating of the type of microswitch chosen. The choice was dictated by the desired physical properties of size and mounting type. But this system, which included several improvements to cure early operational ills, performed in excess of 500,000 camera cycles without serious maintenance problems.

APPENDIX E: Momentum determination

The momentum of the muons studied was determined using the total depth of stopping material penetrated following observation in the spark chamber until coming to rest in the stopping counter. Referring to Fig. II-1 for vertical dimensions of the apparatus, there existed, in addition to the 40-inch lead pile, a 1/2-inch thick aluminum plate upon which the chamber is mounted and a 1/4-inch thick steel plate upon which the lead pile rests. The total stopping thickness in gm/cm^2 was found from the formula

$$R_{(gm/cm^2)} = \sum_i \rho_i d_i \epsilon_i$$

where ρ_i is the density of the i-th type of stopping material; d_i is the total depth in centimeters of the i-th type of material; and ϵ_i is the relative efficiency of this material as an absorber compared to Pb. The average density of the lead bricks used in this experiment was determined to be 11.08 gm/cm^3, while the remaining densities were taken from the handbook. The ϵ_i values for aluminum and iron were taken from information contained in Cosmic Ray Physics[15] by Dr. D. J. Montgomery.

Using these values

$R = (11.08\ gm/cm^3)(40\ in)(2.54\ cm/in)(1) + (2.70\ gm/cm^3) \cdot (\frac{1}{2}\ in)(2.54\ cm/in)(1.46) + (7.6\ gm/cm^3)(\frac{1}{4}\ in) \cdot (2.54)(1.25) = 1137\ gm/cm^2$ (Pb equivalent)

This corresponds to 1.56 Bev/c[15] for the momentum of the muons passing through the chamber. This value of the momentum is the minimum value a particle may have if it enters the apparatus from a vertical direction. Muons entering from directions lying at some non-zero angle with respect to the vertical will have a somewhat larger depth of stopping material through which to pass in reaching the stopping counter. The maximum value this may have is determined by the maximum angle about the vertical which can be accepted by the geometry of the counter telescope arrangement. It was determined from the tabulated experimental measurements of the incoming track direction with respect to the vertical Z axis, that 95 percent of all accepted events entered the apparatus within a vertical cone extending 15.4 degrees from the vertical. Using this angle the corresponding maximum path length in lead was calculated from right triangle geometry to be $(40'') \sqrt{1 + \tan^2 (15.4^o)} = 41.5''$. The corresponding maximum range in lead is 1178 gm/cm^2. In calculating the range for the fastest particles accepted by the apparatus, the effective stopping power of the stopping counter must be included. This counter has a usable thickness of 6-inches, a density of 0.9 gm/cm^3 and an absorbing efficiency of 1.90 from the same curves used above[15]. This yields a range contribution of 26.0 gm/cm^2. The maximum total range of an acceptable particle (i.e., that stopped in the stopping counter)

is then 1204 gm/cm^2. This corresponds to a maximum momentum of 1.65 Bev/c. The median momentum for this experiment was taken as 1.60 Bev/c; this is slightly less than the arithmetic mean of 1.605 Bev/c. This choice is based on the fact that the relative muon incidence rate decreases as the cosine^2 of θ_{IN} measured from the vertical, the effect of which can be seen in the data for incoming tract direction. Thus the momentum of the muons in this experiment was taken to be 1.60 Bev/c + 0.05, - 0.04 or approximately 1.60 Bev/c ± 2.8%.

In view of the narrow momentum limits held in this experiment, it was unnecessary to integrate over the muon intensity distribution within the accepted range interval. This results from the fact that the ± 2.8% spread in momentum stated above causes an expected change of only ± 1.8% in the muon incidence rate as determined from the plot of the differential muon range spectrum found in the cosmic ray survey article by B. Rossi[16]. Further, it can be seen from the equations of Section IV. A. that the major effect of the value of pc upon the predicted scattering distribution is its effect on the conversion factor between the variable x used in the calculation and the projected angle variable φ. Specifically φ is proportional to x/pc, where x is the reduced scattering variable used in the theory. Thus a ± 2.8% spread in momentum causes

only a ± 2.77% change in the value of the scattering distribution in its region of steepest slope (in the vicinity of 1.0 degree) and less change for other values of angle φ. The uncertainty resulting from assuming the momentum to be a constant is therefore sufficiently small to be neglected.

APPENDIX F:

```
      PROGRAM SPARK
    2 DIMENSION MNAME(50),PZS(35),PY(35),PZ(35),PX(35),TITLE(10)
      DIMENSION NAME(50),X(35),Y(35),Z(35)
   30 FORMAT(10A8)
   31 FORMAT(4I10)
    4 REWIND 4
    5 REWIND 5
    6 READ 30,(TITLE(I),I = 1,10)
    8 PRINT 30,(TITLE(I),I = 1,10)
    9 READ 31, NPAGE,NETOT, NSTOT, NMAX
   10 CALL TAPE1(KARDZ)
   14 CALL SPAC1(NPAGE,NETOT,NSTOT)
      STOP
   16 END



      SUBROUTINE TAPE1(KARDZ)
      DIMENSION MNAME(50),NAMES(50),NAMER(50),PX(35),PY(35),PZ(35)
      DIMENSION PZS(35), R(14), X(35), Y(35), Z(35)
      DIMENSION TITLE(10)
   16 FORMAT(1I6,4I1,14F5.5)
   18 FORMAT(102H DATA CARD IS NOT FOR THE SAME EVENT. CHECK ORDER OF CA
  181RDS FOR EACH EVENT. THE EVENT NUMBER SHOULD BE ,I6/40H THE CARD OU
  182T OF ORDER HAS EVENT NUMBER ,I6,4I4)
   19 FORMAT(11H DATA CARD ,I6,4I1,44H HAS THE WRONG VIEW NUMBER IN COLU
  191MN SEVEN. )
   20 FORMAT(11H DATA CARD ,I6,4I1,44H HAS THE WRONG CARD NUMBER IN COLU
  201MN EIGHT. )
   21 FORMAT( 36H THERE ARE TOO MANY CARDS FOR EVENT ,I6,34H.  CHECK DAT
  211A DECK FOR THIS EVENT.)
  131 FORMAT(1H1,1H ,40X,32H LIST OF EVENTS STORED ON TAPE 4 /)
  134 FORMAT(40X,I3,5X,I6)
   30 FORMAT(10A8)
  137 FORMAT(1H1,1H ,40X,20H REJECTED DATA LIST.   /1H ,10X, 47HTHIS DAT
 1371A IS REJECTED DUE TO DECK OUT OF ORDER.  //)
```

```
31 READ 30,(TITLE(I),I = 1,10)
   PRINT 30,(TITLE(I),I = 1,10)
   AL1 = 222.898
   AL2 = 234.033
   AW = 11.144
   AD = 0.5
   AL1 = (2.54)*AL1
   AL2 = (2.54)*AL2
   AW = (2.54)*AW
   AD = (2.54)*AD
32 KARDZ = 0
33 WRITE TAPE 4, KARDZ
   JEND = 1
36 JA = 0
   JB = 0
   I = 0
   NOW = 0
37 IF(JEND)40,45,40
40 IF(I - 50)41,122,122
41 MCARD = 0
44 READ              16, NAME,IA,IB,IC,ID,(R(J),J = 1,14)
45 I = I + 1
46 MNAME(I) = NAME
   NOW = NOW + 1
47 DO 48 K = 1,35
   PX(K) = 0
   PY(K) = 0
   PZ(K) = 0
48 PZS(K) = 0
49 IF(999990 - MNAME(I))195,50,50
50 KARDZ = KARDZ + 1
60 GO TO 74
70 READ              16, NAME,IA,IB,IC,ID,(R(J),J = 1,14)
71 IF(MNAME(I) - NAME)72,74,72
72 PRINT 18,MNAME(I),NAME,IA,IB,IC,ID
   GO TO 115
```

```
 74 IF(IA)174,75,174
174 IF(2-IA)75,76,76
 75 PRINT 19;NAME,IA,IB,IC,ID
    GO TO 115
 76 IF(IB)176,77,176
176 IF(5-IB)77,80,80
 77 PRINT 20,NAME,IA,IB,IC,ID
    GO TO 115
 80 MCARD = MCARD + 1
 81 GO TO(90,92),IA
 90 CALL SORTA(IB,PX,PZ,R)
 91 GO TO 95
 92 CALL SORTA(IB,PY,PZS,R)
 95 IF(10 - MCARD)97,102,70
 97 PRINT 21,MNAME(I)
    GO TO 115
102 CALL SPAC(AL1,AL2,AW,AD,X,Y,PX,PY,PZ,PZS,NAME,NOW,Z)
105 WRITE TAPE 4,MNAME(I) , (X(L),Y(L),Z(L),L = 1,35)
106 JA = JA + 1
107 NAMES(JA) = MNAME(I)
108 GO TO 120
115 JB = JB + 1
    NAMER(JB) = MNAME(I)
116 IF(MNAME(I) - NAME)118,117,118
117 READ              16, NAME,IA,IB,IC,ID,(R(J),J = 1,14)
    GO TO 116
118 KARDZ = KARDZ - 1
    MCARD = 0
    IF(I - 50)45,119,119
119 JEND = 0
    GO TO 130
120 IF(999990 - MNAME(I))129,129,40
122 JEND = 1
123 GO TO 130
129 JEND = 2
130 PRINT 131
```

```
132 DO 135 J = 1,JA
133 PRINT 134,J,NAMES(J)
135 CONTINUE
136 PRINT 137
138 DO 140 K = 1,JB
139 PRINT 134,K,NAMER(K)
140 CONTINUE
141 IF(JEND - 2)36,195,195
195 ENDFILE 4
196 REWIND 4
200 RETURN
201 END
```

```
    SUBROUTINE SORTA(IB,X,Z,R)
  2 DIMENSION R(14),X(7),Z(7)
 10 GO TO(12,17,22,27,32),IB
 12 DO 15 I = 1,7
 13 X(I) =R(2*I - 1)
 14 Z(I) = R(2*I)
 15 CONTINUE
 16 GO TO 40
 17 DO 20 I = 8,14
 18 X(I) = R(2*I - 15)
 19 Z(I) = R(2*I - 14)
 20 CONTINUE
 21 GO TO 40
 22 DO 25 I = 15,21
 23 X(I) = R(2*I - 29)
 24 Z(I) = R(2*I - 28)
 25 CONTINUE
 26 GO TO 40
 27 DO 30 I = 22,28
 28 X(I) = R(2*I - 43)
 29 Z(I) = R(2*I - 42)
```

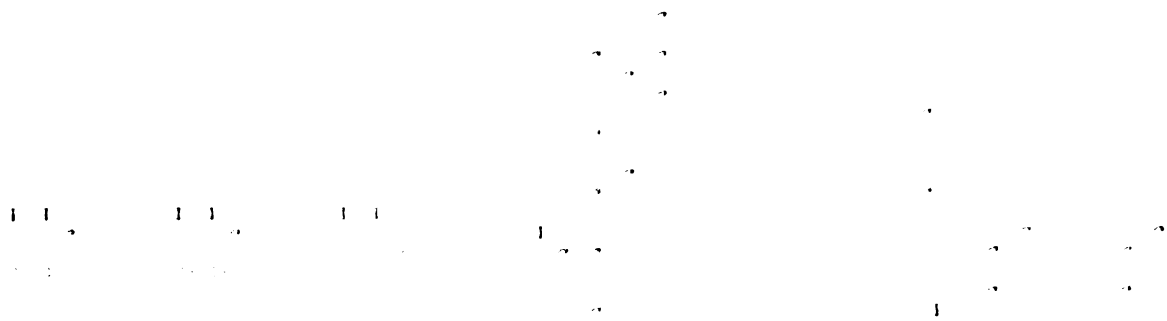

```
30 CONTINUE
31 GO TO 40
32 DO 35 I = 29,35
33 X(I) = R(2*I - 57)
34 Z(I) = R(2*I - 56)
35 CONTINUE
36 DO 37 K = 1,14
37 R(K) = 0.0
40 RETURN
41 END


   SUBROUTINE SPAC(AL1,AL2,AW,AD,X,Y,PX,PY,PZ,PSZ,NAME,KK,Z)
 2 DIMENSION NAME(50),PX(35),PY(35),PZ(35),PSZ(35),X(35),Y(35),Z(35)
10 IF(PX(2))12,11,12
11 TA = 0.07525
   TB = 0
   GO TO 13
12 TA = PZ(2)-PZ(1)
   TB = PX(2)- PX(1)
13 PSLOPE = TB/TA
14 IF(PY(2))16,15,16
15 TC = 0.07160
   TD = 0
   GO TO 17
16 TC = PSZ(2)-PSZ(1)
   TD = PY(2)-PY(1)
17 QSLOPE = TD/TC
23 FD = (22,780625)/TA
   FS = (22,780625)/TC
   P1Z = PZ(1)
   P1SZ = PSZ(1)
   DO 32 K = 1,35
25 IF(PZ(K))26,28,26
26 PZ(K) = PZ(K) - P1Z
```

```
      PZ(K) = FD*PZ(K)
   28 IF(PSZ(K))29,31,29
   29 PSZ(K) = PSZ(K) - P1SZ
   30 PSZ(K) = FS*PSZ(K)
   31 PY(K) = FS*PY(K)
   32 PX(K) = FD*PX(K)
   35 SC = AL1 + AW
   36 SD = AL1*AL2
   37 P1X = PX(1)
   40 DO 58 I = 3,35
   41 Z(I)=(PZ(I)+PSZ(I))/(2.0)
   42 IF(PX(I))44,43,44
   43 X(I) = 0
      Y(I) = 0
      GO TO 58
   44 IF(PY(I))45,43,45
   45 QU = PX(I) - (P1X + PSLOPE*Z(I)) + AD
   46 QV = PY(I) - (PY(1) + QSLOPE*Z(I))
   47 SA = 1.0 + QV/AL1
   48 SB = AW - QV
   50 SE = (QU*SB)/SD  + 1.0
   52 SF = 1.0 + (QU)*(SC/SD)
   54 X(I) = (QU*SA)/(SE) - AD
   56 Y(I) = AW - (SB*SF)/(SE)
   58 CONTINUE
   60 RETURN
   61 END


      SUBROUTINE SPAC1(NPAGE,NETOT,NSTOT)
      DIMENSION NAME(50),X(35),Y(35),Z(35)
      DIMENSION ALPO(50),ALPI(50),BETO(50),BETI(50),EROS(50),EROD(50)
      DIMENSION ERIS(50),ERID(50),YOO(50),YOI(50),XOO(50),XOI(50)
      DIMENSION NOS(50),NOD(50),NIS(50),NID(50),THETO(50),THEGI(50)
```

```
   DIMENSION ANALI(50),ANALO(50),ANBEI(50),ANBEO(50),THEDD(50),THEDS(
  150),THEDDC(50),THEI(50)
   DIMENSION FII(50),IQI(50),FIO(50),IQO(50),NAMES(50),NAMER(50)
   DIMENSION TITLE(10)
   DIMENSIONXA(26),XB(26),YA(26),YB(26),ZA(26),ZB(26),ZSA(26),ZSB(26)
   DIMENSION NAMGI(50)
   DIMENSION NFII(110),NFIO(110),NTHI(110),MFII(110),MFIO(110),MTHI(1
  110),NZD(110),MTHEDCP(110)
   DIMENSION NTHEI(110),MTHEI(110),NTHEDCP(110),NTHEDCN(110),
  1MTHEDCN(110), NALPTP(110),NALPTN(110),MALPTP(110),MALPTN(110)
   DIMENSION LNAME(50)
15 FORMAT(4F7.3)
30 FORMAT(10A8)
81 FORMAT(1H1,1H ,55X,9HLINE DATA ,41X,5HPAGE ,14//
811                                20X,16H  INCOMING TRACK ,45X,14HOUTG
8120ING TRACK/   5X,1HX,7X,5HALPHA,7X,1HY,8X,4HBETA,7X,11HCORRELATION
813,9X,1HX,7X,5HALPHA,7X,1HY,8X,4HBETA,7X,11HCORRELATION/10H INTERCEP
814T,11X,9HINTERCEPT,13X,6HDIRECT,4X,6HSTEREO,2X,9HINTERCEPT,11X,9HIN
815TERCEPT                ,13X,6HDIRECT,4X,6HSTEREO//69X,9HEVENT NO.
  6/)
83 FORMAT(1H ,   43X,1I1,9X,1I1,15X,I6,29X,1I1,
  1                                        9X,1I1/2H  ,F8.3,2X,F8.4,2
  22X,F8.3,2X,F8.4,3X,F6.4,4X,F6.4,3X,F8.3,2X,F8.4,2X,F8.3,2X,F8.4,
  33X,F6.4,4X,F6.4 )
86 FORMAT(1H1,1H ,52X,16HSPACE ANGLE DATA ,37X,5HPAGE ,14//
  1                              13X,14HINCOMING TRACK,28X,14HOUTGO
  2ING TRACK/            7X,8HANGLE FI, 5X,8HQUADRANT,7X,8HTHETA IN,
  36X,8HANGLE FI,
  410X,8HQUADRANT ,11X,5HTHETA,16X,13HTHETA GREATER   /6X,9H(DEGREES)
  5, 4X,10H(5=NORMAL),11X, 9H(DEGREES),16X,12H(5 = NORMAL),7X,9H(DEGR
  6EES),14X,13HTHAN 1 DEGREE//58X,9HEVENT NO./)
88 FORMAT(59X,16/7X,F8.3, 8X,I1,10X,F8.3,5X,F8.3,
  1                                    15X,I1,13X,F8.3,18X,F8.3)
91 FORMAT(53X,15HREJECTED EVENTS // 93H     THESE EVENTS ARE REJECTED
911 FOR INSUFFICIENT DATA POINTS.
94 FORMAT(20X,13,5X,16)
```

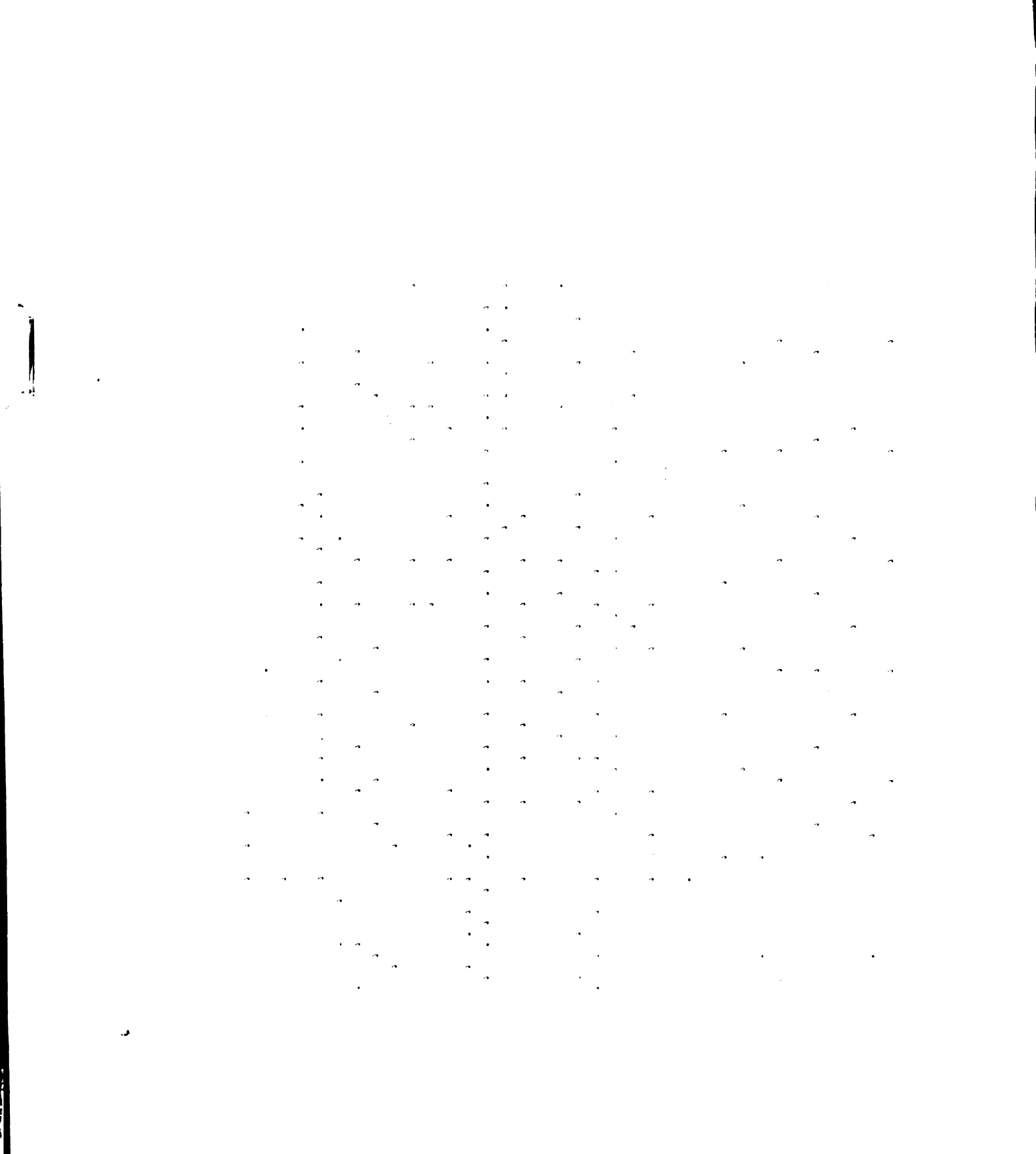

```
 96 FORMAT(1H1)
 98 FORMAT(1H1,        35X,17HLAST PAGE NUMBER ,14/1H ,35X,43HTOTAL NU
 981MBER OF EVENTS PROCESSED TO DATE=  ,18/1H ,35X,29HTOTAL NUMBER SAV
 982ED TO DATE=    ,18/1H ,35X,       42HNUMBER OF EVENTS SAVED DURING
 983THIS RUN=    ,14//1H ,42X,35HEVENT NUMBERS SAVED DURING THIS RUN /
 98430X,           58HLIST OF EVENTS WITH SPACE ANGLES GREATER THAN O
 985NE DEGREE      /)
100 FORMAT(1H ,50X,I3,10X,I6)
153 FORMAT(1H1,1H ,15X,7HFI IN    ,10X,I5//1H ,18X,32HPARTITIONED IN 10
   1DEG. INTERVALS. //(1H ,14X,I5))
253 FORMAT(1HO,14X,I5)
161 FORMAT(1H1,1H ,15X,7HFI OUT   ,10X,I5//1H ,18X,32HPARTITIONED IN 10
   1DEG. INTERVALS. //(1H ,14X,I5))
162 FORMAT(1H1,1H ,15X,7HTHETA    ,10X,20HNUM. 7DEG. OR MORE= ,I5//
   11H ,19X,34HPARTITIONED IN 0.25DEG. INTERVALS. //(1H ,14X,I5))
169 FORMAT(1H1,1H ,15X,23HTHETA IN (ZENITH ANGLE),10X,20HNUM. 20DEG. O
   1R MORE= ,I5//1H , 19X,34HPARTITIONED IN 0.20DEG. INTERVALS. //
   2(1H ,14X,I5))
171 FORMAT(1H1,1H ,10X,31HTHETA DIR., PROJ. DEFL. (CORR.),10X,
   121HNUM. +7DEG. OR MORE= ,I5,10X,21HNUM. -7DEG. OR LESS= ,I5//1H ,
   214X, 34HPARTITIONED IN 0.25DEG. INTERVALS.,44X,19HNUM. EXACTLY ZER
   30= ,
   415,  //1H ,12X,4HPOS.,20X,4HNEG.//(1H ,10X,I5, 23X,I5)//10,I5,
   523X,I5)
271 FORMAT(1HO,25X,I5)
173 FORMAT(1H1,1H ,10X,33HALPHA DIR., PROJ. ANGLE (UNCORR.),10X,
   121HNUM. +20DEG. OR MORE=,I5,10X,21HNUM. -20DEG. OR LESS=,I5//1H ,
   214X, 34HPARTITIONED IN 0.20DEG. INTERVALS.,44X,19HNUM. EXACTLY ZER
   30= ,
   415,  //1H ,12X,4HPOS.,20X,4HNEG.//(1H ,10X,I5, 23X,I5)//10X,I5,
   523X,I5//25X,I5)
201 FORMAT(1H1,53X,15HREJECTED EVENTS   / 78H  THESE EVENTS REJECTED B
2011ECAUSE R**2 LESS THAN 0.960. REMEASURE THESE EVENTS.          /)
 31 READ 30,(TITLE(I),I = 1,10)
 32 PRINT 30,(TITLE(I),I = 1,10)
    NRUN = 0
```

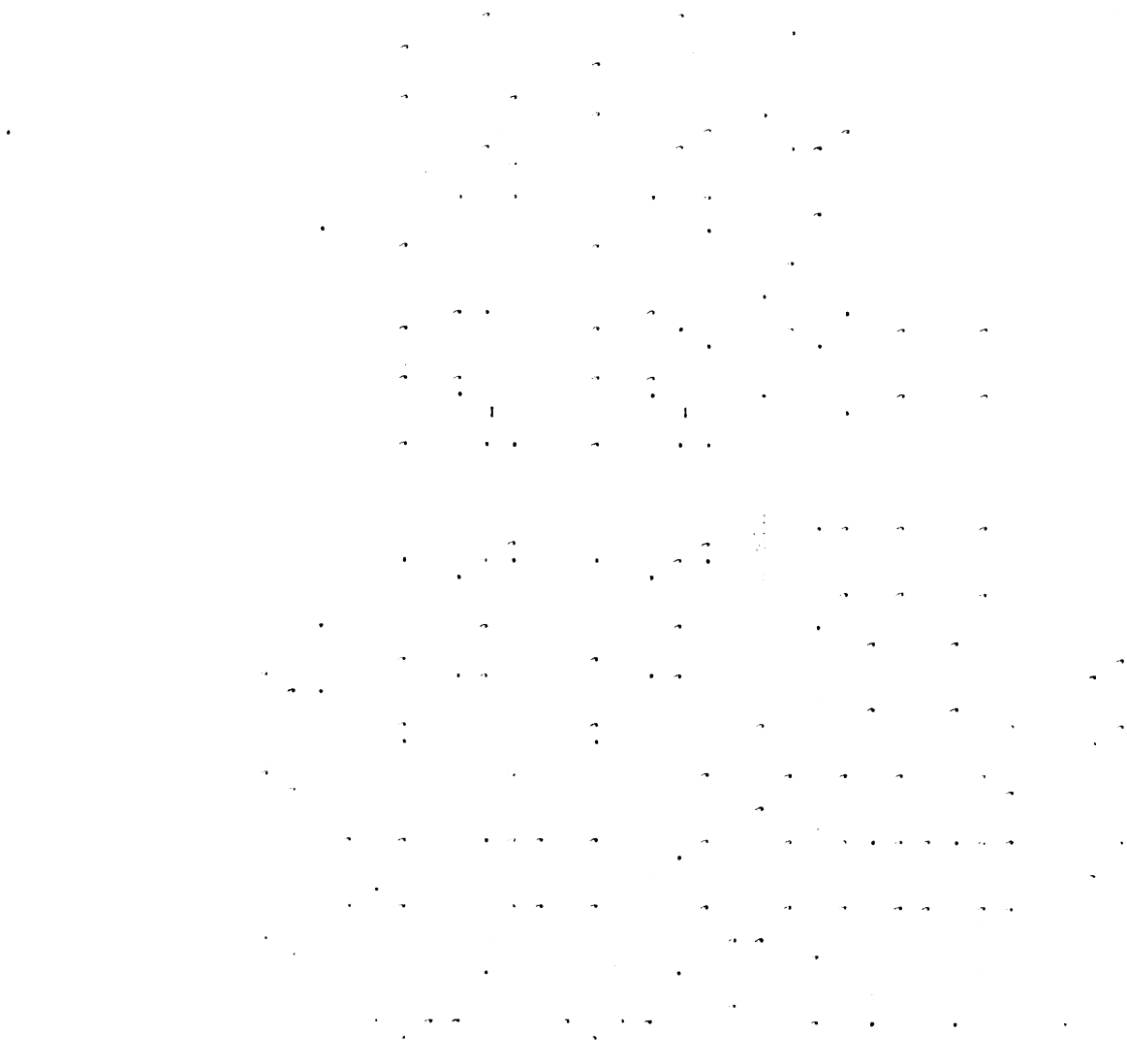

```
      NPRO = 0
      NCRUN = 0
      WRITE TAPE 5,NRUN
      ENDFILE 5
      BACKSPACE 5
      DO 33 I = 1,110
      MALPTP(I) = 0
      MALPTN(I) = 0
   33 MTHEI(I) = 0
      DO 34 I = 1,52
      MFII(I) = 0
      MFIO(I) = 0
      MTHI(I) = 0
      MTHEDCP(I) = 0
   34 MTHEDCN(I) = 0
      MFIG = 0
      MFOG = 0
      MTHG = 0
      MTHEIG = 0
      MTHDCGP = 0
      MTHDCGN = 0
      MTHDCGO = 0
      MALPTGP = 0
      MALPTGN = 0
      MALPTGO = 0
      MFIIT = 0
      MFIOT = 0
      MTHIT = 0
      LTHEDCP = 0
      LTHEDCN = 0
      LTHEDC = 0
      MTHEIT = 0
      MALPTPT = 0
      MALPTNT = 0
      MALPTT = 0
   35 READ TAPE 4,IKM
```

```
      IF(EOF,4)36,36
   36 IK = 0
      JA = 0
      JB = 0
      JC = 0
   37 IF(IKM - NPRO)41,41,41
   38 IF(NAME(IK) - 1000000)36,99,99
   41 IK = IK + 1
   42 READ TAPE 4,NAME(IK),(X(L),Y(L),Z(L),L = 1,35
      IF(EOF,4)74,43
   43 NETOT = NETOT + 1
      CALL CURV(X, Z,ALPB,XOB,ALPT,XOT,ID,RRBD,RRTD,SDEVBD,SDEVTD,NBD,NT
     1D,XA,ZA,XB,ZB,IE)
      IF(IE - 3)44,50,44
   44 IF(ID- 3)45,48,45
   45 CALL CURV(Y, Z ,BETB,YOB,BETT,YOT,ID,RRBS,RRTS,SDEVBS,SDEVTS,NBS,N
     1TS,YA,ZSA,YB,ZSB,IE)
      IF(IE - 3)47,50,47
   47 IF(ID - 3)49,48,49
   48 JB = JB + 1
      NAMER(JB) = NAME(IK)
      GO TO 72
   50 JC = JC + 1
      LNAME(JC) = NAME(IK)
      GO TO 72
   49 JA = JA + 1
      NCRUN = NCRUN + 1
      NAMES(JA) = NAME(IK)
   52 CALL QUAD(ALPT,BETT,IQT,FIT)
      FII(JA) = FIT
      IQI(JA) = IQT
   54 CALL QUAD(ALPB,BETB,IQB,FIB)
      FIO(JA) = FIB
      IQO(JA) = IQB
   60 THETO(JA) = (57.296)*THETA(ALPB,ALPT,BETB,BETT)
   61 ANG = THETO(JA)
```

```
      NID(JA) = NTD
      NIS(JA) = NTS
      NOD(JA) = NBD
      NOS(JA) = NBS
      XOI(JA) = XOT
      XOO(JA) = XOB
      YOI(JA) = YOT
      YOO(JA) = YOB
      ERID(JA) = RRTD
      ERIS(JA) = RRTS
      EROD(JA) = RRBD
      EROS(JA) = RRBS
      ALPI(JA) = ALPT
      ALPO(JA) = ALPB
      BETI(JA) = BETT
      BETO(JA) = BETB
      ANBETT = ATANF(BETT)
      ANBET = ABSF(ANBETT)
      COSBET = COSF(ANBET)
      ALPOT = ALPT*COSBET
      ALPOB = ALPB*COSBET
      ANALPT = (57.296)*ATANF(ALPOT)
      ANALPB = (57.296)*ATANF(ALPOB)
      THEDDC(JA) = ANALPB - ANALPT
      ANALI(JA) = (57.296)*ATANF(ALPT)
      ANALO(JA) = (57.296)*ATANF(ALPB)
      ANBEI(JA) = (57.296)*ATANF(BETT)
      ANBEO(JA) = (57.296)*ATANF(BETB)
      THEDD(JA) = ANALO(JA) - ANALI(JA)
      THEDS(JA) = ANBEO(JA) - ANBEI(JA)
      TANTHI = SQRTF(ALPT*ALPT + BETT*BETT)
      THEI(JA) = (57.296)*ATANF(TANTHI)
   65 IF(THETO(JA) - 1.0)70,66,66
   66 THEGI(JA) = ANG
   67 WRITE TAPE 5,NAME(IK) , (X(L),Y(L),Z(L),L = 1,35)
   68 NRUN = NRUN + 1
```

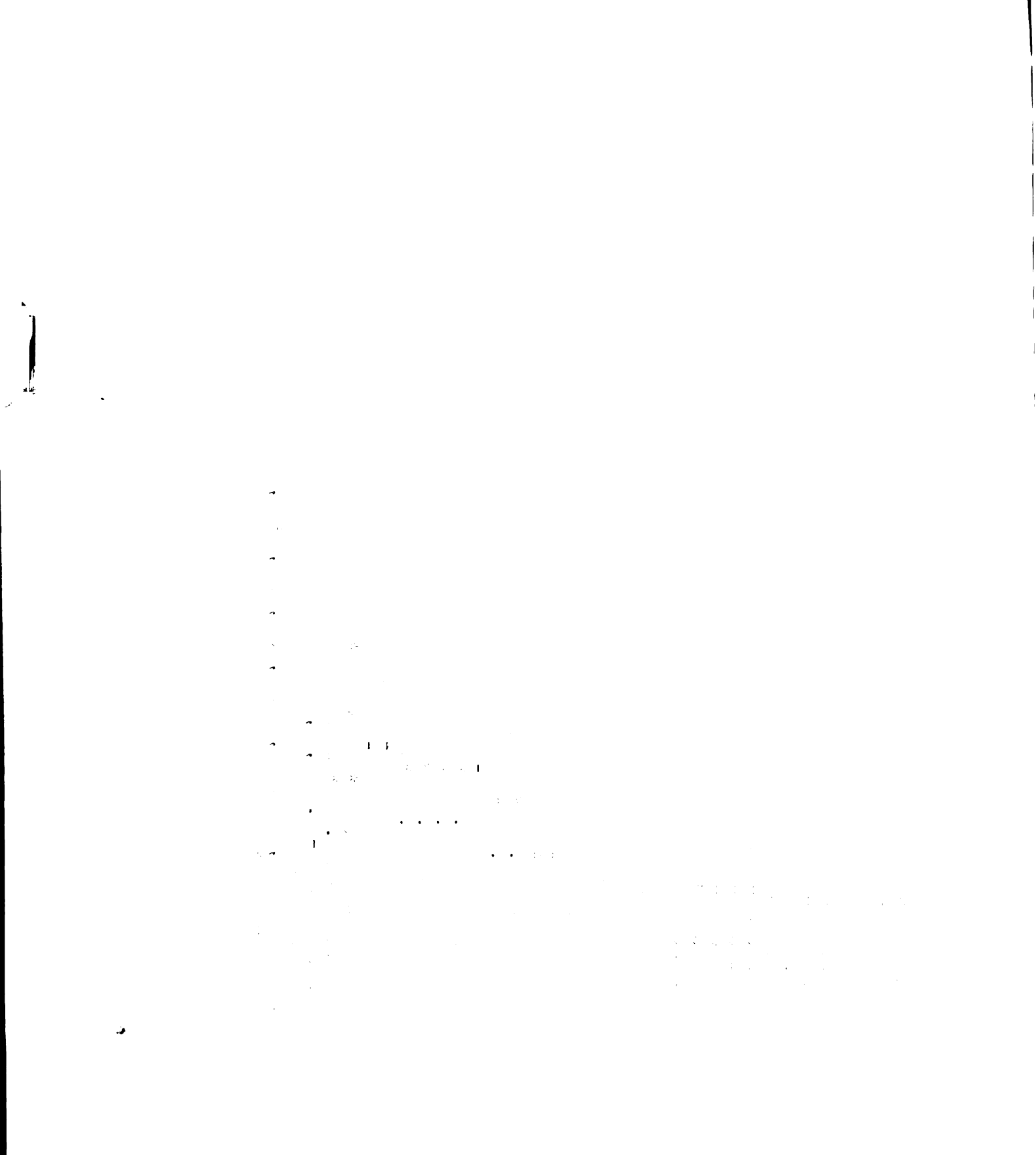

```
 69 GO TO 72
 70 THEGI(JA) = 0.0
 72 NPRO = NPRO + 1
 73 IF(IK - 50)37,74,74
 74 IF(JA)90,90,75
 75 JS = 1
    JM = JA - 25
    IF(JM)76,76,77
 76 L = 1
    GO TO 79
 77 L = 2
    JA = 25
 79 NPAGE = NPAGE + 1
 80 PRINT 81,NPAGE
 82 PRINT 83,(NID(J),NIS(J),NAMES(J),NOD(J),NOS(J),XOI(J),ALPI(J),YOI(
   1J),BETI(J),ERID(J),ERIS(J),XOO(J),ALPO(J),YOO(J),BETO(J),EROD(J),E
   2ROS(J),J = JS,JA)
 85 PRINT 86,NPAGE
 87 PRINT 88,(NAMES(J),FII(J),IQI(J),THEI(J),FIO(J),IQO(J),THETO(J),
   1THEGI(J), J = JS,JA)
    PRINT 301, NPAGE
301 FORMAT(1H1,51X,20HPROJECTED ANGLE DATA,36X,5HPAGE ,14//  14X,14HIN
   1COMING TRACK,26X,14HOUTGOING TRACK30X,5H     /7X,8H DIRECT ,12X,8
   2H STEREO  ,12X,8H DIRECT ,12X,8H STEREO ,2X,10HTHETA DIR.,2X,16HTHE
   3TA D. (CORR.),2X,11HTHETA STER./18X,45H(MEASURED IN DEGREES CLOCKW
   4ISE FROM VERTICAL),22X,28H(CLOCKWISE DEFLECTION ANGLE)//57X,5HEVEN
   5T/)
    PRINT 302,(NAMES(J),ANALI(J),ANBEI(J),ANALO(J),ANBEO(J),THEDD(J),T
   1HEDDC(J),THEDS(J),J = JS,JA)
302 FORMAT( 58X,16/6X,F8.3,12X,F8.3,12X,F8.3,12X,F8.3, 2X,F8.3, 4X,F8.
   13,6X,F8.3)
    IF(L - 2)90,89,90
 89 JS = 26
    JA = JM + 25
    L = 3
    GO TO 79
```

```
 90 PRINT 96
    PRINT 91
 92 DO 95 J = 1,JB
 93 PRINT 94 ,J,NAMER(J)
 95 CONTINUE
    PRINT 201
203 DO 205 J = 1,JC
205 PRINT 100,J,LNAME(J)
148 S = 10.0
149 MPART = 36
150 CALL PART(FII,JA,MPART,S,NFII,NZD,NFIG,NZD,NFIGO)
    MFIG = MFIG + NFIG
    NFII(1) = NFII(1) + NFIGO
155 CALL PART(FIO,JA,MPART,S,NFIO,NZD,NFOG,NZD,NFOGO)
    MFOG = MFOG + NFOG
    NFIO(1) = NFIO(1) + NFOGO
    DO 156 L = 1,MPART
    MFII(L) = MFII(L) + NFII(L)
    MFIO(L) = MFIO(L) + NFIO(L)
    MFIIT = MFIIT + MFII(L)
156 MFIOT = MFIOT + MFIO(L)
    MFIIT = MFIIT + MFIG
    MFIOT = MFIOT + MFOG
157 S = 0.25
158 MPART = 28
159 CALL PART(THETO,JA,MPART,S,NTHI,NZD,NTHG,NZD,NTHGO)
    MTHG = MTHG + NTHG
    NTHI(1) = NTHI(1) + NTHGO
    CALL PART(THEDDC ,JA,MPART,S,NTHEDCP,NTHEDCN,NTHDCGP,NTHDCGN,NTHDC
   1GO)
    MTHDCGP = MTHDCGP + NTHDCGP
    MTHDCGN = MTHDCGN + NTHDCGN
    MTHDCGO = MTHDCGO + NTHDCGO
    DO 160 L = 1,MPART
    MTHI(L) = MTHI(L) + NTHI(L)
    MTHEDCP(L) = MTHEDCP(L) + NTHEDCP(L)
```

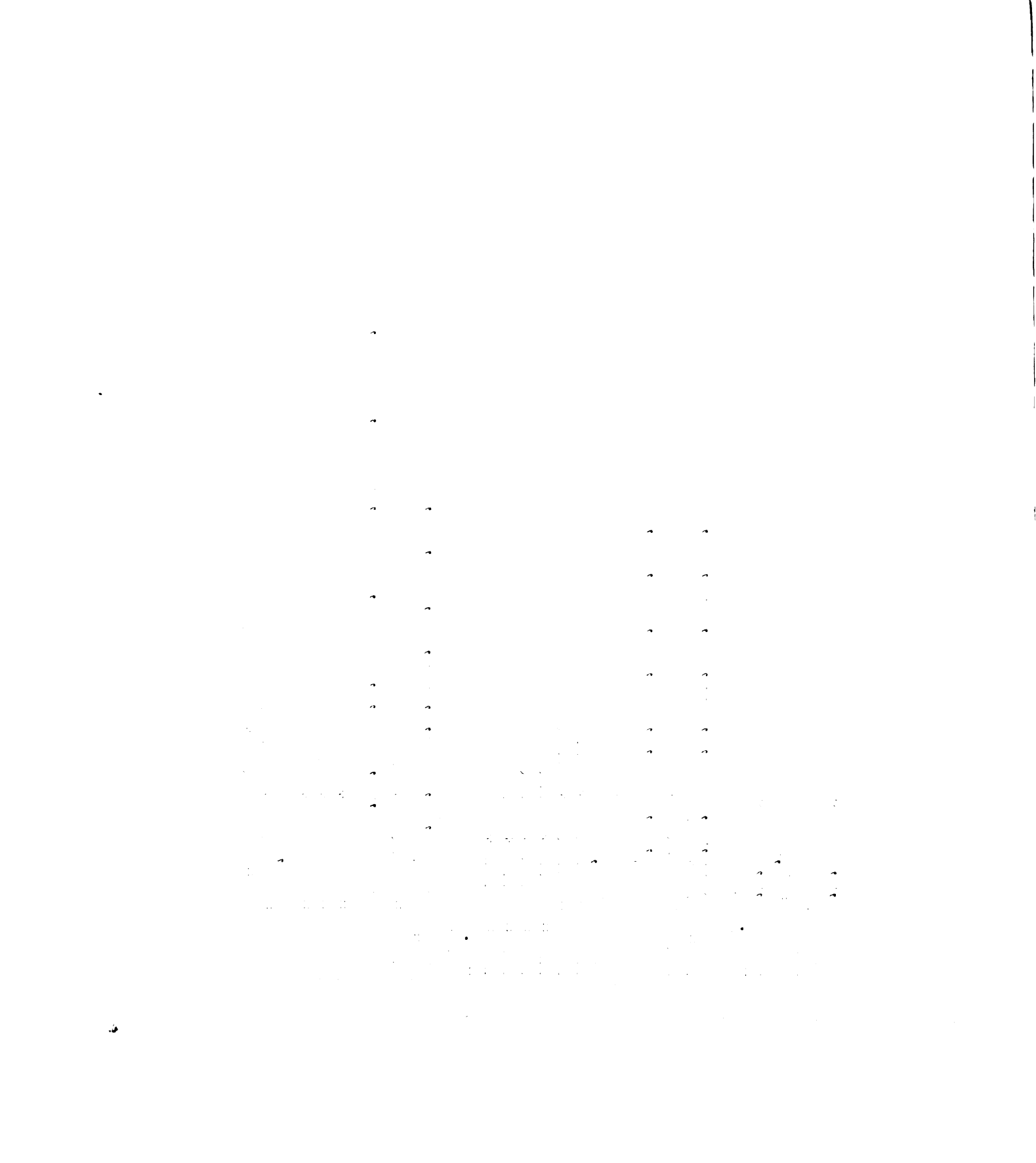

```
    MTHEDCN(L) = MTHEDCN(L) + NTHEDCN(L)
    MTHIT = MTHIT + MTHI(L)
    LTHEDCP = LTHEDCP + MTHEDCP(L)
160 LTHEDCN = LTHEDCN + MTHEDCN(L)
    LTHEDC = LTHEDCP + LTHEDCN + MTHDCGP + MTHDCGN + NTHDCGO
    MTHIT = MTHIT + MTHG
    S = 0.2
    MPART = 100
    CALL PART(THEI,JA,MPART,S,NTHEI,NZD, NTHEIG,NZD,  NTHEIGO)
    MTHEIG = MTHEIG + NTHEIG
    NTHEI(1) = NTHEI(1) + NTHEIGO
    CALL PART(ANALI ,JA,MPART,S,NALPTP,NALPTN,NALPTGP,NALPTGN,NALPTGO)
    MALPTGP = MALPTGP + NALPTGP
    MALPTGN = MALPTGN + NALPTGN
    MALPTGO = MALPTGO + NALPTGO
    DO 163 L = 1,MPART
    MALPTP(L) = MALPTP(L) + NALPTP(L)
    MALPTN(L) = MALPTN(L) + NALPTN(L)
    MTHEI(L) = MTHEI(L) + NTHEI(L)
    MALPTPT = MALPTPT + MALPTP(L)
    MALPTNT = MALPTNT + MALPTN(L)
163 MTHEIT = MTHEIT + MTHEI(L)
    MALPTT = MALPTPT + MALPTNT + MALPTGP + MALPTGN + MALPTGO
    MTHEIT = MTHEIT + MTHEIG
 97 IF(IKM - NPRO)99,99,38
 99 NSTOT = NRUN + NSTOT
    NETOT = NETOT - 1
    PRINT 98,NPAGE,NETOT,NSTOT,NRUN
101 ENDFILE 5
102 REWIND 5
105 READ TAPE 5,MMMM
    DO 108 I = 1,NRUN
106 READ TAPE 5,NAME5
107 PRINT 100 ,I,NAME5
108 CONTINUE
165 PRINT 153,MFIG,(MFII(L),L = 1,36   )
```

```
      PRINT 253, MFIIT
  166 PRINT 161,MFOG,(MFIO(L),L = 1,36    )
      PRINT 253, MFIOT
  167 PRINT 162,MTHG,(MTHI(L),L = 1,28    )
      PRINT 253, MTHIT
  170 PRINT 171, MTHDCGP,MTHDCGN,MTHDCGO,(MTHEDCP(L),MTHEDCN(L),L=1,28),
     1LTHEDCP,LTHEDCN
      PRINT 271, LTHEDC
  168 PRINT 169,MTHEIG,(MTHEI(L),L = 1,100)
      PRINT 253, MTHEIT
      PRINT 173, MALPTGP, MALPTGN,MALPTGO,(MALPTP(L),MALPTN(L),L=1,100),
     1MALPTPT,MALPTNT
      PRINT 271, MALPTT
  114 REWIND 4
  115 REWIND 5
  116 RETURN
  117 END
```



```
      FUNCTION THETA(ALPB,ALPT,BETB,BETT)
   10 DENT = SQRTF(1.0 + ALPT**2 + BETT**2)
   11 DENB = SQRTF(1.0 + ALPB**2 + BETB**2)
      DCAT = ALPT/DENT
      DCBT = BETT/DENT
      DCCT = (1.0)/DENT
      DCAB = ALPB/DENB
      DCBB = BETB/DENB
      DCCB = (1.0)/DENB
   14 CTHTA = DCAT*DCAB + DCBT*DCBB + DCCT*DCCB
   15 THETA = ACOSF(CTHTA)
   20 RETURN
   21 END
```

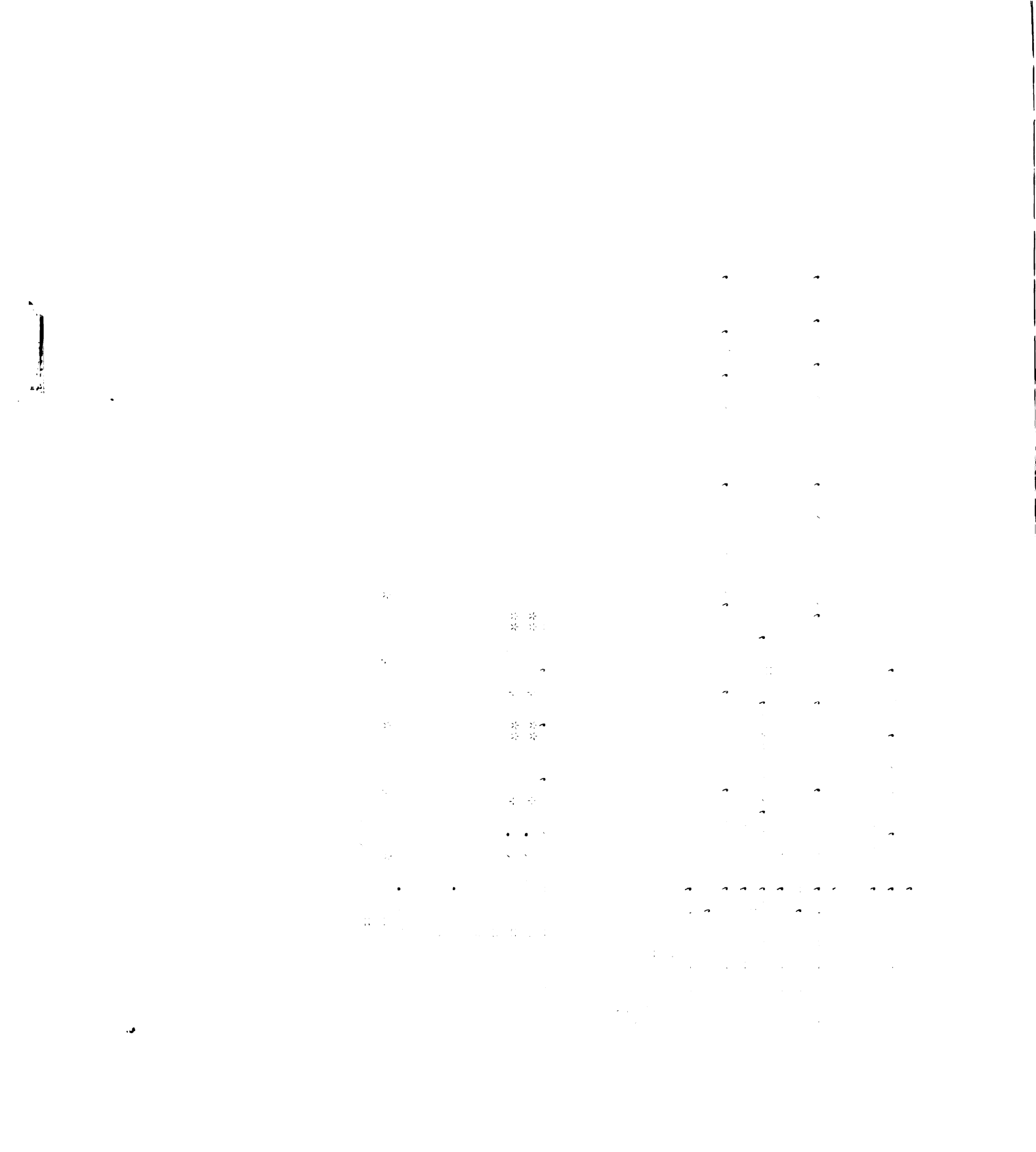

```
      SUBROUTINE CURV(X,Z,ALPB,XOB,ALPT,XOT,ID,RRB,RRT,SDEVB,SDEVT,NB,NT
     1,XA,ZA,XB,ZB,IE)
     2 DIMENSION X(35),Z(35),XA(26),ZA(26),XB(26),ZB(26)
C    SUBROUTINE CURV WRITTEN TO ACCEPT EVENTS HAVING TWO POINTS ANYWHERE IN
C    BOTTOM CHAMBER AND ONE POINT IN EACH OF THE GAP PAIRS IN THE TOP CHAMBER
     5 DO 7 I = 1,26
       XA(I) = 0
       ZA(I) = 0
     7 CONTINUE
     8 NC = 1
       NB = 0
       ILOW = 3
       IUP = 4
       ND = 3
    10 CALL A(X,Z,XA,ZA,NC,NB,ILOW,IUP,ND)
    17 GO TO 20
    18 ID = 3
       IE = 1
       GO TO 80
    20 NC = 1
       ILOW = 5
       IUP = 6
    21 CALL A(X,Z,XA,ZA,NC,NB,ILOW,IUP,ND)
    27 IF(NB - 2)18,30,30
    30 NC = 1
       ILOW = 7
       IUP = 10
    31 CALL A(X,Z,XA,ZA,NC,NB,ILOW,IUP,ND)
    32 IF(NC - 3)18,40,40
    40 IF(NB - 4)18,41,41
    41 CALL LINE(XA,ZA,NB,XOB,ALPB,RRB,SDEVB,IE)
    42 IF(IE-3)50,75,50
    50 DO 52 I = 1,26
    51 XB(I) = 0
    52 ZB(I) = 0
    53 NT = 0
```

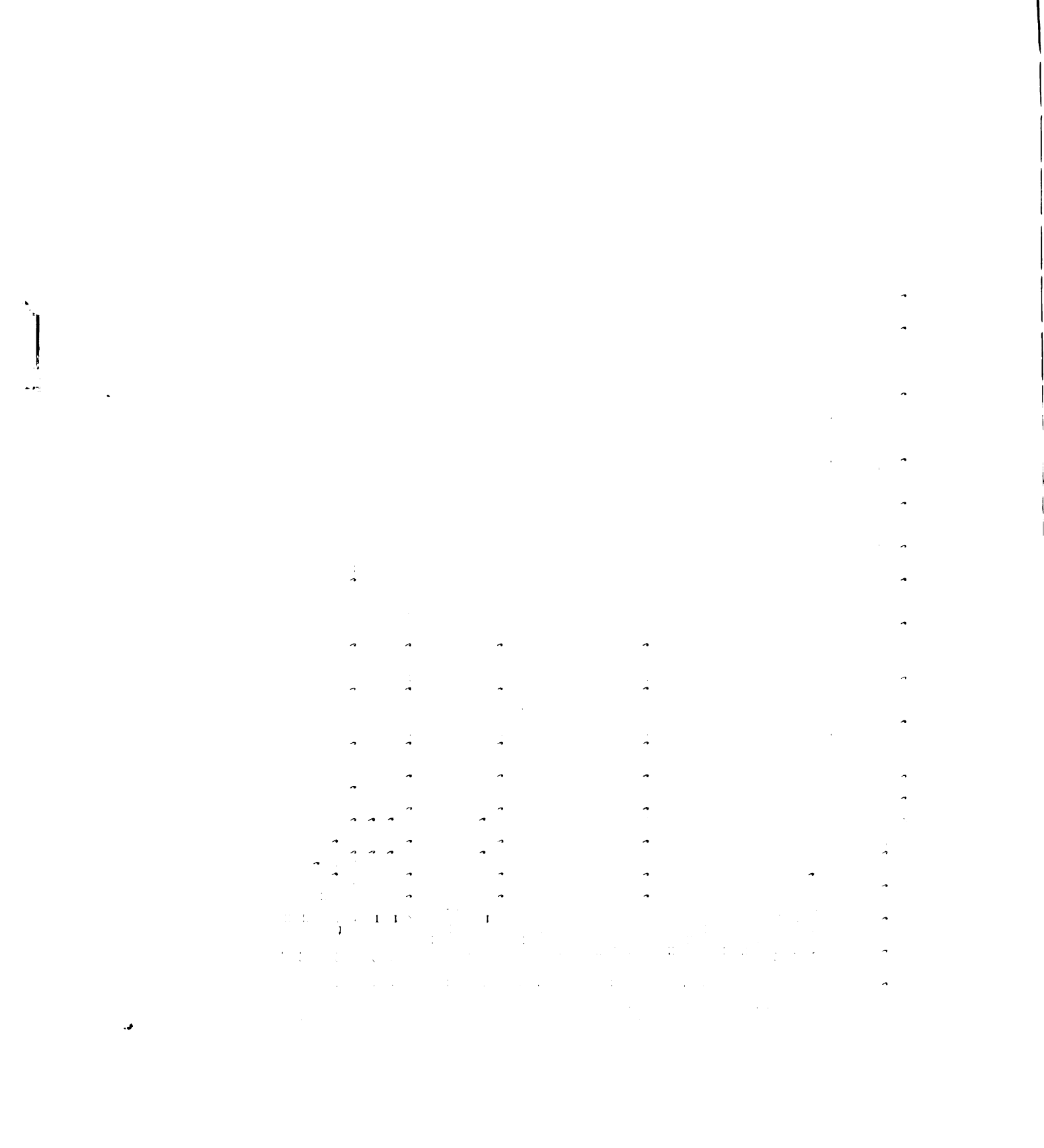

```
      NC = 1
      ND = 3
      ILOW = 29
      IUP = 30
54    CALL A(X,Z,XB,ZB,NC,NT,ILOW,IUP,ND)
56    GO TO(18,57,57),NC
57    NC = 1
      ILOW = 31
      IUP = 32
58    CALL A(X,Z,XB,ZB,NC,NT,ILOW,IUP,ND)
60    GO TO(18,61,61),NC
61    NC = 1
      ILOW = 28
      IUP = 28
62    CALL A(X,Z,XB,ZB,NC,NT,ILOW,IUP,ND)
      ILOW = 27
      IUP = 27
63    CALL A(X,Z,XB,ZB,NC,NT,ILOW,IUP,ND)
      IF(NC - 3)64,71,71
64    ILOW = 26
      IUP = 26
65    CALL A(X,Z,XB,ZB,NC,NT,ILOW,IUP,ND)
      IF(NC - 2)18,66,71
66    ILOW = 25
      IUP = 25
67    CALL A(X,Z,XB,ZB,NC,NT,ILOW,IUP,ND)
68    IF(NC - 3)18,71,71
71    IF(NT - 4)18,72,72
72    CALL LINE(XB,ZB,NT,XOT,ALPT,RRT,SDEVT,IE)
73    IF(IE-3)74,75,74
74    ID = 1
      IE = 1
      GO TO 80
75    IE = 3
      ID = 1
80    RETURN
81    END
```

```
      SUBROUTINE A(X,Z,XA,ZA,NC,NB,ILOW,IUP,ND)
 5    DIMENSION X(35),Z(35),XA(26),ZA(26)
10    DO 20 I = ILOW,IUP
11    XA(I) = 0
      ZA(I) = 0
      IF(X(I))15,20,15
15    N = NB + 1
16    XA(N) = X(I)
17    ZA(N) = Z(I)
18    NB = N
19    NC = NC + 1
      IF(NC - ND)20,21,21
20    CONTINUE
21    RETURN
22    END
```

```
      SUBROUTINE LINE(XA,ZA,N,XO,ALP,RR,SDEV,ID)
 5    DIMENSION XA(26),ZA(26),EB(26),EBS(26)
10    XSUM = 0
      ZSUM = 0
      EB = 0
      ECA = 0
      ECB = 0
      XX = 0
      XZ = 0
      ZZ = 0
15    DO 20 I = 1,N
      XSUM = XA(I) + XSUM
      ZSUM = ZA(I) + ZSUM
19    XX = XA(I)**2 + XX
      XZ = XA(I) * ZA(I) + XZ
20    ZZ = ZA(I)**2 + ZZ
      AN = N
      AX = XSUM*ZZ - XZ*ZSUM
```

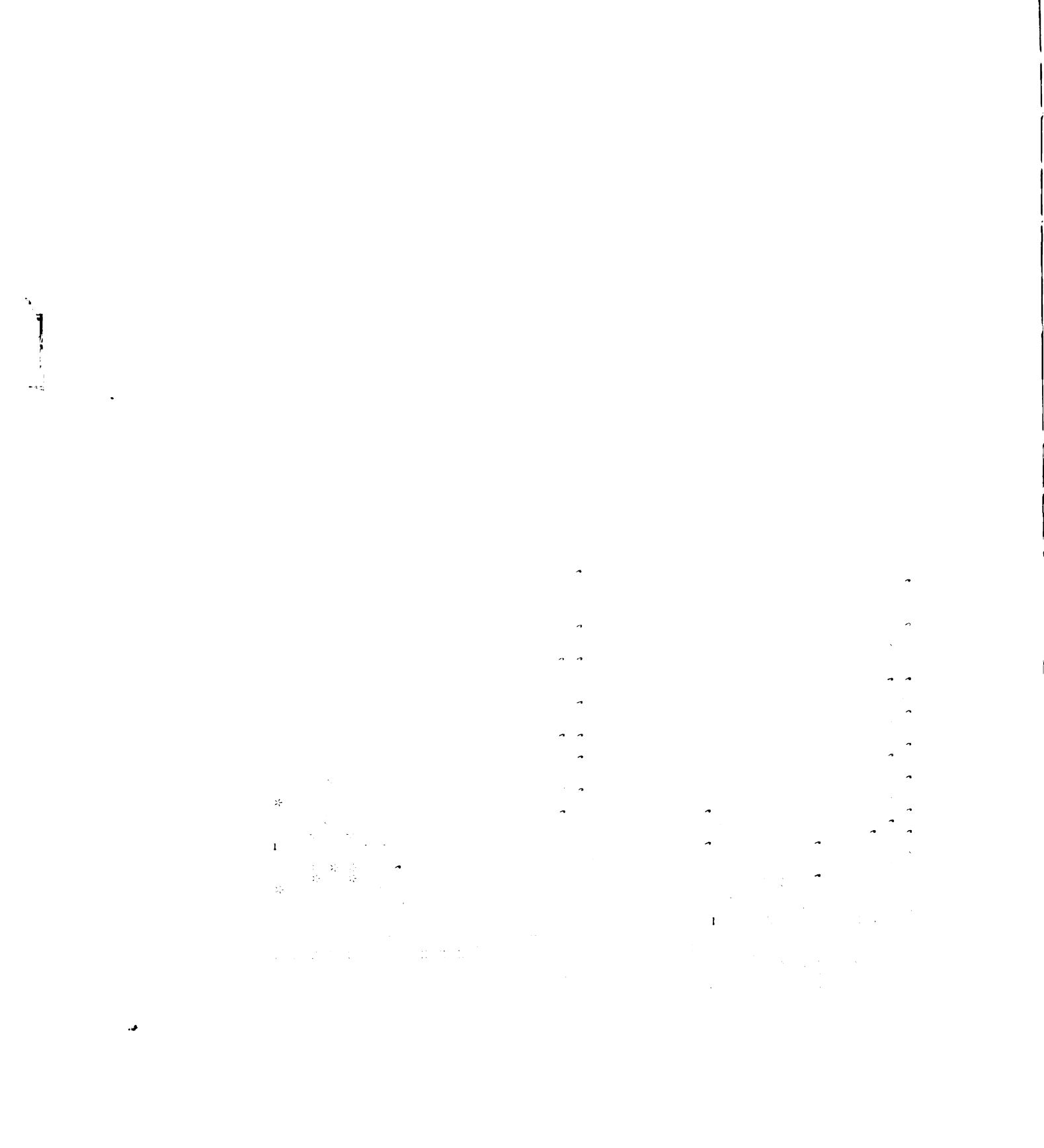

```
      BX = AN*ZZ - ZSUM**2
   25 XO = AX/BX
      CX = XZ - XO*ZSUM
   30 ALP = CX/ZZ
      DO 35 I = 1,N
      EB(I) = XA(I) - XO-ALP*ZA(I)
   33 ECB = EB(I) + ECB
      EBS(I) = EB(I)**2
   35 ECA = EBS(I) + ECA
   36 V = ECA/(AN - 2.0)
   37 SDEV = SQRTF(V)
   38 AA = XSUM/AN
   39 AB = ZSUM/AN
   40 AC = AN*(AA**2)
   41 AD = AN*(AB**2)
   42 AE = (XX - AC)/(AN - 1.0)
   43 AF = SQRTF(AE)
   44 AG = (ZZ - AD)/(AN - 1.0)
   45 AH = SQRTF(AG)
   46 AI = 0
   47 DO 50 J = 1,N
   48 AJ =  XA(J) - AA
   49 AK =  ZA(J) - AB
   50 AI = AJ*AK + AI
   51 R = AI/(AF*AH)
      R = R/(AN - 1.0)
   52 RR = R**2
   54 IF(RR - 0.960)56,58,58
   56 ID = 3
   57 GO TO 60
   58 ID = 1
   60 RETURN
   61 END
```

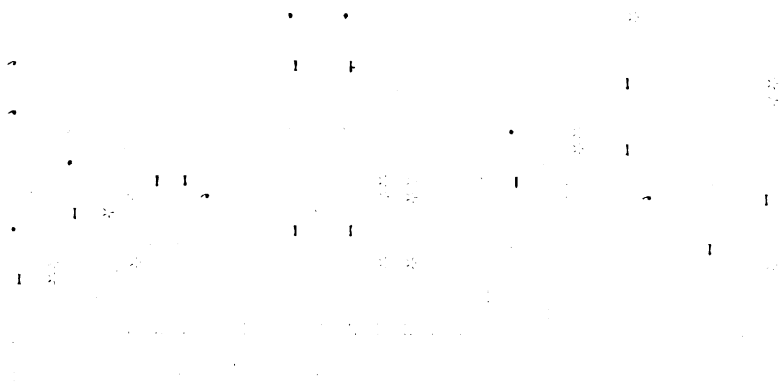

```
   SUBROUTINE QUAD(ALPHA,BETA,IQ,FI)
10 IF(ALPHA)14,16,12
12 IF(BETA)34,18,28
14 IF(BETA)32,22,30
16 IF(BETA)24,26,20
18 FI = 0.0
   IQ = 1
   GO TO 45
20 FI = 90.0
   IQ = 2
   GO TO 45
22 FI = 180.0
   IQ = 3
   GO TO 45
24 FI = 270.0
   IQ = 4
   GO TO 45
26 FI = 0.0
   IQ = 5
   GO TO 45
28 IQ = 1
   GO TO 36
30 IQ = 2
   GO TO 36
32 IQ = 3
   GO TO 36
34 IQ = 4
36 T = BETA/ALPHA
37 FI = ATANF(T)
38 FI = (57.296)*FI
40 GO TO(45,41,41,43,45), IQ
41 FI=180.0 + FI
42 GO TO 45
43 FI=360.0 + FI
45 RETURN
46 END
```

```
      SUBROUTINE PART(X,N,NA,S,NPI,NNI,NGP,NGN,NGO)
      DIMENSION X(50),NPI(105),NNI(105)
   10 DO 11 I = 1,105
      NPI(I) = 0
   11 NNI(I) = 0
      NGP = 0
      NGN = 0
      NGO = 0
   13 SNA = NA
   14 A = SNA*S
   15 DO 46 IA = 1,N
   16 IF(X(IA) - A)17,44,44
   17 IF(X(IA) + A)45,45,18
   18 IF(X(IA))24,19,20
   19 NGO = NGO + 1
      GO TO 46
   20 DO 23 I = 1,NA
      C = I
      B = C*S
      IF(X(IA) - B)21,23,23
   21 NPI(I) = NPI(I) + 1
      GO TO 46
   23 CONTINUE
   24 DO 26 I = 1,NA
      C = I
      B = C*S
      IF(X(IA) + B)26,26,25
   25 NNI(I) = NNI(I) + 1
      GO TO 46
   26 CONTINUE
   44 NGP = NGP + 1
      GO TO 46
   45 NGN = NGN + 1
   46 CONTINUE
      RETURN
      END
```

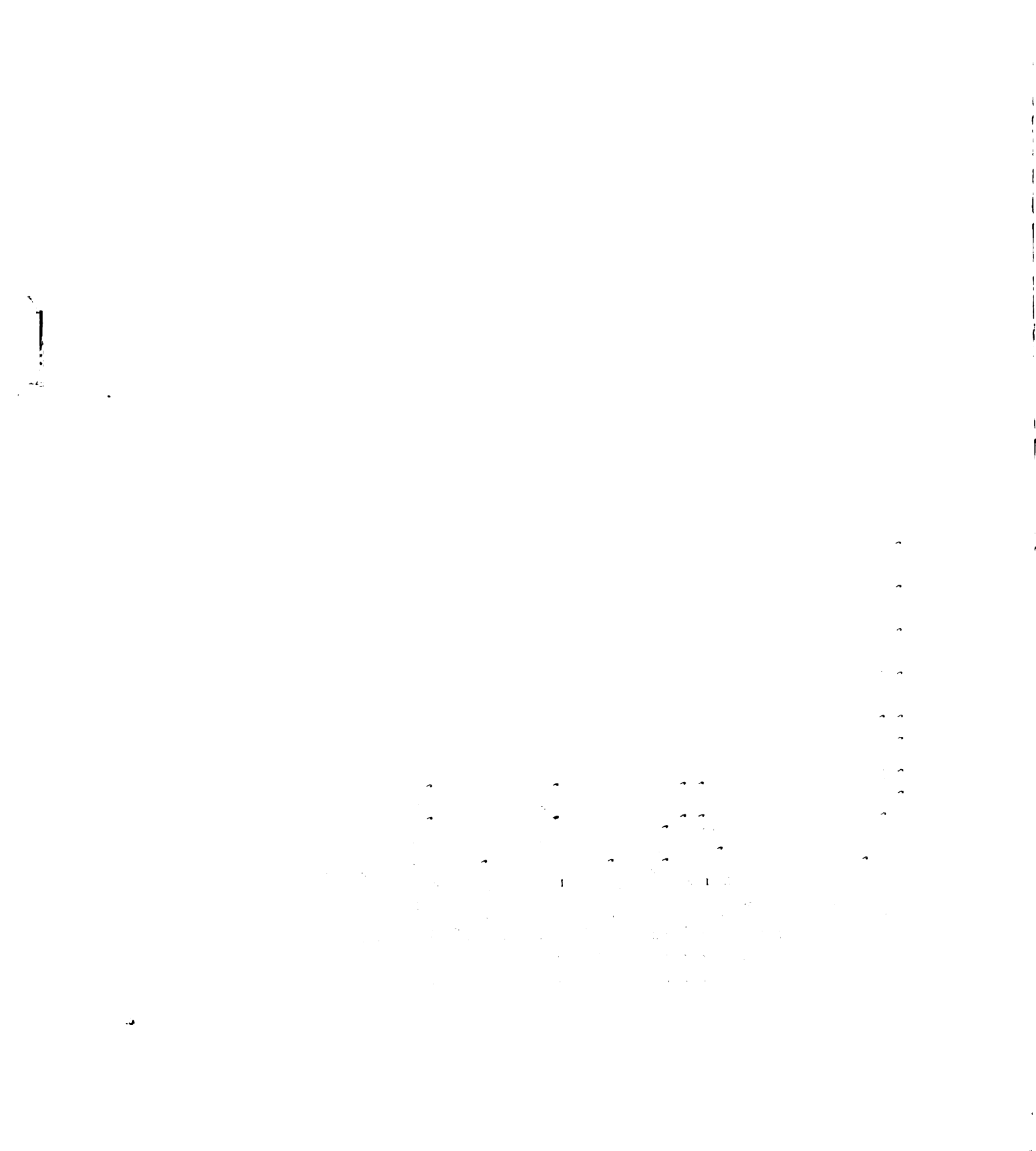

APPENDIX G: Calculation of theoretical multiple scattering distributions

I. Calculation of the Cooper-Rainwater distribution

A. The differential scattering distribution M(x)

As given in Section IV. B., the form of the differential distribution that describes large angles as well as small is

$$M^{C-R}(x) = \frac{e^{-x^2}}{\sqrt{\pi}}\left[1 + \frac{q(1,x)}{4G}\right] + \frac{1}{4G\sqrt{\pi}} N(1,x)$$

The parameters and functions in this expression for M(x) are as defined in the main text.

In performing the calculation of M(x) the program written for the task was arranged in the following manner: Subroutine COOP calculates the quantities G, Q, x_0, φ_0, φ_m, t (in gm/cm^2), $(2 \cdot GQ)^{\frac{1}{2}}$, all of which are needed later on in the calculation. In addition to these quantities, the form factors $F_N^C(y)$ and $\mathcal{F}_{N(y)}$ are calculated in this subroutine.

To perform this, a table of 21 values of $F_N^C(y)$ for values of y from y = 0 to y = 4 increments of 0.25 is entered in an array in the machine memory. These values of F_N^C were obtained from plotting the four values for y = 0, 1, 2, 3, that Cooper and Rainwater suggest,[9] which is then to be matched to the function $F_N^C = 12/y^4$ for $y \geq 4$. A function routine FORM (y) interpolates this table of F_N^C values or uses the assmptotic value of $F_N^C(y)$ for any required value of y. The values of

$F_N^C(y)$ thus generated are used in COOP by which to obtain the corresponding values of $\mathcal{F}_{N(y)}$ from the relation

$$\mathcal{F}_{N(y)} = F_N^C(y) + (1 - F_N^C(y))/Z.$$

The values of $\mathcal{F}_{N(y)}$ obtained in this manner are stored in an array under Labelled Common for later use.

Subroutine RAIN, called successively for each value of x, controls the remaining operations involved in calculating the differential scattering distribution M(x). Function TXLAM is called a number of times to furnish, for each value of x, an array of values of the function $T(x, \lambda)$ as defined above. Function QLX is called to evaluate the function $q(L, x)$ as defined above. The integral represented by $N(L, x)$ is evaluated by means of Weddle's rule in Function WEDL. The value of M(x) then is merely the sum of each of the terms whose value was just calculated. Each value of M(x) thus obtained is entered in an array in Labelled Common containing the set of M(x) values that correspond to the set of required values of x. M(x) is also printed out at this point along with the corresponding value of φ and x. Printed out also is the value of $q(L, x)$ and the number of terms found necessary for convergence of the series used to calculate $q(L, x)$.

B. The corrected differential scattering distribution

The next step in the calculation is to obtain a differential scattering distribution corrected for noise level scattering. This is done as discussed in in the main text by evaluating the following integral

$$g(x') = \frac{1}{\sqrt{2\pi}\,\sigma}\int_{-\infty}^{\infty} M(x)\, e^{\frac{-(x-x')^2}{2\sigma^2}}\, dx$$

where $g(x')$ is the corrected distribution, x' = measured deflection, $e^{\frac{-(x-x')^2}{2\sigma^2}}$ is the normal distribution function used as a weighting factor upon M(x) as a method of obtaining the expected value of the differential distribution function at x' due to the total of all the contributions from deflections having all values of x. This integral is evaluated by numerical integration in Function GPTHTA, which in turn calls Function FNTGRL to do the actual integration using an extended five-point Newton-Cotes quadrature method.

A set of $g(x')$ values is obtained by repeating the above procedure for various values of x' by which a corrected differential distribution $g(x')$ for each x' needed is made available. These values of $g(x')$ are printed out at this point together with their corresponding φ' and x' values.

C. The integral scattering distribution

From the set of $g(x')$ values obtained in Function GPTHTA an integral distribution is obtained by numerical integration of these values in Function GTHETA. This is done to evaluate the integral

$$G_{(x_L')} = \int_{x_L'}^{\infty} g(x')\, dx'$$

For purposes of normalization this may be rewritten as

$$G_{N\,(x_L')} = \frac{1}{G_{(0)}} \int_{x_L'}^{\infty} g(x')\, dx'$$

The integration of this expression is performed by the same Newton-Cotes function routine mentioned above. Normalization is performed after integration by dividing each value of $G(X_L')$ by $G_{(0)}$ to obtain $G_N(X_L')$ for each value of X_L' to be used. The values of X_L' were generated stepwise in the machine upon reading in values of the step size and upper limit on X_L'. The calculated values of $G(X_L')$ and $G_N(X_L')$ were printed out at this point together with the corresponding values of θ'_L and X'_L.

II. Calculation of the Moliere scattering distribution

The Moliere differential scattering distribution was calculated using the same program as described in Section I. above, making the proper identification concerning $\mathcal{F}_N$ in the calculation of M(x). $(F_N{}^C)^{\frac{1}{2}}$ is the Fourier transform of the nuclear charge distribution. Thus the point charge nucleus which is assumed in the Moliere theory will, since it has negligible extent, have a corresponding $F_N{}^C \longrightarrow 1.00$. From the expression for $\mathcal{F}_N = F_N{}^C + \frac{1}{Z}(1 - F_N{}^C)$ we see that $\mathcal{F}_N \longrightarrow 1.00$ also. Thus to calculate the Moliere differential distribution, the integrand of $N_{(L,\ N)}$ was merely rewritten with the $\mathcal{F}_N$ factor omitted--effectively setting $\mathcal{F}_N = 1.00$.

The Moliere corrected differential distribution and the Moliere corrected integral distribution were then calculated in exactly the same manner as described in B. and C. above.

III. Calculation of the Drell-Schwartz scattering distribution

To obtain the Drell-Schwartz predicted distribution, a subroutine DRELL was written in a straight-forward manner to calculate the function $dN/d\theta$ developed in section IV.-C. Values of this function were obtained at 260 points in the range of the experiment. Printed out at each of the 260 points were the following quantities: θ, q_o(in Mev/c), $f^2(q_o)$, $F(q_o)$, $\mathcal{F}(q_o)$, $\mathcal{F}_{mag}(q_o)$, $d\sigma_o/d\Omega$, $d\sigma/d\Omega$, $dN/d\theta$.

A second subroutine MSCOR was written to calculate the multiple scattering correction factor required to correct the single scattering law of Drell-Schwartz to one which includes the effects of multiple scattering. This was done by calculating the ratio of the multiple to single scattering laws of Cooper-Rainwater at each point. This ratio was then stored in the memory until after the following step.

Next a third subroutine DRELPR was written to calculate $dN/d\varphi$ from the appropriate linear combination of the $dN/d\theta$ values, as developed in Section IV.-C. Values for $dN/d\varphi$ were obtained at each of the 260 values of φ as above. These values were then corrected by using the correction factors generated in subroutine MSCOR, giving a differential distribution for multiple scattering based on the Drell-Schwartz single scattering results. Printed out at this point were the following quantities: φ, x, $(dN/d\varphi)_S$, $(dN/d\varphi)_M$, %MS. The terms $(dN/d\varphi)_S$ and

$(dN/d\varphi)_M$ are respectively the single scattering distribution of Drell-Schwartz converted to projected angles and this distribution corrected for multiple scattering.

The set of values obtained for $(dN/d\varphi)_M$ were then operated on by function GPTHTA and then by function GTHETA whose purposes and printed results are described in sections I.-B. and I.-C. of this appendix.

In addition both $(dN/d\varphi)_s$ and $(dN/d\varphi)_M$ were operated on directly by function GTHETA. By comparing the resulting distributions printed out from this step, an estimate of the precent difference in the integral distribution due to multiple scattering was made.

A listing of the computer program described above, written in CDC-3600 Fortran, follows:

```
      PROGRAM THEORY
      COMMON TOL, PI
      COMMON /B/ XL,DEL,FN(601),Q,G,NMAX,PC,A,Z,THICK,DEN,PHIM,FNC(601).
     1XZERO, FNCS(601), FNS(601), PHIZR
      COMMON /C/ AMX(300),BMX(300),CMX(300),FRDF(300),DMX(300)
      COMMON /D/ GPTA(300)
      COMMON /E/ DNDTHA(300),Q0(300),F2EL(300),DSIG0(300),
     1DSIGC(300),F2MAG(300)
      DIMENSION  IW(16)
      READ 400, IW
      PRINT 600, IW
  400 FORMAT(16A5)
  401 FORMAT(215)
  402 FORMAT(8F10.5)
  600 FORMAT(1H1,16A5)
  100 READ 400, IW
      PRINT 600, IW
      IF(IW,EQ,5HSTOP ) GO TO 1000
      READ 401, NUM, NTIMES
      ICOUNT = 0
      IF (NUM) 1000,2,101
  101 IF(NUM-6)102,102,1000
  102 IF(NUM-1)2,2,5
C     NUM = OPTION NUMBER
C     OPTION 0 *** CALCULATION OF G,Q, X-0, PHI-0, SQRT(2GQ), GM/CM2
C         IN SUBROUTINE COOP ONLY
C     OPTION 1 *** CALCULATION OF M(X) FOR READ-IN SET OF X VALUES
C     OPTION 2 *** CALCULATION OF G(X) CORRECTED DIFF. DIST, FOR READ-IN SET
C              OF XPR VALUES.
C     OPTION 3 *** CALCULATION OF  G(X0) CORRECTED INTEGRAL DISTRIBUTION.
C     OPTION 4 *** CALCULATION OF  G(X0) UNCORR.   INTEGRAL DISTRIBUTION,
C            USING M2(X) INSTEAD OF G(P-THETA).
C     OPTION 5 *** CALCULATION OF G(X0) CORR. INT. DISTR.,
C                         USING G()-THETA) FROM MOLIERE DISTRIBUTION.
C            MOLIERE DISTRIBUTION OBTAINED BY SETTING FORM FACTOR=1.0(I.E. RE-
C            MOVING IT FROM CALCULATION) IN RAIN.
C     OPTION 6 *** CALCULATION OF G(X0) CORRECTED INTEGRAL DISTRIBUTION,
C            USING DRELL SUM RULE.
```

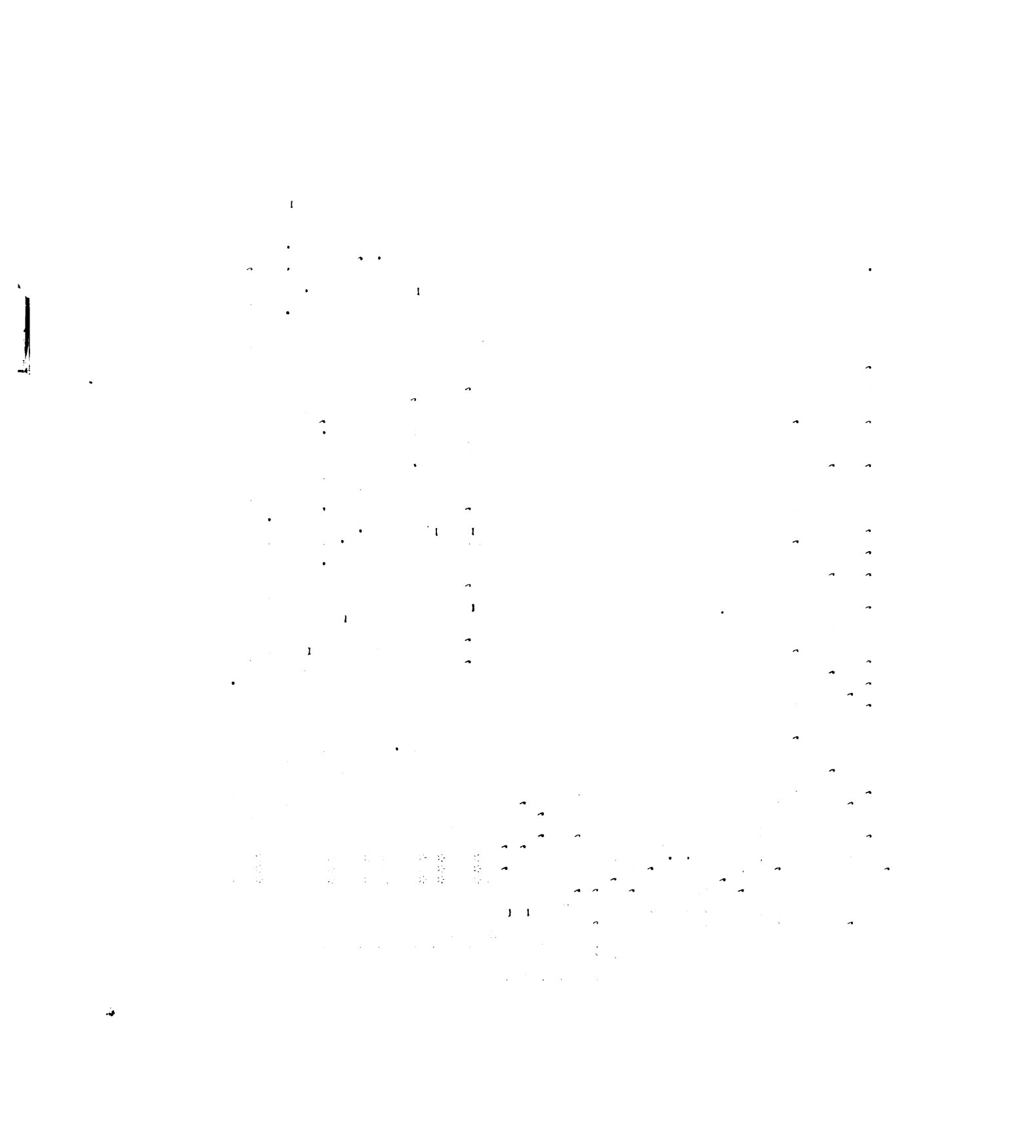

```
  2 CALL COOP
    IF(NUM - 1)100,3,1000
  3 PRINT 604
604 FORMAT (1H0,66HCOOPER-RAINWATER DIFFERENTIAL DISTRIBUTION FOR MULT
   1IPLE SCATTERING /)
 30 READ 402, X
    KF = 1
    CALL RAIN(X, VM2X, NUM,KF)
    ICOUNT = ICOUNT + 1
    IF (NTIMES - ICOUNT) 4,4,30
  4 GO TO 100
  5 CALL COOP
    DO 50 I = 1,300
    AMX(I) = 0.0
    BMX(I) = 0.0
    CMX(I) = 0.0
    DMX(I) = 0.0
    FRDF(I) = 0.0
    DNDTHA(I) = 0.0
    GPTA(I) = 0.0
 50 CONTINUE
    READ 402, SIGMA, ULIM, DELX, ULIMI, DELXI
    PRINT 603, SIGMA, ULIM, DELX, ULIMI, DELXI
603 FORMAT(1H0,2X,5HSIGMA,9X,4HULIM,9X,4HDELX,9X,5HULIMI,8X,5HDELXI/
   16(F10.5,3X))
    IF(NUM-5)55,56,55
 55 PRINT 604
    GO TO 62
 56 PRINT 606
606 FORMAT(1H0,58HMOLIERE DIFFERENTIAL DISTRIBUTION FOR MULTIPLE SCATT
   1ERING /)
 62 X = 0.0
    INDEX = ULIM/DELX + 1
    DO 64 K = 1,INDEX
    KF = K
    CALL RAIN(X,AMX(K),NUM,KF)
    X = X + DELX
```

```
 64 CONTINUE
    IF(NUM-6)69,70,70
 69 IF(NUM-2)1000,6,10
 70 CALL DRELL (ULIM,DELX,NUM)
    PRINT 607
607 FORMAT(1H0,76HDRELL-SCHWARTZ DIFFERENTIAL DISTRIBUTION, CORRECTED
   1FOR MULTIPLE SCATTERING. /)
    X = 0.0
    INDEX = ULIM/DELX + 1
    DO 74 K=1,INDEX
    KM = K
    CALL DRELPR(X,CMX(K),DMX(K),ULIM,DELX,NUM,KM)
    X = X + DELX
 74 CONTINUE
    GO TO 11
  6 READ 402, XPR
    KL = XPR/DELX + 1
    GPT = GPTHTA(XPR,SIGMA,ULIM,DELX,NUM,KL)
    ICOUNT = ICOUNT + 1
    IF(NTIMES - ICOUNT) 7,7,6
  7 GO TO 100
 10 IF(NUM - 4)11,17,11
 11 X = 0.0
    NGPT = ULIM/DELX + 1
    DO 84 K = 1,NGPT
    KL = K
    GPTA(K) = GPTHTA(X,SIGMA,ULIM,DELX,NUM,KL)
    X = X + DELX
 84 CONTINUE
    IF (NUM-5)17,14,15
 14 PRINT 605
605 FORMAT(1H0,50HMOLIERE CORRECTED INTEGRAL SCATTERING DISTRIBUTION,
   1 /)
    GO TO 17
 15 PRINT 608
608 FORMAT(1H0,65HDRELL-SCHWARTZ CORRECTED INTEGRAL  MULT. SCATTERING
   1DISTRIBUTION /)
```

```
 17 NUMGP = 1
 18 SLIM = 0.0
    INDEXI=ULIMI/DELXI+1
    DO 28  I=1,INDEXI
    ANS = GTHETA(ULIM,DELX,SIGMA,SLIM,NUM,INDEXL,NUMGP)
    PHIO   = SLIM*(57.296)*SQRTF(2.*G*Q)
    IF(SLIM)27,26,27
 26 ANORM = ANS
 27 ANSN = ANS/ANORM
    PRINT 602, PHIO  , SLIM, ANS, ANSN, INDEXL
602 FORMAT(1H ,  15HPHI-0(IN DEG.)= ,F7.3, 3X,11H(I.E.) X-0= ,F6.2,
   13X,   9HG(PHI-0)=,E11.4,3X,  14HG(PHI-0)NORM.= ,E11.4,3X,7HINDEXL=
   2,I3/)
    SLIM = SLIM + DELXI
 28 CONTINUE
    IF(NUM-6)300,150,300
150 GO TO(160,170,180,190,300),NUMGP
160 PRINT 609
609 FORMAT(1H0,67HDRELL-SCHWARTZ UNCORRECTED INTEGRAL MULT. SCATTERING
   1DISTRIBUTION   /)
    NUMGP = 2
    GO TO 18
170 PRINT 610
610 FORMAT(1H0,68HDRELL-SCHWARTZ UNCORRECTED INTEGRAL SINGLE SCATTERIN
   1G DISTRIBUTION      /)
    NUMGP = 3
    GO TO 18
180 PRINT 611
611 FORMAT(1H0,69HCOOPER-RAINWATER UNCORRECTED INTEGRAL MULT. SCATTERI
   1NG DISTRIBUTION      /)
    NUMGP = 4
    GO TO 18
190 PRINT 612
612 FORMAT(1H0,70HCOOPER-RAINWATER UNCORRECTED INTEGRAL SINGLE SCATTER
   1ING DISTRIBUTION       /)
    NUMGP = 5
    GO TO 18
300 GO TO 100
1000 STOP
    END
```

```
      SUBROUTINE COOP
      COMMON TOL, PI, TOLM
      COMMON /B/ XL, DEL, FN(601), Q, G, NMAX
      DIMENSION FNC(601)
   10 PI = 3.14159265
C    HBARC IS IN UNITS OF MEV-CM(SINCE 1 MEV=E+6 JOUL./COUL.(1.602E-19)= 1.602E-6
C        ERGS.
```

```
    HBARC = 3.1632E-17/1.602E-6
    CALL TABLE
    READ 402, XL, DEL, TOL, NMAX, TOLM
402 FORMAT(3F10.5,I10,F10.5)
    READ 401, PC,A, Z, BETA, THICK, DEN
401 FORMAT (8F10.5)
    PHIZR = HBARC/(PC*A**(1./3.)*1.1E-13)
    TERM10 = 1.1E-13*(A*Z)**(1./3.)
    TERM11 = 1.67E4*2.818E-13
    PHIM = TERM10/TERM11
    DENOM = (1.13*BETA*BETA*3.76*((Z/137.)**2))*A
    TOP = (Z**(4./3.))*THICK*DEN*2.54
    BRKT1 = TOP/DENOM
    TERM1 = 1.24*LOGF(BRKT1)*0.43429
    G = 5.66 + TERM1
    BRKT2 = (Z/BETA)*2.818E-13*(0.511/PC)
    BRKT3 = BRKT2**2
    GMCM2 = DEN*THICK*2.54
    Q = ((4.*PI)*6.02E23*GMCM2/A)*BRKT3
    BRKT4 = 2.*G*Q
    BRKT4 = SQRTF(BRKT4)
    XZERO = PHIZR/BRKT4
    CALL FORMC (XZERO,XL, DEL, FNC)
    NZIP = NMAX + 1
    DO 6 I = 1,NZIP
    FN(I) = FNC(I) + ((1.-FNC(I))/Z)
  6 CONTINUE
    PRINT 606
606 FORMAT (1H0,52H     L             DEL           TOL             NMAX
   1 )
    PRINT 607, XL, DEL, TOL, NMAX
607 FORMAT (1H , 3(F10.5,3X),I10)
    PRINT 604
604 FORMAT (1HO,97H  PC (MEV)     A             Z             BETA
   1  THICK.(INCHES)    DEN.(GM/CM3)
    PRINT 601,PC,A,Z,BETA,THICK,DEN
```

```
601 FORMAT (1H , 6(F10.5,3X))
    PRINT 605
605 FORMAT(1H0,5X,1HG,13X,1HQ,10X,5HXZERO,7X,7HPHIZERO,6X,4HPHIM,8X,
   19HSQRT(2GQ),5X,6HGM/CM2)
    PRINT 602,G,Q,XZERO,PHIZR,PHIM,BRKT4,GMCM2
602 FORMAT(1H ,F10.5,3X,F10.8,3X,5(F10.5,3X))
    RETURN
    END



    SUBROUTINE TABLE
    COMMON /A/ ARRAY(21)
    ARRAY(1) = 1.0
    ARRAY(2) = 0.979
    ARRAY(3) = 0.946
    ARRAY(4) = 0.910
    ARRAY(5) = 0.868
    ARRAY(6) = 0.820
    ARRAY(7) = 0.765
    ARRAY(8) = 0.708
    ARRAY(9) = 0.640
    ARRAY(10) = 0.570
    ARRAY (11)= 0.500
    ARRAY(12) = 0.420
  . ARRAY(13) = 0.345
    ARRAY(14) = 0.275
    ARRAY(15) = 0.210
    ARRAY(16) = 0.150
    ARRAY(17) = 0.110
    ARRAY(18) = 0.083
    ARRAY(19) = 0.063
    ARRAY(20) = 0.052
    ARRAY(21)=12./256.
    RETURN
    END
```

```
      SUBROUTINE FORMC (XZERO,XL,DEL,FNC)
      DIMENSION FNC(601)
      COMMON/B/DXL,DE,FN(601),Q,G,NMAX
      NZIP = NMAX + 1
      DO 10 I = 1,NZIP
      EI = I
      X = (EI-1.)*DEL + XL
      Y = X/XZERO
      FNC(I) = FORM(Y)
   10 CONTINUE
      RETURN
      END



      FUNCTION FORM (ARG)
      COMMON /A/ ARRAY(21)
      IF(ARG) 2,1,2
    1 FORM = ARRAY(1)
      GO TO 1000
    2 IF(ARG - 4.0) 3,4,4
    3 I = ARG/.2
      EI = I
      ISUB = I + 1
      IUP = I + 2
      FORM = ARRAY(ISUB) - (ARRAY(ISUB) - ARRAY(IUP))*((ARG/0.2) - EI)
      GO TO 1000
    4 FORM = 12./(ARG**4)
 1000 CONTINUE
      RETURN
      END



      SUBROUTINE RAIN(X, VM2X, NUM)
C  DIFFERENTIAL DISTRIBUTION CALCULATION
```

```
      COMMON TOL, PI, TOLM
      COMMON /B/ XL, DEL, FN(601), Q, G, NMAX
      DIMENSION IW(16), TLM3(601), Y(601), C(601)
      NZIP = NMAX + 1
   11 DO 70 M = 1,NZIP
      EM = M
      XLAM = XL + (EM - 1.)*DEL
      TLM3(M) = TXLAM(X, XLAM)
   70 CONTINUE
      DO 8 J = 1,NZIP
      IF (NUM - 4)7,7,6
C  FORM INTEGRAND VALUES WITH OR WITHOUT MULTIPLICATIVE FACTOR FN(J), AS NEEDED
C        FOR C-R OR MOLIERE DISTRIBUTION, RESPECTIVELY.
    6 Y(J) = TLM3(J)
      GO TO 8
    7 Y(J) = TLM3(J)*FN(J)
    8 CONTINUE
      QMX=QLX(XL,X,NMAXQ)
      BRKT5 = (1.0 + (QMX/(4.0*G)))
      RTPI = SQRTF(PI)
      COEF1 = EXPF(-X*X)/RTPI
      TERM1 = COEF1*BRKT5
      TERM 2 = WEDL(Y,NMAX,DEL)
      TERM 2 = (1.0/(4.0*G*RTPI))*TERM 2
      VM2X = TERM1 + TERM2
      THETA = X*(57.296)*SQRTF(2.*G*Q)
      PRINT 604, THETA, X, VM2X, QMX, NMAXQ
  604 FORMAT (1H ,15HTHETA(IN DEG.)= ,F7.3,3X,9H(I.E.) X= , F6.2,5X,
     15HM(X)= ,E11.4,5X,7HQ(L,X)= ,E11.4,4X,15HNMAX IN Q(L,X)= ,I4)
      RETURN
      END
```

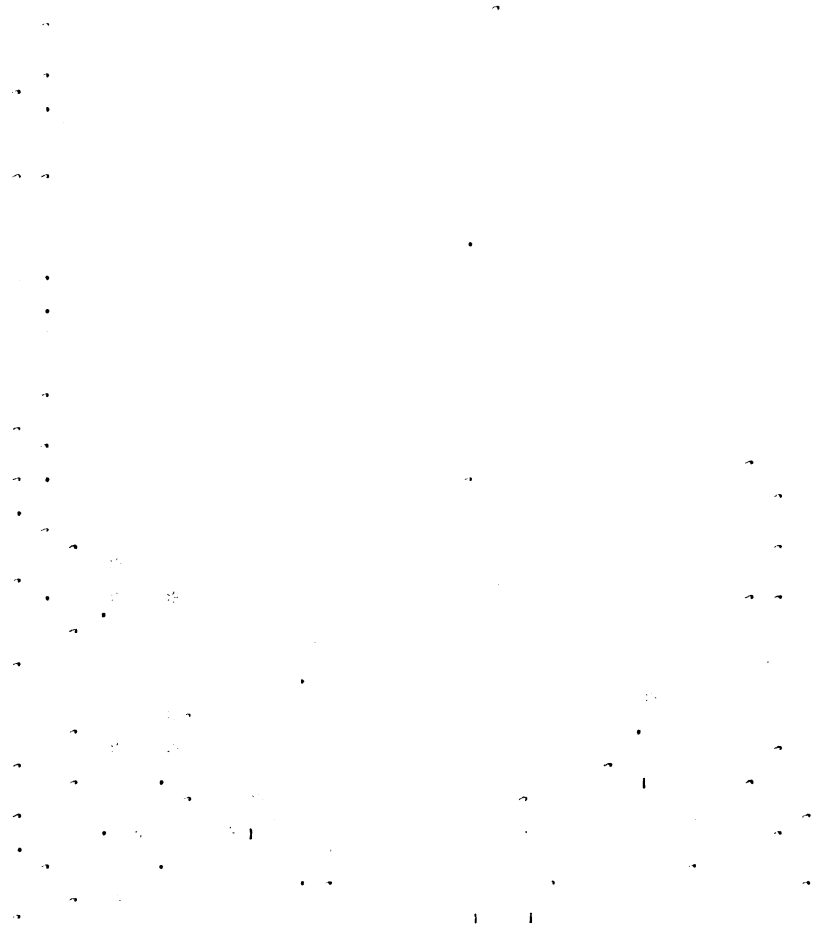

```
      SUBROUTINE DRELL (ULIM,DELX,NUM)
C   DIFFERENTIAL SINGLE SCATTERING DISTRIBUTION OF DRELL-SCHWARTZ
      COMMON TOL,PI
      COMMON /B/ XL,DEL,FN(601),Q,G,NMAX,PC,A,Z,THICK,DEN,PHIM
      COMMON /C/ AMX(300),BMX(300),CMX(300),FRDF(300),DMX(300)
      COMMON /E/ DNDTHA(300),Q0(300),F2X0(300),F2EL(300),DSIG0(300),
     1DSIGC(300),F2MAG(300)
C   HBARC IS IN UNITS OF MEV-CM(SINCE 1 MEV=E+6 JOULE/COUL.(1.602E-19)*(1.0E+7)=
C    1.602E-6 ERGS PER MEV.
      HBARC = 3.1632E-17/1.602E-6
      ANO = 6.02E23
      RE = 2.81E-13
      AME = 0.5
      AMN = 938.8
      AMUP = 2.793
      AMUN = -1.91
      TBAR=30.0
      AR = 1.86E-13
C    AKO IS IN UNITS OF MEV, AK01 IS IN UNITS OF INVERSE CM.
      AKO = PC
      AK01 = AKO/HBARC
      DELFI = DELX*SQRTF(2.*G*Q)
      INDEX=ULIM/DELX+1
      THETA = DELFI/100
      PRINT 602
  602 FORMAT(1H0,38HRESULTS OF DRELL-SCHWARTZ CALCULATION. /2X,5HTHETA ,
     16X,2HQ0 ,10X,5HF2Q0 ,7X,5HDSIG0 ,7X,4HF2X0 ,8X,4HF2EL ,8X,
     25HF2MAG ,7X,5HDSIGO ,7X,6HDNDTHA /)
      DO 5   I=1,INDEX
      EI = I
      Q0(I) = (2.)*AK01*SINF(THETA/2,)
      X0 = ((AR*Q0(I))**2)/2.
      TERM 1 = EXPF(-(X0/2.))
      TERM2 = 1. - (16.)*X0/39. +(5.)*(X0*X0)/156
      F2X0(I) = TERM1*TERM2
      F2EL(I) = Z + Z*(Z-1.)*F2X0(I)
C    HERE Q0MUST BE PUT IN INVERSE FERMIS INSTEAD OF INVERSE CM. AS ABOVE.
```

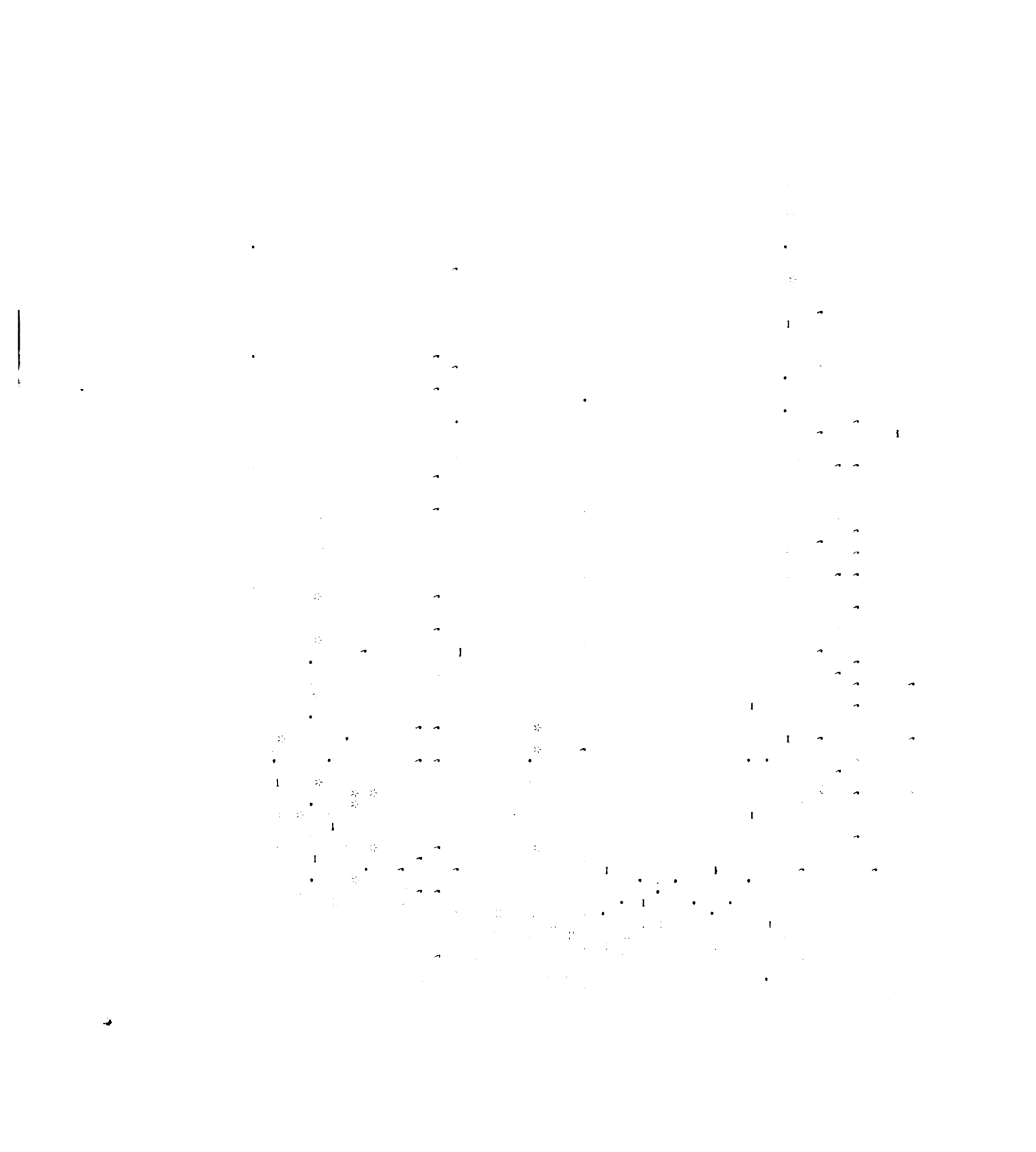

```
      EF2Q0 = (Q0(I)*Q0(I)*1.E-26)/6.1
      IF(EF2Q0-600.)3,3,2
    2 F2Q0 = 1.0
      GO TO 4
    3 F2Q0 = EXPF(-(EF2Q0))
    4 TERM1 =RE*AME/(2.*AK0)
      TERM 1 = TERM1*TERM1
      TERM 2 = COSF(THETA/2.)/((SINF(THETA/2.))**2)
      TERM 2 = TERM2*TERM2
      DSIG0(I) = TERM1*TERM2
C     Q01 IS IN UNITS OF MEV(NUMERICALLY = MOM. TRANSFER IN MEV/C)
      Q01 = Q0(I)*HBARC
      TERM1 = Z*Q01*Q01/(2.*A*AMN*AMN)
      TERM2 = 2./((COSF(THETA/2.))**2) - 1
      TERM3 = 2.*Z*TBAR/(3.*A*AMN)
      TERM4 = Q01*Q01/(4.*AMN*AMN)
      TERM5 = Z*AMUP*AMUP + (A-Z)*AMUN*AMUN
      F2MAG(I) = TERM1 + TERM2*(TERM3 + TERM4*TERM5)
      DSIGC(I)=DSIG0(I)*F2Q0*(F2EL(I)+F2MAG(I))
C     CALCULATION OF DNDTHETA (DNDTHA) FROM DSIGC
      TERM 1=(2.)*PI*SINF(THETA)
      TERM2 = ANO*DEN*2.54*THICK/A
      DNDTHA(I) = TERM1*TERM2*DSIGC(I)
      THETAP = THETA*(57.296)
      PRINT 601,THETAP,Q01, F2Q0, DSIG0(I), F2X0(I), F2EL(I)
     1F2MAG(I), DSIGC(I), DNDTHA(I)
  601 FORMAT(1H ,F7.3,3X,8(E10.3,2X))
      THETA = EI*DELFI
    5 CONTINUE
      CALL MSCOR(ULIM,DELX)
      RETURN
      END
```

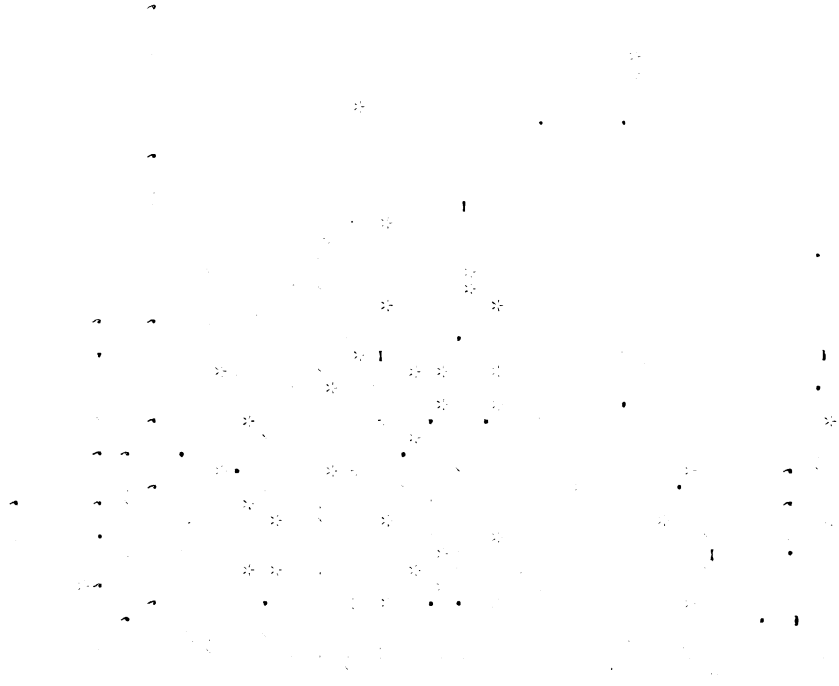

```
      SUBROUTINE MSCOR(ULIM, DELX)
C   CALCULATION OF MULTIPLE SCATTERING CORRECTION TO D-S DISTRIB.,
      DONE BY COMPARING C-R CALC. FOR MULTIPLE AND SINGLE SCATTERING.
      COMMON /B/ XL,DEL,FN(601),Q,G,NMAX,PC,A,Z,THICK,DEN,PHIM,FNC(601),
     1XZERO, FNCS(601), FNX(601), PHIZR
      COMMON /C/ AMX(300),BMX(300),CMX(300),FRDF(300),DMX(300)
      INDEX = ULIM/DELX + 1
      SLIM = 0.0
      NUMGP = 4
      GO TO 16
      ANORMA = GTHETA(ULIM,DELX,SIGMA,SLIM,NUM,INDEXL,NUMGP)
      DO 15 I = 1,INDEX
      AMX(I) = AMX(I)/ANORMA
   15 CONTINUE
   16 X = 0.0
      DO 20 J = 1,INDEX
      Y = X/XZERO
      YM = PHIM/PHIZR
      TERM 1 = (Y**2 + YM**2)**(3./2.)
      BQ = Q/(PHIZR**2)
      BMX(J) = BQ*FNS(J)/(2.*TERM1)
      X = X + DELX
   20 CONTINUE
      DO 23 I = 1,INDEX
      EI = I - 1
      IF(BMX(I)-1.0)21,21,23
   21 SLIM = EI*DELX
      GO TO 24
   23 CONTINUE
   24 NUMGP=5
      GO TO 27
      ANORMB = GTHETA(ULIM,DELX,SIGMA,SLIM,NUM,INDEXLB,NUMGP)
      DO 25 I = 1,INDEX
      BMX(I) = BMX(I)/ANORMB
   25 CONTINUE
      PRINT 604, ANORMA, ANORMB, INDEXLB
```

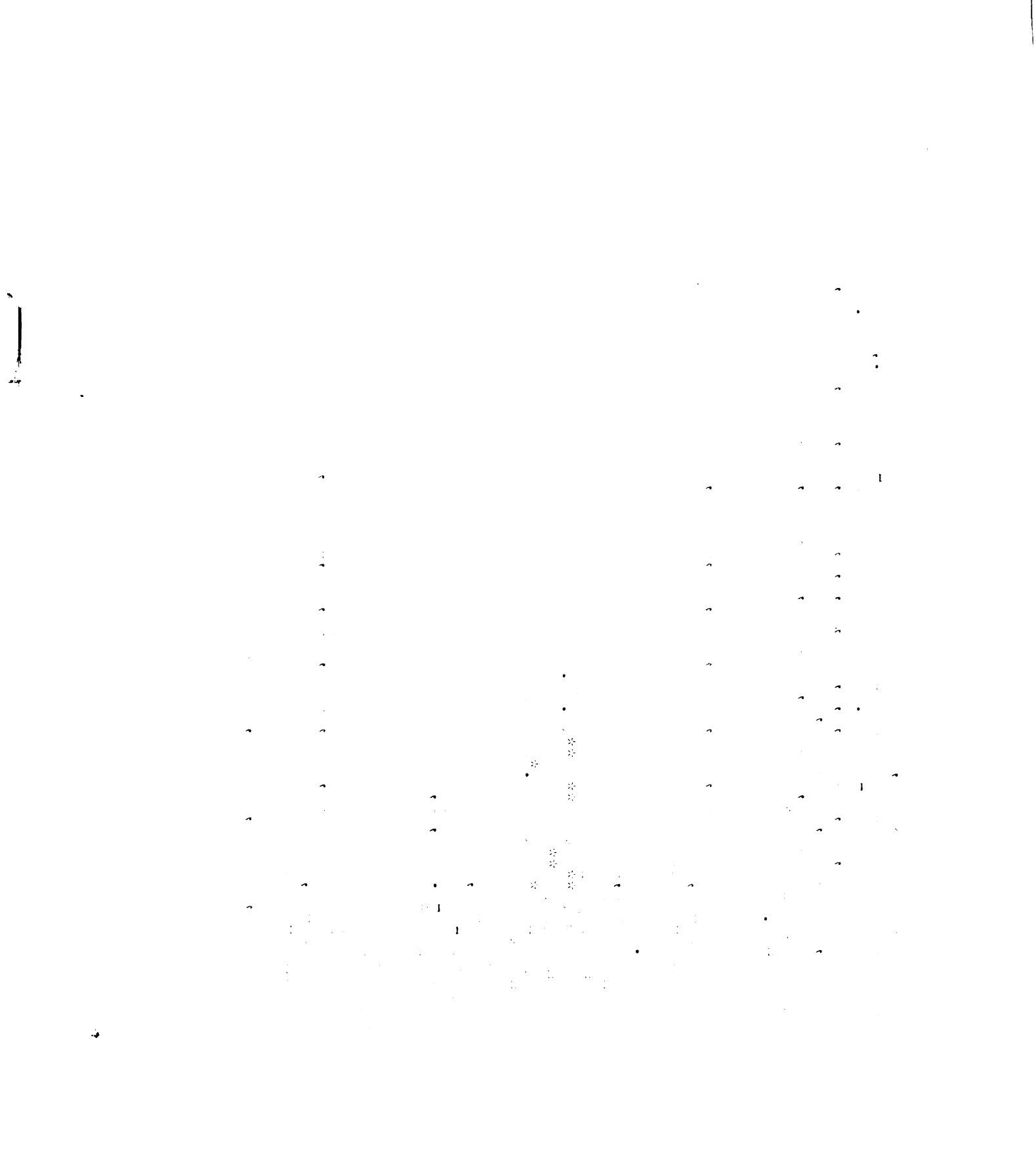

```
  604 FORMAT(1H0.7HANORMA= ,E11.4,3X,7HANORMB= ,E11.4,3X,8HINDEXLB= ,I3)
   27 X = 0.0
      DO 30 I = 1,INDEX
      FRDF(I) = (AMX(I) - BMX(I))/BMX(I)
      X = X + DELX
   30 CONTINUE
      RETURN
      END
```

```
      SUBROUTINE DRELPR(X,DNDPHI,DNDPHIS,ULIM,DELX,NUM,KM)
C     CONVERSION OF DNDTHA TO PROJECTED ANGLES.
      COMMON TOL,PI
      COMMON /B/ XL,DEL,FN(601),Q,G,NMAX,PC,A,Z,THICK,DEN,PHIM
      COMMON /C/ AMX(300),BMX(300),CMX(300),FRDF(300),DMX(300)
      COMMON /E/ DNDTHA(300)
      DIMENSION GAMMA(300),CA(300),THETAR(300)
      FI = X*SQRTF(2.*G*Q)
      DELFI = DELX*SQRTF(2.*G*Q)
      LO = X/DELX + 1
      INDEX=ULIM/DELX+1
      DO 10   I=LO,INDEX
      EI = I
      THETAR(I) = FI + EI*DELFI
    9 GAMMA(I) =ACOSF(TANF(FI)/TANF(THETAR(I))
      GAMMA(I) = ABSF(GAMMA(I))
   10 CONTINUE
C     FRACTIONAL CONTRIBUTION OF AREA FOR I = LO.
      TERM 1 = 2.*GAMMA(LO) -SINF(2.*GAMMA(LO))
      TERM 2 = (TANF(THETAR(LO)))**2
      TERM 3 = (TANF(THETAR(LO)))**2 - (TANF(FI))**2
      CA(LO) = TERM1*TERM2/(PI*TERM3)
C     FRACTIONAL CONTRIBUTION OF AREA FOR I GREATER THAN LO.
      LOP1 = LO + 1
```

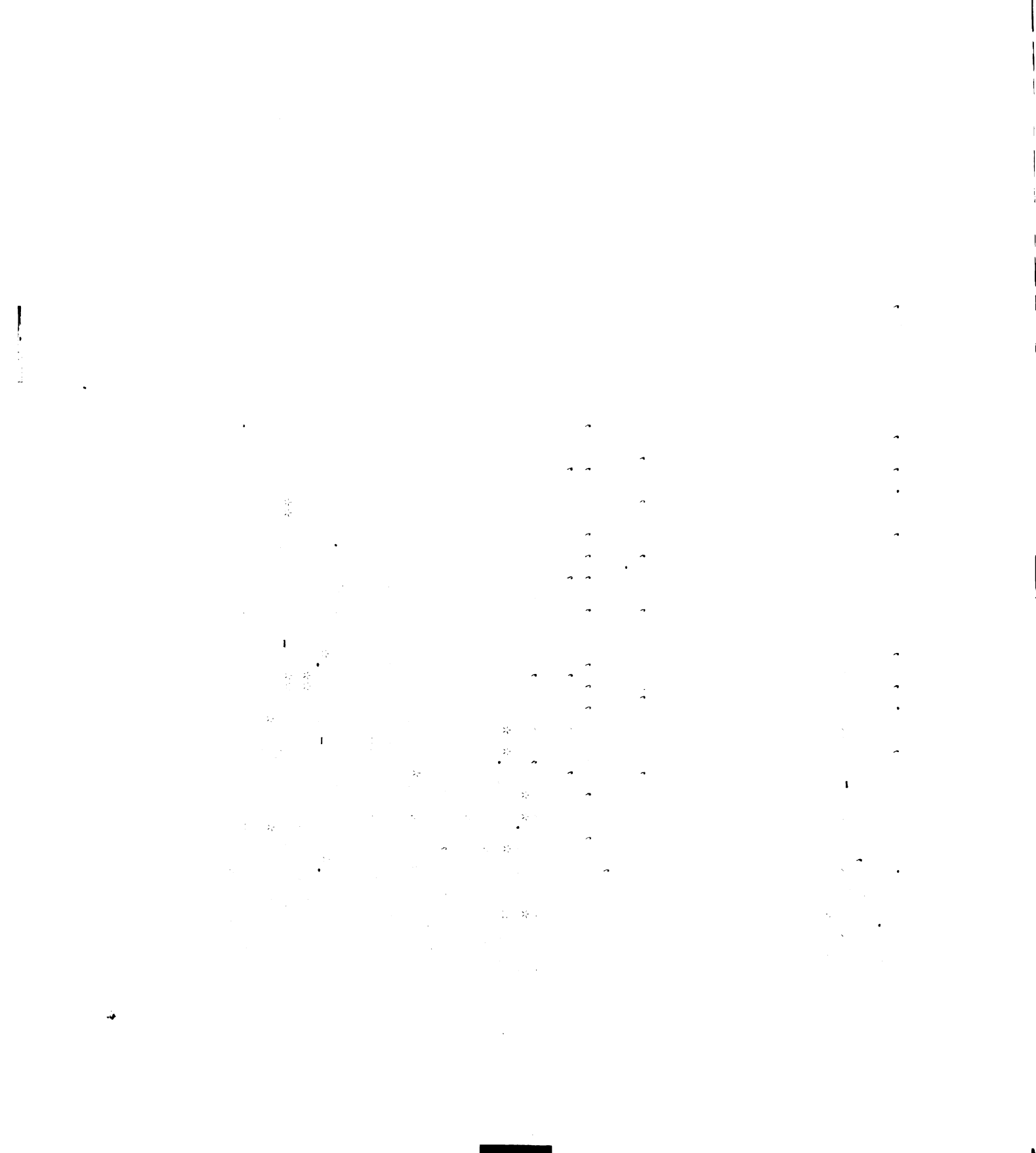

```
      DO 20    I=LOP1,INDEX
      TERM 1 = DELFI**2
      K = I - 1
      TERM2 = (TANF(THETAR(I)))**2 - (TANF(THETAR(K)))**2
      TERM 3 = SINF(GAMMA(I)) + 1.E-30
      CA(I) = 4.*TERM1/(PI*TERM2*TERM3)
   20 CONTINUE
      SERIES = 0.0
      DO 30  I=LO,INDEX
      TERM = CA(I)*DNDTHA(I)
      SERIES = SERIES + TERM
   30 CONTINUE
      DNDPHIS = SERIES
      DNDPHI = SERIES + FRDF(LO)*SERIES
      PHI = FI*(57.296)
      FRDFP = FRDF(LO)*100
      PRINT 601,PHI,X,DNDPHIS,DNDPHI,FRDFP
  601 FORMAT(1H ,4HPHI= ,F7.3,2X, 2HX= , F5.2, 2X,11HDNDPHIS(X)= ,E11.4,
     12X, 10HDNDPHI(X)= ,E11.4, 2X, 7H0/0 MS= ,E17.10)
      RETURN
      END
```

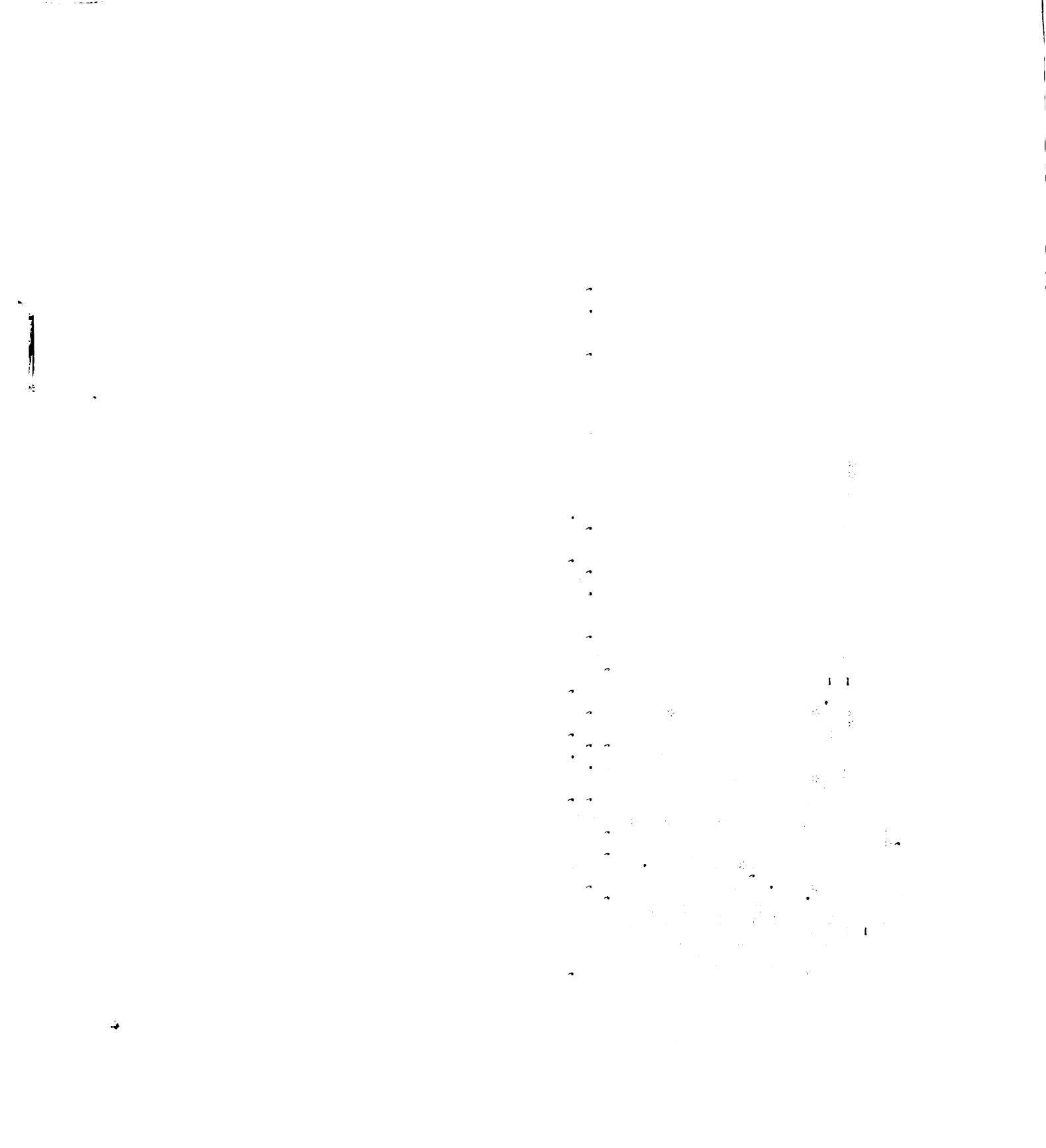

```
      FUNCTION TXLAM (X,XLDA)
C  AN EXPONENT OF 835 IS STILL PERMISSABLE.  USING 785 LIMITS X TO 28.0.
      ET1 = (X + XLDA)**2
      IF(ET1-785)2,1,1
    1 TERM1 = 0.0
      GO TO 3
    2 TERM1 = EXPF(-(X + XLDA)**2
    3 ET2 = (X-XLDA)**2
      IF(ET2-785)5,4,4
    4 TERM2 = 0.0
      GO TO 6
    5 TERM2 = EXPF(-(X - XLDA)**2)
    6 ET3 = X*X
      IF(ET3-785)8,7,7
    7 TERM3 = 0.0
      GO TO 9
    8 TERM3 = -2.*EXPF(-X*X)
    9 XMULT = XLDA**3
      TXLAM = (TERM1 + TERM2 + TERM3)/XMULT
      RETURN
      END


      FUNCTION QLX(XL,X,NMAX)
      COMMON TOL, PI, TOLM
      SERIES = 0.0
      COMP=0.01
      N = 2
      IF(X) 1,3,1
    1 EN=N
      TERM = ((2.*XL*X)**N)/(EN*FACT(N))
      SERIES = SERIES + TERM
      C=ABSF(TERM/COMP)
      IF(C - TOL) 3,3,2
    2 N = N+2
```

```
      COMP = TERM
      GO TO 1
    3 XMULT = 2.*(2.*X*X - 1.)
      BRKT1 = LOGF(XL/1.26) + SERIES
      BRKT2 = 6.*X*X - (1./(XL*XL)) * (CSNH(2.*
     1XL*X) - 1.) - (2.*X/XL)*ZINH(2.*XL*X)
      QLX = XMULT*BRKT1 + BRKT2
      NMAX = N
      RETURN
      END


      FUNCTION FACT (I)
      FACT = 1.0
      IF(I) 2,1,2
    1 RETURN
    2 DO 10 M = 1,I
      XM = M
      FACT = FACT*XM
   10 CONTINUE
      RETURN
      END


      FUNCTION CSNH(X)
      CSNH = (EXPF(X) + EXPF(-X))/2.
      RETURN
      END


      FUNCTION ZINH(X)
      ZINH = (EXPF(X) - EXPF(-X))/2.
      RETURN
```

```
      END


      FUNCTION WEDL (FX,NMAX,DEL)
      DIMENSION C(601), FX(601)
C     SET THE FIRST SEVEN COEFFICIENTS
      C(1) = 1.0
      C(2) = 5.0
      C(3) = 1.0
      C(4) = 6.0
      C(5) = 1.0
      C(6) = 5.0
      C(7) = 2.0
C     SET ALL BUT THE LAST
      DO 1 K = 8,NMAX
      C(K) = C(K-6)
    1 CONTINUE
C     SET THE LAST COEFFICIENT
      C(NMAX + 1) = 1.0
      SUM = 0.0
      NZIP=NMAX+1
      DO 2  K=1,NZIP
      SUM = SUM + FX(K)*C(K)
    2 CONTINUE
      WEDL = 0.3*DEL*SUM
      RETURN
      END


      FUNCTION GPTHTA(XPR, SIGMA ULIM, DELX,NUM)
      DIMENSION XINTG(800)
      COMMON TOL, PI, TOLM
      COMMON /B/ XL, DEL, FN(601), Q, G, NMAX
```

```
      COMMON /C/ AMX(500)
      X = ULIM
      N1 = ULIM/DELX
C    PREPARE THE INTEGRAND
      XNORM = 1./(SQRTF(2.*PI)*SIGMA)
      EPT = (XPR + X)**2/(2.*SIGMA*SIGMA)
      IF(EPT-300.)10,5,5
    5 DO 8 J = 1,N1
      EP = (XPR + X)**2/(2.*SIGMA*SIGMA)
      IF(EP-300)6,7,7
    6 LC = J
      GO TO 12
    7 XINTG(J) = 0.0
      X = X-DELX
    8 CONTINUE
      GO TO 18
   10 LC = 1
   12 DO 15 I = LC,N1
      EI = I
      NI = ULIM/DELX - EI + 1
      K = NI + 1
      EP = (XPR + X)**2/(2.*SIGMA*SIGMA)
      XINTG(I) = AMX(K)*EXPF(-EP)
      AMXP = AMX(K)
      XINTP = XINTG(I)
C    STATEMENT READING   GO TO 115   INSERTED HERE WILL PREVENT PRINTING XINTG.
      GO TO 115
      IF(XPR-1.5)201,200,202
  200 GO TO 612
  201 GO TO 115
  202 IF(XPR-3.0)201,200,204
  204 IF(XPR-4.5)201,200,206
  206 IF(XPR-6.0)201,200,208
  208 IF(XPR-7.5)115,200,115
  612 PRINT 602,I,XPR,X,AMXP,EP,K,XINTP
```

```
  602 FORMAT(1H ,2HI= ,I3,3X,4HXPR= ,F6.2,3X,2HX= ,F6.2,3X,7HAMX(K)= ,
     1E11.4,3X,3HEP= ,E11.4,3X,2HK= ,I3,3X,9HXINTG(I)= ,E11.4)
  115 X = X - DELX
   15 CONTINUE
   18 X = 0.0
      N2 = N1 + ULIM/DELX + 1
      EPT = XPR*XPR/(2.*SIGMA*SIGMA)
      N1 = N1 + 1
      IF(EPT - 300)33,25,25
   25 DO 28 J = N1,N2
      EP = (XPR - X)**2/(2.*SIGMA*SIGMA)
      IF(EP - 300)26,27,27
   26 LC = J
      GO TO 35
   27 XINTG(J) = 0.0
      K = J - N1 + 1
      AMXP = AMX(K)
      XINTP = XINTG(J)
C     STATEMENT READING   GO TO 128   INSERTED HERE WILL PREVENT PRINTING XINTG.
      GO TO 128
      IF(XPR-1.5)301,300,302
  300 GO TO 613
  301 GO TO 128
  302 IF(XPR-3.0)301,300,304
  304 IF(XPR-4.5)301,300,306
  306 IF(XPR-6.0)301,300,308
  308 IF(XPR-7.5)128,300,128
  613 PRINT 603,J,XPR,X,AMXP,EP,K,XINTP
  603 FORMAT(1H ,2HI= ,I3,3X,4HXPR= ,F6.2,3X,2HX= ,F6.2,3X,7HAMX(K)= ,
     1E11.4,3X,3HEP= ,E11.4,3X,2HK= ,I3,3X,9HXINTG(I)= ,E11.4)
  128 X = X + DELX
   28 CONTINUE
   33 LC = N1
   35 DO 100 I = LC,N2
      EP = (XPR - X)**2/(2.*SIGMA*SIGMA)
      IF(EP - 300.)29,21,21
```

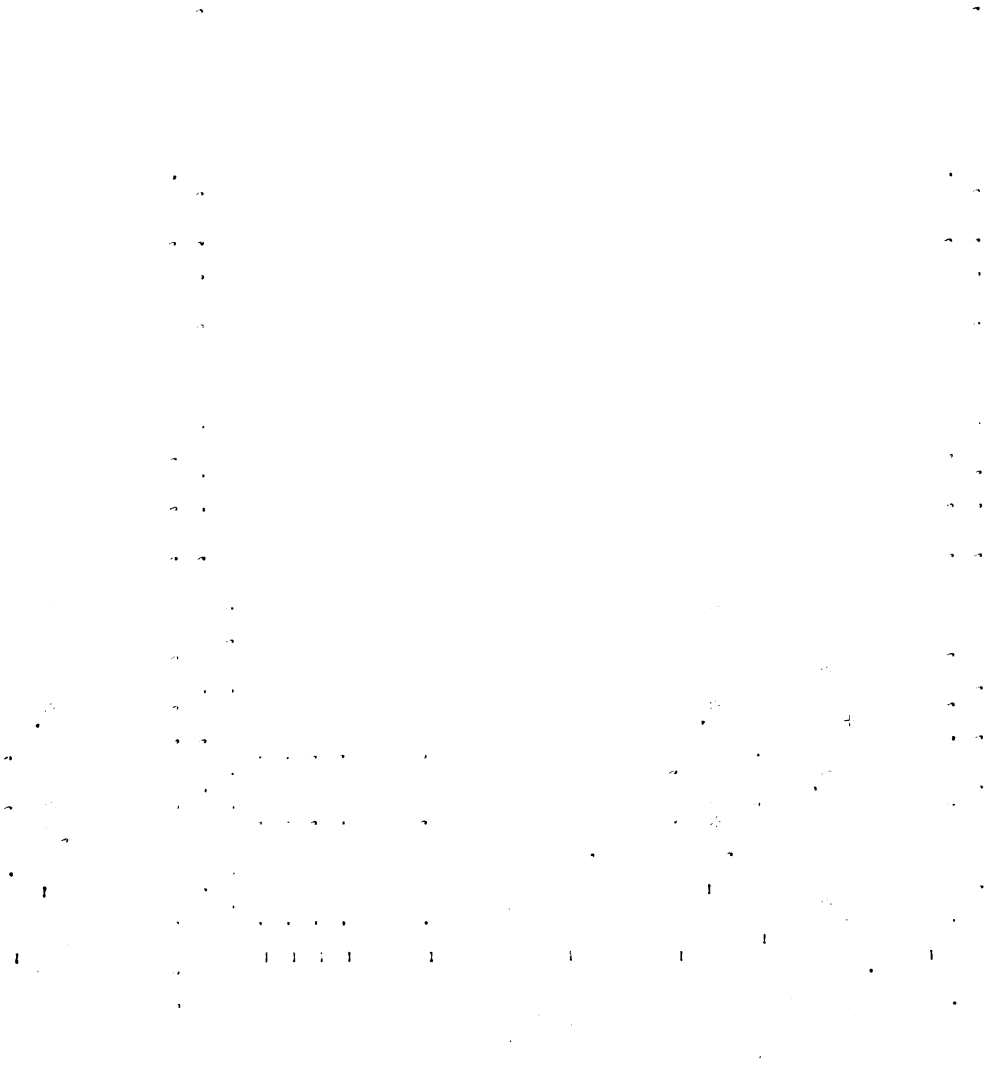

```
   21 DO 22 K = I,N2
   22 XINTG(K) = 0.0
      GO TO 1000
   29 L = I - N1 + 1
      XINTG(I)= AMX(L)*EXPF(-EP)
      AMXP = AMX(L)
      XINTP = XINTG(I)
C     STATEMENT READING   GO TO 30   INSERTED HERE WILL PREVENT PRINTING XINTG.
      GO TO 30
      IF(XPR-1.5)401,400.402
  400 GO TO 614
  401 GO TO 30
  402 IF(XPR-3.0)401,400,404
  404 IF(XPR-4.5)401,400,406
  406 IF(XPR-6.0)401,400,408
  408 IF(XPR-7.5)30,400,30
  614 PRINT 604,I,XPR,X,AMXP,EP,L,XINTP
  604 FORMAT(1H ,2HI= ,I3,3X,4HXPR= ,F6.2,3X,2HX= ,F6.2,3X,7HAMX(L)= ,
     1E11.4,3X,3HEP= ,E11.4,3X,2HK= ,I3,3X,9HXINTG(I)= ,E11.4)
   30 X = X + DELX
  100 CONTINUE
 1000 GPTHTA = XNORM*FNTGRL(N2,DELX,XINTG)
      THETAPR = XPR*(57.296)*SQRTF(2.*G*Q)
  601 FORMAT(1H ,18HTHETA-PR(IN DEG.)=,F7.3, 5X,12H(I.E.) XPR =,F6.2, 5X
     1,11HG(P*THETA)= ,E11.4)
      IF(GPTHTA-3.0E-5)1002,102,102
  102 PRINT 601, THETAPR, XPR, GPTHTA
 1002 RETURN
      END


      FUNCTION GTHETA (ULIM,DELX,SIGMA,SLIM,NUM,INDEX)
C     CALC. OF INTEGRAL SCATTERING DISTRIB., CORR. FOR NOISE LEVEL SCATT
C     PREPARE THE INTEGRAND
```

```
      DIMENSION U(500)
      COMMON /B/ XL, DEL, FN(601), Q, G, NMAX
      COMMON /C/ AMX(500)
      COMMON /D/ GPTA(500)
      N=ULIM/DELX+1.
      INDEX = SLIM/DELX + 1
      X = SLIM
      GO TO(3, 3,3,4,3,4),NUM
    3 DO 10 I = INDEX,N
      U(I) = GPTA(I)
   10 CONTINUE
      GO TO 30
    4 DO 20 I = INDEX,N
      U(I) = AMX(I)
   20 CONTINUE
   30 GTHETA = FNTGRL(N-INDEX+1,DELX,U(INDEX))
      RETURN
      END
```



```
      FUNCTION FNTGRL(N,DELTA,F)
CFNTGRL      NUMERICAL INTEGRATION SUBROUTINE
C        FUNCTION  FNTGRL(N,DELTA,F)
C     EXTENDED FIVE-POINT NEWTON-COTES QUADRATURE
C     EXACT FOR FOURTH-DEGREE POLYNOMIAL
C     REQUIRES MINIMUM OF FIVE POINTS ... NO MAXIMUM
C        N = TOTAL NUMBER OF NET POINTS (AEQUALLY-SPACED)
C        DELTA = INCREMENT BETWEEN NET POINTS
C        F = INTEGRAND TABULATED AT EACH NET POINT
      DIMENSION F(5)
      S=0.0
      DO 20 J=5,N,4
      M=J
   20 S=S+7.*(F(J-4)+F(J))+32.*(F(J-3)+F(J-1))+12.*F(J-2_
      IF(N-M) 50,50,25
```

```
25 M=M+1
   DO 30 J=M,N
30 S=S+7.84375*F(J)+20.1875*F(J-1)-8.25*F(J-2)+3.3125*F(J-3)-0.59375*
  1F(J-4)
50 FNTGRL=DELTA*S/22.5
   RETURN
   END
```

REFERENCES

1. J. Rainwater, Annual Review of Nuclear Science, Vol. 7, (1957).

2. G. N. Fowler and A. W. Wolfendale, Progress in Elementary Particles and Cosmic Ray Physics, Vol. 4, (1958).

3. E. Amaldi and G. Fidecaro, Nuovo cimento, 7, 535 (1950).

4. W. L. Whittemore and R. P. Shutt, Phys. Rev. 88, 1312 (1952).

5. I. B. McDiarmid, Phil. Mag. 46, 177 (1955).

6. J. L. Lloyd and A. W. Wolfendale, Proc. Phys. Soc. (London) A68, 1045 (1955).

7. J. L. Lloyd, E. Rossle, and A. W. Wolfendale, Proc. Phys. Soc. (London) A70, 421 (1957).

8. S. Olbert, Phys Rev. 87, 319 (1952); Annis, Bridge and Olbert, Phys. Rev. 89, 1216 (1953).

9. L. N. Cooper and J. Rainwater, Phys. Rev. 97, 492 (1955).

10. G. Moliere, Z. Naturforsh 2a, 133 (1947); 3a, 78 (1948).

11. S. Fukui, T. Kitamura, and Y. Watase, Phys. Rev. 113, 315 (1959).

12. J. L. Lloyd and A. W. Wolfendale, Phys. Rev. 117, 247 (1960).

13. G. E. Masek, L. D. Heggie, Y. B. Kim, and R. W. Williams, Phys. Rev. 122, 937 (1961).

14. B. McDiarmid, Phil. Mag. 45, 933 (1954).

15. D. J. Montgomery, Cosmic Ray Physics, Princeton University Press, 1949.

16. B. Rossi, Rev. Mod. Phys. 20, 537 (1948)

17. S. D. Drell and C. L. Schwartz, Phys. Rev. 112, 568 (1958).

18. R. Hofstadter, Rev. Mod. Phys. 30, 458 (1958).

19. Chollet, Bounin, and Bishop, Laboratoire de Accel. Lineaire, Orsay, LAL 1091 (Jan., 1964).

20. D. Halliday, "Introductory Nuclear Physics," John Wiley, Inc., 1955 (Page 326).

21. G. Shapiro and L. M. Lederman, Phys. Rev. 125, 1022 (1962).

22. Nuclear Data Chart, UCRL-8030 (Revised), June 1964.

23. G. Danby, J. M. Gaillard, K. Goulianos, L. M. Lederman, N. Mistry, M. Schwartz, and J. Steinberger, Phys. Rev. Letters 9, 36 (1962).

24. Feinberg and Lederman, Ann. Rev. Nucl. Sci. 13, 431 (1963).

25. R. H. Hildebrand, Phys. Rev. Letters 8, 34 (1962).

26. E. Bertolini, D. Citron, G. Gianlanella, S. Focardi, A. Muklin, C. Rubia, and S. Saporetti, "Proc. International Conf. High Energy Phys.," CERN, Geneva, 421 (1962).

27. E. Bleser, L. M. Lederman, J. Rosen, J. Rothberg, and E. Zavaltini, Phys. Rev. Letters 8, 128 (1962).

28. J. Rothberg, "Columbia Univ. Nevis Rept." 116 (1963).

29. F. Charpak, F. J. M. Farley, R. L. Garwin, T. Muller, J. C. Sens, and A. Zichichi, Phys. Letters 1, 16 (1962).

30. R. Hofstadter, Rev. Mod. Phys. 28, 214 (1956); Ann. Rev. Nucl. Sci. 7, 231 (1957) (contains a summary of electron scattering results up to that time).

31. D. G. Ravenhall, Rev. Mod. Phys. 30, 430 (1958).

32. L. N. Hand, D. G. Miller, and R. Wilson, Rev. Mod. Phys. 35, 335 (1963)(contains a summary of eight e-p experiments between 1961-1963).

33. J. R. Dunning, Jr., K. W. Chen, A. A. Cone, G. Hartwig, N. F. Ramsey, J. K. Walker, and R. Wilson, Phys. Rev. Letters 13, 631 (1964).

34. H. F. Davis, T. E. Ewart, G. E. Masek, E. D. Platner, J. P. Toutonghi, and R. W. Williams, Phys. Rev. 131, 2192 (1963).

35. R. Cool, A. Maschke, L. M. Lederman, and M. Tannenbaum, Phys. Rev. Letters 14, 724 (1965).

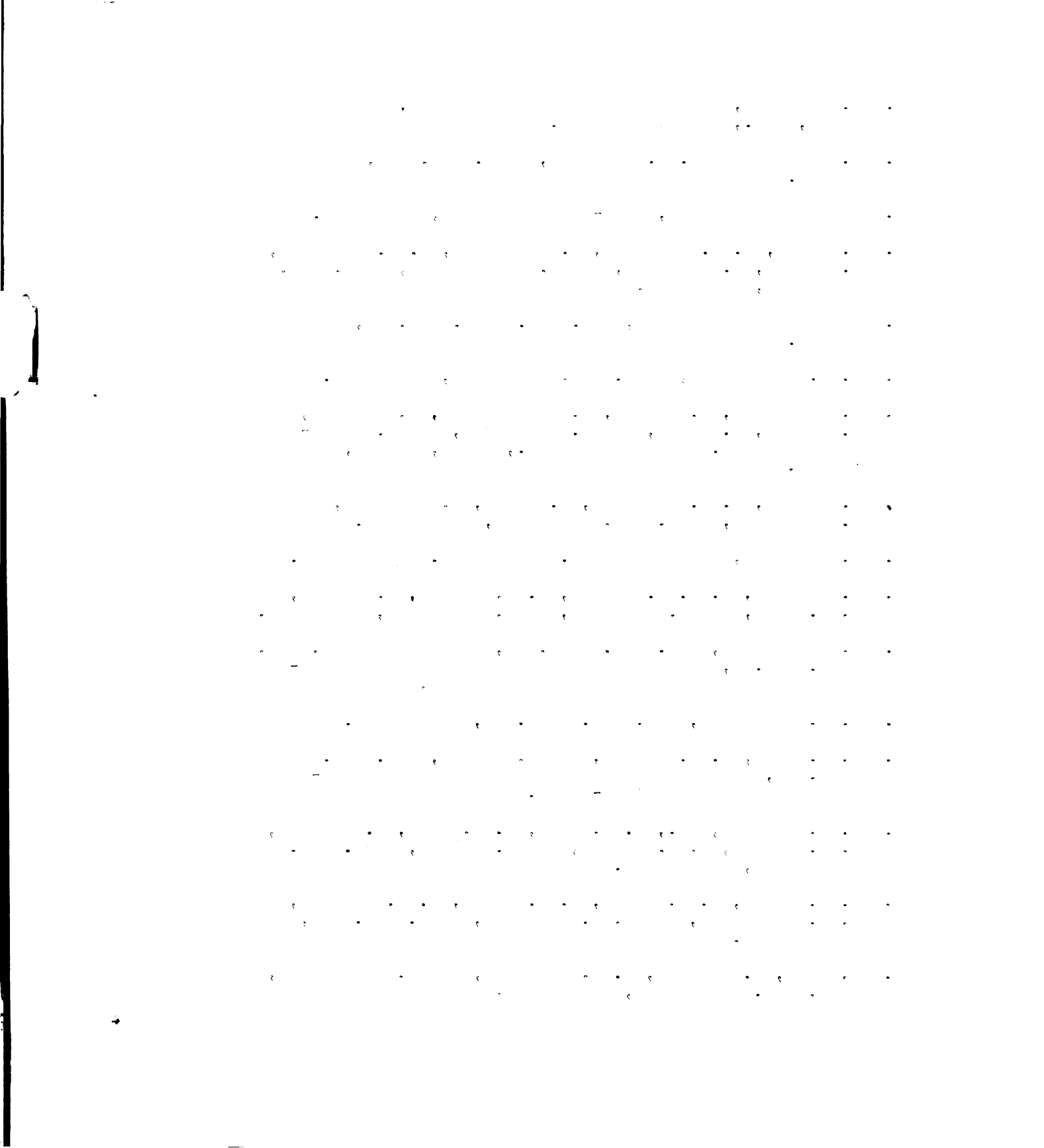

36. Whetstone and Kounosu, Rev. Sci. Instr. 33, 423 (1962).

37. Private communication with Professor L. Jones, Univ. of Michigan.

38. Tables for statisticians, Biometrika 32 (1941).